ABSTRACT

JIANG, ZONGLIANG. Application of an Entropy-Assisted Optimization Model in the Prediction of Agonist and Antagonist Muscle Forces. (Under the direction of Dr. Gary A. Mirka and Dr. Shu-Cherng Fang.)

Work-related musculoskeletal disorders are a significant problem in industry. A considerable amount of research has been conducted to try to reduce the incidence and severity of these injuries/illnesses. Biomechanical modeling techniques are often employed to estimate the muscle forces and joint loading that occur during physical exertions. One class of these models utilizes optimization techniques to arrive at predictions. Unfortunately, most existing optimization-based biomechanical models fail to predict antagonist muscle activity, which results in an underestimation of overall muscle force requirements and an underestimation of joint reaction forces. Some optimization models predict such a co-contraction, but they either lack a compelling physiological basis or are computationally formidable. The current study takes advantage of the flexible definition of entropy as a scientific measure, and utilizes it in the objective function of an optimization formulation to construct a new optimization model for predicting both agonist and antagonist muscle forces. Recent neurophysiological studies suggested that there exist two separate central nervous systems for generation of two motor patterns: agonist only contraction and agonist-antagonist co-contraction. These have provided a sound physiological basis for a novel optimization-based approach.

In the proposed model (Entropy-ASsisted Optimization Model, or EASOM), the objective function consists of a weighted combination of two components: the sum of cubed muscle stresses, which promotes agonist muscle only exertion, and an entropy related term

which encourages the agonist and antagonist co-contraction. The weight factor assigned to the entropy term (W) is set between 0.1 and 1, and it represents the level of co-contraction associated with EASOM muscle force predictions. The constraints include a moment equilibrium constraint and a muscle stress limit constraint. This study focused on a single-plane model in the elbow where the elbow flexion motion in the sagittal plane was investigated. The task variables (or input to the optimization model) included load magnitude, angular velocity, and elbow flexion angle. EMG data were collected and used to obtain the relationship between W and task variables. The muscle forces generated from these empirical EMG data were considered the gold standard and used during model validation.

The results showed that the value of W increases with higher load magnitude, higher angular velocity, and greater elbow extension, which confirms the physiological basis of EASOM, thereby providing support for the theoretical foundations of the approach. The performance of EASOM was compared with three of the most often used optimization-based approaches that exist in the literature (linear programming (LP), double linear programming (DLP) and non-linear programming (NLP) formulations). For predicted muscle forces, EASOM yielded consistently reduced average absolute errors in the prediction of the individual muscle forces for both agonist and antagonist muscle groups. When these muscle forces were used to calculate the joint reaction forces, EASOM showed superiority where it produced average absolute percent errors from 21.13% to 25.23%. The other three approaches generated average absolute percent errors ranging from 77.99% to 107.79% for LP, 21.70% to 58.87% for DLP, and 23.71% to 55.91% for NLP. This evidence supports the

EASOM modeling approach in more accurate prediction of muscle forces than LP, DLP and NLP.

EASOM employs neurophysiology to construct a computationally economical optimization model that predicts muscle co-contraction, which leads to more accurate prediction of joint loading. It also helps quantify level of muscle co-contraction relative to different task variables. The current study established a sound protocol and solid foundation that will facilitate the expansion of EASOM to other body segments (e.g. the lumbar region of the torso). Data generated from such models can be used as more accurate guidelines in designing safer work postures that can lower the risks of musculoskeletal disorders.

Application of an Entropy-Assisted Optimization Model in the Prediction of Agonist and Antagonist Muscle Forces

by

Zongliang Jiang

A dissertation submitted to the Graduate Faculty of
North Carolina State University
In partial fulfillment of the
Requirements for the Degree of
Doctor of Philosophy

Industrial Engineering

Raleigh, North Carolina

2007

APPROVED BY:

Simon M. Hsiang, PhD.

David B. Kaber, PhD.

Gary A. Mirka, PhD.
Co-chair of Advisory Committee

Shu-Cherng Fang, PhD.
Co-chair of Advisory Committee

BIOGRAPHY

Zongliang Jiang was born on September 30th, 1980 in Shanghai China, where he spent his childhood and most of his teen years. In August of 1999, he graduated from Shanghai Jiao Tong University (China) with dual Bachelor of Science degree in Engineering Mechanics and Computer Science. To pursue advanced degrees, he came to the United States in August of 2000. After spending one year in the graduate program in Engineering Mechanics at the University of Texas at Austin, he transferred to the graduate program in Computer Science at North Carolina State University, where he received Master of Science degree in August of 2003. In the spring of 2003, he discovered the ergonomics program at NC State and decided to pursue his PhD degree in this fascinating area. After obtaining the admission for Fall 2003, he joined the Ergonomics Laboratory in the Department of Industrial Engineering at NC State, where he has served as a research assistant and teaching assistant.

ACKNOWLEDGEMENTS

I wish to express my deep gratitude to Dr. Gary Mirka, my mentor, who never ceases to show me what it takes to be a top-notch researcher and educator. I want to express my sincere thankfulness to Dr. Shu-Cherng Fang for providing me with the inspiration that I desperately needed throughout this work. Special thanks to Dr. Simon Hsiang and Dr. Dave Kaber whose encouragement and invaluable advice have made this journey so much easier and more enjoyable. Finally, I dearly owe my family, my mom, and friends (Garry Pigg in particular) for their emotional and moral support during the time when I was working on this dissertation.

TABLE OF CONTENTS

LIST OF FIGURES

LIST OF TABLES

1. INTRODUCTION

Musculoskeletal disorders (MSDs) are a major health issue in the US and worldwide. For example, previous studies have shown that about four out of five members of the general population will have activity-altering low back pain sometime in their lifetime (Andersson, 1998; Vonkorff *et al.*, 1988). Further, the economy suffers tens of billions of dollars' loss each year from worker compensation costs due to low back pain (Webster and Snook, 1994). Therefore, the fact that researchers across various academic fields have been continuously striving to understand the mechanisms underlying MSDs is well justified. MSDs can be caused by strains of the musculature, sprains to the ligamentous tissues, compression of nerves and/or problems associated with other passive tissues such as the intervertebral discs of the spine. Disorders associated with injury to the tissues of the joints (e.g. the intervertebral discs) often result in more chronic problems and understanding the loading of these structures has been given focused attention from researchers. This focus is on developing a relationship between joint loading and various kinds of external conditions, such as loads lifted, postures assumed, duration of task and repetitiveness of jobs, etc. Therefore, development of robust biomechanical models that can provide satisfactory estimates on joint loading (compression, shear and torsion) as well as estimates of the forces produced by individual muscles, has often been at the core of such studies.

Early researchers in biomechanics realized it was impossible to solve for joint loading analytically since the force generating components around the joint (numerous muscles, ligaments, discs, etc.) outnumber the mechanical equilibrium equations (three force equations (x,y,z) and three moment equations (x,y,z)) available for an analytical solution. To overcome this challenge, researchers attempted various simplifications of the biomechanical system to

allow for an analytical solution. Some reduced the number of force generating components by grouping those with the same function into one unit (i.e. to decrease the number of unknowns); others increased the number of constraints as to how the system functioned (i.e. increase the number of equations). These approaches generally were found to oversimplify the system to such a degree that the results suffered serious loss of physiological reality. To address these limitations, more advanced models have been developed that have included electromyography (EMG)-assisted models and optimization-based models. EMG-assisted models utilize the well-established relationship between the electrical activity of a muscle and the force that it generates and then use this information to predict joint loading. Such an approach has its roots in basic muscle physiology and represents physiological reality to a greater degree than any other method. It is also sensitive to individual differences between people. However, the data acquisition procedure can be cumbersome and complicated and therefore is not easily applied.

Optimization-based approaches, on the other hand, have no instrumentation requirements, but instead assume that the human body is optimizing the way it performs a physical exertion. A typical result of this optimization approach is that antagonist muscle activity is often not predicted – a result that contradicts the results of empirical studies. Some researchers have introduced joint stability constraints into their optimization models (to force certain levels of antagonist muscle activity for control), but these results do not show general agreement with experimental results.

The model proposed in the current work is an alternative approach to existing optimization techniques, and this new modeling strategy relies on the concept of entropy. The motivation for this model originates from two differing perspectives on the

neurophysiologic aspect of motor control. Reciprocal inhibition of agonist-antagonist muscle pairs has been shown to be an important concept that underlies motor control. This concept states that when an exertion is being performed, the antagonist muscle that acts to oppose the desired action is inhibited. More recent studies have shown that a separate central nervous system function actually produces co-contraction of antagonist muscles. This phenomenon results from the discharge of Renshaw cells that depress the function of the Ia interneurons from agonist muscles that cause inhibition on related antagonist muscles. In the proposed model presented in this work a weighted combination of commands from both systems is suggested, with one activating reciprocal inhibition and one generating antagonist co-contraction. Based on this idea, this study introduces an optimization objective function consisting of the weighted sum of two factors, one favoring agonist contraction (reciprocal inhibition) and one favoring agonist-antagonist co-contraction (entropy).

Based on the literature, there are a number of lifting exertion characteristics (e.g. load magnitude, speed of motion) that may affect the balance between these two central neuronal systems. In the proposed work, experiments will be conducted to reflect various levels for those conditions. The experimental results are to be compared with predicted values from the objective functions with varying combinations of weights. The pair of weights (for both components of the objective function) that generates predicted values closest to the experimental results will be chosen for that specific condition.

The goal of this study is to develop and validate an entropy-assisted optimization modeling technique for the prediction of muscle co-contraction patterns. This study provides a new approach to optimization-based biomechanical modeling, offering a fresh perspective into trunk muscle co-contraction based on underlying neurophysiological principles.

2. BACKGROUND

2.1. Musculoskeletal Disorders (MSDs)

2.1.1. Epidemiology

As reported in Praemer et al. (1999), one out of seven Americans have a MSD that limits or reduces their ability of function at all aspects of daily life. MSDs are a leading cause of work loss, and they cost the US economy over $215 billion per year. Among all kinds of MSDs, back pain accounts for more hospitalizations than any other form of MSD. Among those back pain induced hospitalizations, disc-related back pain accounts for more than half of the incidents. Praemer et al. (1999) reported that back and spine impairments were present in about 6% of US population. Furthermore, back pain affects up to 85% of the population sometime during their lifetime (Andersson, 1998; Praemer et al., 1999). It was estimated that worker compensation costs resulting from work-related back pain were in the tens of billions of dollars annually (Webster and Snook, 1994). The severity of MSDs, especially of back pain, supported by these statistics has driven researchers' focus on searching for the causes. Because back pain has been identified as such an important form of MSD, many of the biomechanical models that have been developed to quantify joint loading have been developed for the low back. Therefore, in the following sections a brief introduction to low back anatomy and mechanisms of low back pain are presented to allow the reader to interpret the specifics of some of the existing biomechanical models that are outlined in subsequent sections.

2.1.2. Anatomy of lumbar region

The anatomy of human lumbar region consists of lumbar vertebra (L1 – L5), joints (or intervertebral discs), soft connective tissues (ligaments, tendons, and fascia), and muscles (Chaffin *et al.*, 2006). Among those components, the intervertebral discs are often considered the most important within the context of chronic low back pain, due to their limited capability of repair/healing. Single intervertebral discs connect and allow motion between adjacent vertebra where each disc bears compression and shear forces (Chaffin et al., 2006).

2.1.3. Mechanisms of back pain

The cause for low back injury is far more complicated than just the excessive external loading. There are many other factors that can jeopardize the integrity of intervertebral discs, such as awkward postures and repetitive exertions (Granata and Marras, 1993). McGill (1998) even stated that most cases of low back injury (muscle tears, herniated discs, etc.) were caused by trauma from cumulative sub-failure magnitude loading (e.g. bending and sitting), particularly at the very end of range of motion. This kind of exertions progressively reduces the tissue failure tolerance. After prolonged strain, ligaments, capsules and intervertebral discs of the lumbar spine start to creep, and may be subject to injury if loading is unexpectedly applied during this vulnerable recovery period (Bogduk and Twomey, 1991). Besides the issue of reduced tissue tolerance, according to Panjabi (1992a), such cumulative trauma can affect proper functioning of motor control system and compromise spinal stability, which can cause serious low back injury in the long run.

2.1.4. Biomechanical models

Due to the nature of MSDs, a better understanding of the relationship between muscle forces / joint loading and external task conditions is considered critical to injury prevention measures. Direct measurement of muscle forces is not practical. Therefore, in order to investigate the mechanisms of MSDs, it is essential to have a robust biomechanical model that can quantify muscle forces and joint loading under various external load conditions. Besides its capability of predicting muscle and joint forces, this type of biomechanical models can also contribute important knowledge to motor control theory and biomedical research. For motor control theory, such biomechanical models provide knowledge of muscle activation strategies during motor tasks that can help explore the functions of central nervous system relative to environmental constraints as well as physiological capabilities of human body. For biomedical research studies, such models are important for understanding mechanical and physiological capabilities of passive and active components of human body, which can contribute to rehabilitation and surgery programs (Tsirakos *et al.*, 1997).

However, even with a simplified anatomical structure, biomechanical models of the lumbar region often face the issue of static indeterminacy where the number of force generating components (muscles, ligaments, discs, etc.) in the system is greater than the number of available equations. This results in an infinite number of feasible solutions. To address this challenge, one has the option of applying an electromyography (EMG) data assisted model (or EMG-assisted model). Such a model is based on the assumption that force generated by the trunk muscles can be estimated based on empirical EMG signals collected from these muscles (McGill and Norman, 1986). The expression of the model is shown below.

$$F_i = \frac{EMG_i(t)}{EMG_{i,\max}} \times f(l_i) \times f(v_i) \times PCSA_i \times gain \qquad (2\text{-}1)$$

where

F_i is the force generated by muscle i;

$EMG_i(t)$ is the EMG measurement of muscle i at that time t;

$EMG_{i,\max}$ is the EMG measurement for muscle i during maximum voluntary isometric contraction (MVIC);

$f(l_i)$ is the force-length factor for muscle i;

$f(v_i)$ is the force-velocity factor for muscle i;

$PCSA_i$ is the physiological cross sectional area of the muscle i;

gain is a constant representing the force generating potential of an individual, and it is the amount of force generated per cross sectional area for all muscles within an individual (in unit N/cm^2).

In addition, the value of *gain* needs to be adjusted so that the torque resulting from EMG generated muscle forces matches the external torque measured during the experiment (Granata and Marras, 1995a). Due to its approximation to physiological reality, results from other models, such as optimization-based models, are often compared with EMG results as a way of model performance evaluation (Hughes *et al.*, 1994). These EMG-assisted biomechanical models represent one approach to estimating muscle forces and joint loading. Optimization-based models represent another approach.

2.2. Optimization-based Models

Unlike EMG-assisted biomechanical models, optimization-based approaches can be applied without complicated instrumentation and data acquisition procedures. Optimization-based models predict muscle exertions by assuming that the central nervous system (CNS) attempts to minimize (or maximize) certain physiological criterion while satisfying a number of constraints such as joint moment equilibrium, muscle stress limits, etc. In an optimization formulation, such a criterion is represented as an objective function.

Research has been undertaken for decades in order to find an objective function that represents physiological reality (i.e. matches empirical EMG responses) while remaining computationally economical. A general form of any objective function can be denoted as $\sum_{i=1}^{n}(\frac{F_i}{C_i})^p$, where F_i is the force generated by muscle i; n is the number of muscles in the system; C_i is a constant associated with muscle i and p is an integer greater than zero. Different combinations of C_i and p result in objective functions with different physiological meanings (Tsirakos et al., 1997). Moreover, the value of p determines whether this optimization is in the form of linear programming (p=1) or nonlinear programming (p>1).

Estimation of joint loading obtained from predicted muscle forces is quite sensitive to choice of objective functions. Hughes et al. (1994) found that the difference in contribution from muscle exertions to spinal compression force prediction between models with different objective functions could be up to 160%. Since direct measurement of muscle forces is impractical, the most often used way to validate those assumptions is to compare the model predicted results with empirical EMG data (Schultz *et al.*, 1982a). Studies have shown that how well an objective function performs is closely related to the characteristic of the task that

is performed, e.g., high load vs. low load (e.g. Schultz et al. (1987, 1983)), static vs. dynamic (e.g. Hughes (1995)), symmetric vs. asymmetric (e.g. Hughes (2000), Hughes and Chaffin (1995)). Besides, accounting for torques generated by ligamentous tissues along with a more realistic anatomical model for the joint region can also contribute to the validity of an optimization model. These issues will be discussed in more detail in the following sections.

2.2.1. Linear programming

For a linear programming (LP)-based biomechanical model, an objective function that is often applied (and minimized) is the sum of muscle forces (i.e. for $\sum_{i=1}^{n}(\frac{F_i}{C_i})^p$, C_i=1 and p=1). This is shown below in a more explicit form.

$$\textit{Minimize} \quad \sum_{i=1}^{n} F_i \tag{2-2}$$

$$\textit{Subject to} \quad \sum_{i=1}^{n}(r_i^k \times F_i) = M_{ext}^k \qquad (k = x, y, z) \tag{2-3}$$

$$0 \le \frac{F_i}{PCSA_i} \le \sigma_0 \qquad (i = 1,\ldots,n) \tag{2-4}$$

where

F_i is the force generated by muscle i;

n is the number of muscles in the model;

r_i^k is the moment arm for muscle i about the k axis through the joint;

M_{ext}^k is the torque generated by external loads and mass of body segments around the k axis through the joint;

$PCSA_i$ is the physiological cross sectional area of muscle *i*;

σ_0 is the upper bound for muscle stress, or muscle stress limit.

It is noted that constraints (2-3) and (2-4) represent, respectively, the joint moment equilibrium condition about all three (*x*, *y* and *z*) axes and muscle stress limit condition (for all *n* muscles). In constraint (2-3), r_i^k is positive if muscle *i* is agonist and negative if muscle *i* is antagonist. The mechanism of this LP approach is such that the model first chooses the muscle with the largest moment arm (r_i^k) and increases its muscle stress ($\frac{F_i}{PCSA_i}$) until either the moment equilibrium (2-3) or the upper limit of muscle stress in (2-4) is reached. If the latter, the model then continues the same process with the muscle with the next largest moment arm. Such a procedure is repeated until the moment equilibrium (2-3) is eventually obtained. In the case of a lumbar model, this objective function would be equivalent to the spinal compression force at a certain lumbar vertebral level (Schultz and Andersson, 1981; Schultz *et al.*, 1982b). Some spine biomechanists have also tried to minimize the spinal shear force which is also a linear form of muscle forces (Gracovetsky *et al.*, 1977).

The drawbacks of such an LP-based model include (1) engagement of muscles with larger moment arms prior to those with smaller moment arms, which is not physiologically realistic most of the times (Bean *et al.*, 1988), and (2) its lack of prediction of co-contraction of antagonist abdominal muscles (Herzog and Binding, 1992). To address the first shortcoming, researchers have tried approaches such as multi-stage linear programming which will be focused on in the following section (Section 2.2.2). The second drawback of the model often results in prediction of unrealistically low spinal compression force

(Cholewicki *et al.*, 1995). Researchers have attempted in various ways in order to overcome the lack of prediction of antagonist muscles, and some of those studies will be discussed in more detail in Section 2.2.5.

2.2.2. Multi-stage linear programming models

When applying an LP-based biomechanical model (e.g., minimization of sum of muscle forces as in formulation (2-2)), the model recruits muscles one at a time in the descending order of their moment arms. That is, only when the stress of the muscle with the largest moment arm has increased and reached its limit, are muscles with the next largest moment arm engaged. This approach has somehow generated unrealistic results (Bean *et al.*, 1988). To address this issue, An et al. (1984) suggested finding the lowest possible muscle stress limit. This way, muscles with larger moments arms would be engaged to a lower level even when the stress limit is reached, and muscles with smaller moment arms would have greater chances of being recruited. This idea became part of a double linear programming (DLP) approach proposed by Schultz et al. (Schultz et al., 1982a; Schultz et al., 1983), which was later reformulated by Bean et al. (1988). It is noted that from now on, DLP will only refer to this reformulated model, which is displayed as follows.

Stage one:

$$\textit{Minimize} \quad \sigma_0 \tag{2-5}$$

$$\textit{Subject to} \ \sum_{i=1}^{n} (r_i^k \times F_i) = M_{ext}^k \quad (k = 1, 2, 3) \tag{2-6}$$

$$0 \le \frac{F_i}{PCSA_i} \le \sigma_0 \quad (i = 1, \ldots, n) \tag{2-7}$$

Stage two:

$$\textit{Minimize} \quad \sum_{i=1}^{n} F_i \tag{2-8}$$

$$\textit{Subject to} \quad \sum_{i=1}^{n} (r_i^k \times F_i) = M_{ext}^k \quad (k = x, y, z) \tag{2-9}$$

$$0 \le \frac{F_i}{PCSA_i} \le \sigma_0^* \quad (i = 1, \ldots, n) \tag{2-10}$$

where

σ_0 is the upper bound for muscle stress, or muscle stress limit;

r_i^k is the moment arm for muscle *i* about the *k* axis through the joint;

F_i is the force generated by muscle *i*;

n is the number of muscles in the model;

M_{ext}^k is the torque generated by external loads and mass of body segments around the *k* axis through the joint;

$PCSA_i$ is the physiological cross sectional area of muscle *i*;

σ_0^* is the minimum value of σ_0 obtained from stage one.

In the DLP-based model, the first stage ((2-5) – (2-7)) of the optimization works to minimize muscle stress limit (σ_0). The minimum value obtained from this stage (i.e. σ_0^*) is then used as the upper bound for muscle stress (as in (2-10)) during the second stage ((2-8) – (2-10)) of the DLP.

The DLP-based model has improved upon an LP-based model in that the DLP-based

model does a better job in balancing force predictions evenly among (agonist) muscles with different moment arms, thus has made one step closer to physiological reality. However, just like an LP-based model, the DLP-based model is unable to predict antagonist muscle exertions. This lack of prediction is especially undesirable during more strenuous tasks, where antagonist muscle contraction is widely evident (Schultz et al., 1987).

Besides the lack of antagonist muscle force prediction, Hughes and Chaffin (1995) found that restricting muscle stress limits resulted in unrealistic predictions of trunk muscle exertions in their studies of physical tasks involving trunk torsion and extension. The specifically compared the DLP-based model with one of the nonlinear programming approaches which will be introduced in the next section. Kee and Chung (1996) investigated the effects of load, lateral and vertical distance of the lifting on peak L5/S1 compression force obtained from the LP, DLP, and EMG-assisted models, during squat lifting. It was found that both LP and DLP predicted peak L5/S1 compression force to occur at the very starting point of the lift, while the EMG-assisted model generated more realistic results showing peak L5/S1 compression force at the end of the lift. Therefore, it was quite obvious that minimizing muscle stress limit was not the golden objective sought by the central nervous system in motor control.

2.2.3. Nonlinear programming (p>1)

When p is greater than 1, the objective term $\sum_{i=1}^{n}(\frac{F_i}{C_i})^p$ becomes a nonlinear function, and the corresponding optimization formulation take the form of nonlinear programming (NLP). The most common examples of an objective function in this category include sum of

cubed muscle stresses (SCS) (i.e., $C_i = PCSA_i$ (or physiologic cross sectional area) and p=3) as well as sum of cubed muscle forces (SCF) (i.e., C_i =1 and p=3) (Brown and Potvin, 2005; Cheng *et al.*, 1998). Taking SCS as an example, with $p > 1$ (compared with $p = 1$), the optimization formulation would impose greater penalties on a muscle with much higher muscle stress than the rest of the muscles, therefore encouraging more balanced level of exertions among (agonist) muscles. This accommodates for muscle endurance (Crowninshield and Brand, 1981) and helps reduce muscle fatigue (Schultz et al., 1983). The formulation of such a model is shown below.

$$\textit{Minimize} \quad \sum_{i=1}^{n} \left(\frac{F_i}{PCSA_i}\right)^3 \text{ (SCS)} \tag{2-11a}$$

$$\textit{or} \quad \sum_{i=1}^{n} (F_i)^3 \text{ (SCF)} \tag{2-11b}$$

$$\textit{Subject to} \quad \sum_{i=1}^{n} (r_i^k \times F_i) = M_{ext}^k \quad (k = x, y, z) \tag{2-12}$$

$$0 \le \frac{F_i}{PCSA_i} \le \sigma_0 \quad (i = 1, \ldots, n) \tag{2-13}$$

where

F_i is the force generated by muscle *i*;

$PCSA_i$ is the physiological cross sectional area of muscle *i*;

n is the number of muscles in the model;

r_i^k is the moment arm for muscle *i* about the *k* axis through the joint;

M_{ext}^k is the torque generated by external loads and mass of body segments around the *k* axis through the joint;

σ_0 is the upper bound for muscle stress, or muscle stress limit.

Unlike the objective functions (i.e. sum of muscle forces) in LP and the second stage of DLP, the objective function of SCS (i.e. sum of cubed muscle stress) is not independent of physiological cross sectional areas of the muscles. Determined by this fact and the mechanism of the SCS formulation, the model therefore will have slight preference in recruiting muscles with larger masses (although the nature of nonlinear programming also reduce this preference to a less degree). This can cause problems when there exists large difference in muscle masses among all muscles in the system such as the lumbar region of the torso. Van Dieen and Kingma (2005) found that overestimation of exertions from large muscles such as internal oblique led to unrealistically high shear force, thus suggested inclusion of a penalty for muscle masses in the objective function. This resulted in the utilization of formulations such as SCF where the objective function is the sum of cubed muscle forces (Brown and Potvin, 2005).

The DLP and SCS (or SCF) are widely applied in spine biomechanical models due to their physiological considerations for optimal muscle endurance and minimal muscle fatigue, resulting in generally more realistic results than an LP-based model. There have been a number of studies comparing DLP with nonlinear programming (NLP), mostly in both static and dynamic loading scenarios.

Hughes et al. found that SCS produced results that were most consistent with EMG data for their experiments on static loading (extension and torsion) with upright standing posture (Hughes et al., 1994). On the contrary, Schultz et al. (1983) showed that DLP generated results with better correlation with EMG measurements than some other objective functions (including SCS) applied alone, for a mixture of isometric exertions (i.e. flexion,

extension, lateral bending, and twisting). However, it is noted that Schultz et al. (1983) selected a wider range of tasks to test than those in Hughes et al. (1994). Stokes and Gardner-Morse (2001) found that when a more realistic anatomical model (e.g. a 180-muscle model in their study) with more degrees of freedom is considered (e.g., intervertebral flexibility, spinal column displacements, etc.), SCS is not as good as some linear criteria (e.g. intervertebral forces) in predicting muscle forces during isometric loading conditions. In agreement, Brown and Potvin (2005) applided a 52-muscle model and found that DLP generated more accurate prediction of spinal compression forces than SCF during sagittal static loading with upright standing posture. It is noted that both studies accounted for torque generated by ligamentous tissues (Brown and Potvin, 2005; Stokes and Gardner-Morse, 2001).

Besides studies on static tasks, Hughes (2000) investigated asymmetric dynamic lifting tasks where the author compared the spinal compression and shear forces predicted from SCS and the DLP. A trunk musculature model with five bilateral muscles (erector spinae, latissimus dorsi, rectus abdominis, external oblique, and internal oblique) was applied. The results showed agreement between these two models, which contrasts the finding that DLP generated substantially higher compression force than SCS as shown in Hughes (1995). The author attributed this to the fact that the tasks performed in Hughes (2000) were predominantly extensions instead of lateral and axial rotations as in Hughes (1995).

Like LP and DLP, NLP-based models are still unable to predict realistic levels of antagonist muscle forces. However, some recent studies have attempted to address this issue. Some of these approaches are described in the following sections.

2.2.4. Optimization-based models involving stability

A major limitation of the previously introduced optimization-based models is the absence of prediction of antagonist trunk muscle co-contraction (Brown and Potvin, 2005; Stokes and Gardner-Morse, 2001). Such co-contraction is widely observed in static (Lavender *et al.*, 1992; Marras and Granata, 1997) and dynamic (Granata and Marras, 1995b; McGill, 1991, 1992) loading conditions. More specifically, Granata and Marras (1995b) found that antagonist trunk muscle co-contraction can account for up to 45% of total spinal compression load. Agonist and antagonist muscle co-contraction results in greater joint stiffness and ultimately higher joint stability, compared with agonist muscle only contraction under the same condition (Bergmark, 1989; Cholewicki *et al.*, 1997; Gardner-Morse and Stokes, 1998; Granata and Orishimo, 2001; Panjabi, 1992b). It is noted that with increased stability, the critical spinal load (i.e. maximum spinal load allowed against buckling) increases. Although higher level of co-contraction leads to larger spinal loading, the margin between the applied and the critical spinal load grows wider with increased cocontraction, meaning reduced risk of injuries (Granata and Marras, 2000).

Although physiologically muscle co-contraction is the cause for improved joint stability, some researchers tried to apply this principle backwards and use it in an optimization-based biomechanical model. They introduce spinal stability into an optimization formulation in order to enforce prediction of antagonist trunk muscle co-contraction. It should be noted that in those studies, second-order partial derivatives of system potential energy with regard to each degree of freedom were used to quantify the system stability level (Brown and Potvin, 2005; Stokes and Gardner-Morse, 2001). Following such an approach, Stokes and Gardner-Morse (2001) introduced spinal stability

into the objective function to investigate isometric loading conditions (applied from anterior to towards posterior with 45-degree intervals) in standing posture. The following is a simplified version of the model formulation, where the objective function (2-14) combines stability with SCS (sum of cubed muscle stresses).

$$\textit{Minimize} \quad -S \tag{2-14a}$$

$$\textit{or} \quad \sum_{i=1}^{n}\left(\frac{F_i}{PCSA_i}\right)^3 - S \tag{2-14b}$$

$$\textit{Subject to} \quad \sum_{i=1}^{n}(r_i^k \times F_i) = M_{ext}^k \quad (k = x, y, z) \tag{2-15}$$

$$0 \le \frac{F_i}{PCSA_i} \le \sigma_0 \quad (i = 1,\ldots,n) \tag{2-16}$$

$$\textit{Minimum stability requirement (void of buckling)} \tag{2-17}$$

where

S is the stability level and is a function of muscle forces and other known anatomical measures, and note that minimizing $(-S)$ is equivalent to maximizing S;

F_i is the force generated by muscle *i*;

$PCSA_i$ is the physiological cross sectional area of muscle *i*;

n is the number of muscles in the model;

r_i^k is the moment arm for muscle *i* about the *k* axis through the joint;

M_{ext}^k is the torque generated by external loads and mass of body segments around the *k* axis through the joint;

σ_0 is the upper bound for muscle stress, or muscle stress limit.

It was found that when spinal stability alone is maximized (2-14a), the model generated unrealistically high intervertebral displacements and high antagonist muscle exertions which in turn produced high spinal compression forces. When stability is applied in conjunction with SCS (2-14b), the results showed unrealistic trunk muscle recruitment patterns where muscle activity level decreased as load level increased. Stokes and Gardner-Morse (2001) concluded that maximizing spinal stability should not be the goal of central nervous system. Apparently, there is a tradeoff between spinal stability and spinal compression force (Granata and Marras, 2000).

Brown and Potvin (2005) hypothesized that there exists an optimal level for spinal stability that allows for a compromise between spinal stability and loading. In their study, with empirical EMG data collected and an 52-muscle fascicle anatomical model, the actual stability levels under all task conditions for all subjects were first calculated as a function of muscle forces, muscle moment arms, muscle lengths, body weight above joint (L4/L5), height of center of body mass above joint (L4/L5), external force, and height of external force about joint (L4/L5). With these data, they were able to establish regression equations relating the stability level to factors including external moment, subject height, body mass, external load height, external load mass, and the combined potential energy resulting from the external load and upper body mass. This way, the spinal stability level could be predicted from these easy to obtain measures. In their optimization model, actual spinal stability under each task condition was constrained to the predicted value. The formulation is shown below.

$$\textit{Minimize} \quad \sum_{i=1}^{n} (F_i)^3 \tag{2-18}$$

$$\textit{Subject to} \quad \sum_{i=1}^{n} (r_i^k \times F_i) = M_{ext}^k \qquad (k = x, y, z) \tag{2-19}$$

$$0 \le \frac{F_i}{PCSA_i} \le \sigma_0 \quad (i = 1, \ldots, n) \tag{2-20}$$

$$S_{act}^k = S_{pred}^k \quad (k = x, y, z) \tag{2-21}$$

where

F_i is the force generated by muscle *i*;

n is the number of muscles in the model;

r_i^k is the moment arm for muscle *i* about the *k* axis through the joint;

M_{ext}^k is the torque generated by external loads and mass of body mass above L4/L5 around the *k* axis through the joint;

$PCSA_i$ is the physiological cross sectional area of muscle *i*;

σ_0 is the upper bound for muscle stress, or muscle stress limit.

S_{act}^k is the actual stability level around *k* axis;

$S_{act}^k = S_{pred}^k$ is the predicted stability level around *k* axis.

It is noted that the objective function (2-18) in the above optimization formulation is the same as SCF (sum of cubed forces). The results from Brown and Potvin (2005) showed more realistic predictions of both antagonist muscle exertions and spinal compression forces than without stability constraints (i.e. SCF), in both sagittal and lateral static loading conditions (during upright standing postures). However, stability levels for each subject under different loading conditions were set according to a regression model generated based on the data collected from the same pool of subjects. These factors limit, to a great extent, the generalizability of the model validation results from this study. The authors also

admitted that some muscles that could potentially stabilize the spine were not modeled in the study, which reveals the complexity of use of stability as a component in optimization models.

Applying stability in an optimization model usually requires a detailed anatomical model representing the spine region (e.g., 180 muscles in Stokes and Gardner-Morse (2001); 52 muscles in Brown and Potvin (2005)). Solving optimization problems of such dimension can have rather high computational cost. Therefore, applying spinal stability in a optimization-based biomechanical model can be formidable.

2.2.5. Other approaches to enforce antagonist co-contraction

Besides direct involvement of stability in optimization formulations, the literature review shows numerous other attempts in enforcing antagonist muscle exertions in predicted results. Raikova (1999) suggested applying weight factors of different signs to agonist and antagonist muscles in the objective function.

$$\textit{Minimize} \quad \sum_{i=1}^{n} \frac{F_i}{C_i} \tag{2-22}$$

$$\textit{Subject to} \quad \sum_{i=1}^{n} (r_i^k \times F_i) = M_{ext}^k \quad (k = x, y, z) \tag{2-23}$$

$$0 \le \frac{F_i}{PCSA_i} \le \sigma_0 \quad (i = 1, \ldots, n) \tag{2-24}$$

where

F_i is the force generated by muscle *i*;

C_i is the weight factor associated with muscle *i*, and it is positive if muscle *i* is agonist and

negative if muscle i is antagonist;

n is the number of muscles in the model;

r_i^k is the moment arm for muscle i about the k axis through the joint;

M_{ext}^k is the torque generated by external loads and mass of body segments around the k axis through the joint;

$PCSA_i$ is the physiological cross sectional area of muscle i;

σ_0 is the upper bound for muscle stress, or muscle stress limit.

No empirical data were collected for model validation or characterization of the weight factors in Raikova (1999), and the physiological interpretation of such an approach remains unclear.

In another attempt, Forster et al. introduced a so-called shift parameter x_s into the objective function to enforce the prediction for antagonist muscle exertions (Forster *et al.*, 2004). The model is shown more explicitly as follows.

$$\textit{Minimize} \quad \sum_{i=1}^{n} \left(\frac{F_i}{F_{\max,i}} - x_s\right)^2 \tag{2-25}$$

$$\textit{Subject to} \quad \sum_{i=1}^{n} (r_i^k \times F_i) = M_{ext}^k \quad (k = x, y, z) \tag{2-26}$$

$$0 \le \frac{F_i}{F_{\max,i}} \le 1 \qquad (i = 1, \ldots, n) \tag{2-27}$$

where

F_i is the force generated by muscle i;

$F_{\max,i}$ is the maximum force allowed for muscle i;

n is the number of muscles in the model;

x_s is the "shift parameter" which is a constant across all muscles with value between 0 and 1;

r_i^k is the moment arm for muscle i about the k axis through the joint;

M_{ext}^k is the torque generated by external loads and mass of body segments around the k axis through the joint.

It should be noted that Forster et al. (2004) did not collect any empirical data to compare with model predictions. Therefore, they only theoretically demonstrated how their model worked relative to varying x_s values, without being able to quantify x_s with regard to internal (physiological) or external (loading) characteristics. Forster et al. (2004) claimed that the shift parameter x_s represented level of stability since the larger the value of x_s, the higher the antagonist muscle exertions, which leads to greater joint stiffness. However, this claim lacks strength and physiological basis until the researchers have validated the model with empirical data and studied the mechanism behind x_s in greater depth.

Due to the rather questionable results and computational complexity from applying spinal stability in optimization (Brown and Potvin, 2005; Stokes and Gardner-Morse, 2001), and lack of physiological meaning behind various antagonist exertion enforcing optimization approaches (Forster et al., 2004; Raikova, 1999), an economical optimization-based model that enforces co-contraction of antagonist trunk muscles and bears physiological meaning is necessary.

2.3. Physiology of Muscle Contraction

2.3.1. Basics of motor control

Motor control is the study of posture and movements controlled by central (cortex) commands and spinal reflexes (Brooks, 1986). Basically the brain and the spinal cord constitute the central nervous system (CNS). Figure 1 shows the feed-forward process of the CNS and its output in the form of muscle exertions. The cortex part of the CNS consists of three components (Figure 1): the limbic cortex generates the demand (e.g., desire for drink due to thirst); the association cortex answers the demand with what to do (e.g., to reaching for and pick up the water glass on the table); the projection cortex comes up with how to do it (e.g., direction, trajectory, speed, and stiffness of the dominant arm). The latter two components (association and projection cortex) form motor plans, and by convention, are usually called the highest and middle command levels of the CNS, respectively. The efficiency and effectiveness of a motor plan is highly related to motor skills (or motor programs) that are developed through previous successful performances and used as guidelines for generating motor plans. The spinal cord (as bounded by the broken line in Figure 1, usually called the lowest command level in CNS) is the interface between the brain and muscles. It executes commands from higher levels (or central commands), and corrects (through stretch reflex) deviations from motor plans using reflex activities to ensure success of the plan.

It is noted that some sensorimotor feedback routes (e.g., visual, audio, etc.) are not shown in Figure 1 for simplicity. This does not mean such feedbacks are not important. On the contrary, sometimes such sensorimotor feedbacks call for deviations from original motor plans, which causes the spinal cord to make effort to correct the movement (Brooks, 1986).

Since the spinal cord bears a great amount of relevance to the current study (as will be explained later), the spinal cord along with the muscle component will be the main focus in the following literature review.

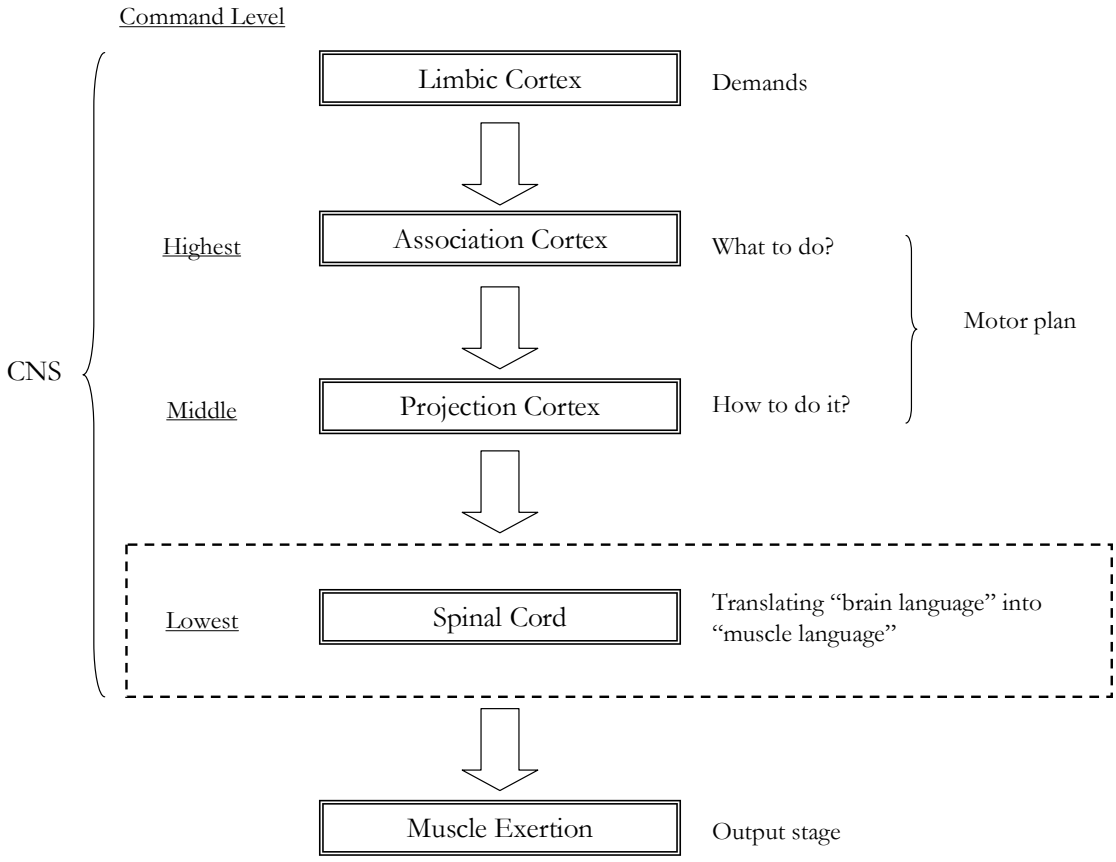

Figure 1 Schematic drawing of the feed-forward process of the CNS. Feedback route is omitted from the diagram for simplicity. (Modified from Fig. 2.4 in Brooks, 1986)

2.3.1.1.Motoneurons and interneurons

Motoneurons (MNs) and interneurons (INs) are the two main components in the spinal cord that take part in motor control activities. They are the ones that play the role of translating "brain language" into "muscle language" (Figure 1). MNs are neurons that activate

and cause contractions in muscles (Enoka, 1994). The two main types of MNs are the alpha MNs and the gamma MNs. INs are neurons that only have connections with other neurons (Enoka, 1994). The major types of INs are of inhibitory nature: Ia IN and Renshaw cells (Brooks, 1986). The function of the two types of MN and the Ia IN will be explained in Section 2.3.1.3. Renshaw cells will be discussed in more detail in Section 2.3.3.

2.3.1.2.Muscles

All muscles consist of two functionally distinct components critical to motor control: muscle fibers and muscle receptors. Muscle fibers when contracted produce muscle exertions, while muscle receptors take on the role of sensing muscle lengths (and length change) or tensions. The two main types of muscle receptors are muscle spindles and Golgi tendon organs (GTOs or tendon organs). Muscle spindles lie in parallel to muscle fibers and are able to sense length and change of length of the muscle fiber in which they are embedded (Figure 2). Golgi tendon organs are located in the tendon at the end of muscle and serve as sensors for muscle tension (Figure 2) (Brooks, 1986; Enoka, 1994).

2.3.1.3.Interaction between neurons and muscles

The neurons that are discussed in this section include alpha MNs, gamma MNs, and Ia INs. For muscles, we are interested in muscle fibers and muscle receptors. Alpha MNs send out signals to muscle fibers and generate active muscle contractions (route 1 in Figures 2 and 3). Gamma MNs adjust the activation of muscle spindles so that the latter maintain the proper sensitivity in sensing muscle length and the rate of length change (route 2 in Figures 2 and 3) (Brooks, 1986; Enoka, 1994). On the other hand, muscle receptors play the role of

sending peripheral feedback to neurons. Properly activated muscle spindles provide facilitation (excitation) to alpha MNs and Ia INs (through Ia axon fibers) (route 3 in Figures 2 and 3). Subsequently, excited Ia INs yield inhibition to the alpha MN of the antagonist muscle (route 5 in Figure 2). Another muscle receptor, Golgi tendon organs sense muscle contraction and inhibit alpha MNs as needed to prevent overexertion (route 4 in Figures 2 and 3). This principle forms the basis of reciprocal inhibition theory and will be discussed in more detail in Section 2.3.2.

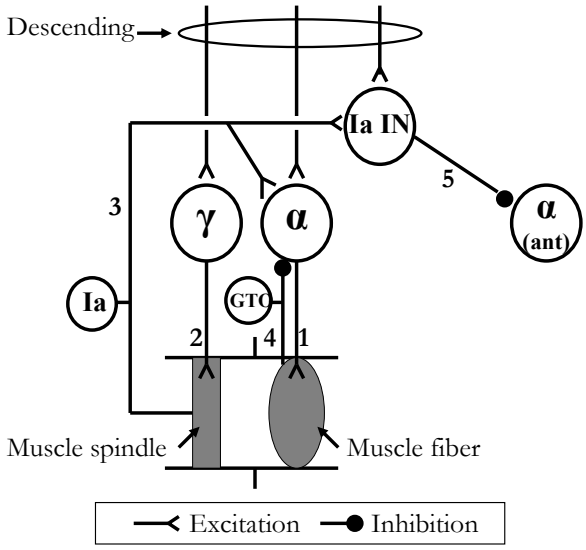

Figure 2 Connections (synapses) between major neurons (minus Renshaw cells) in the spinal cord and muscle components (muscle fiber and muscle spindle). (α – alpha MN; γ – gamma MN; Ia – Ia axon fiber; Ia IN – Ia interneuron; R: Renshaw cell, GTO: Golgi tendon orgon; α(ant): alpha MN for the antagonist muscle) (Modified from Loeb (1984) and Hultborn et al. (1976))

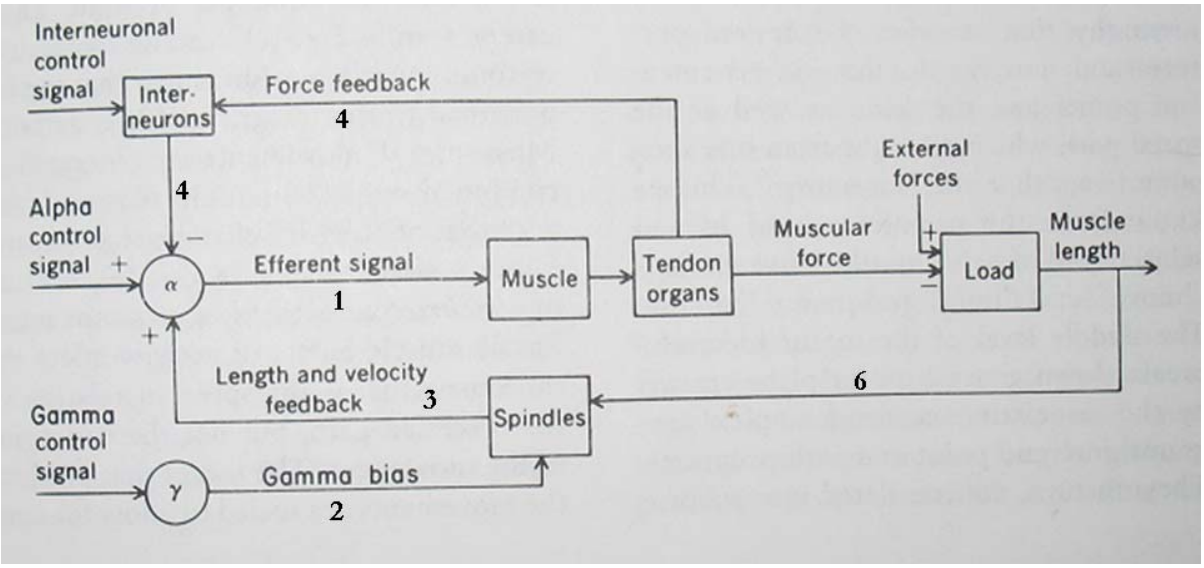

Figure 3 Schematic diagram of interaction between spinal cord and muscle upon withstanding external forces. (Ia afferent from spindles to Ia IN is not shown in this figure.) (Modifed from Houk (1974) in Brooks (1986))

2.3.1.4.Response of spinal-cord-muscle system to higher commands (motor plans)

Motor plans are executed in spinal cord by conversion of the plans into instructions directed to the alpha and gamma MNs and Ia IN (as well as Renshaw cells as will be discussed later). This is combined with peripheral feedbacks generated by muscle receptors (muscle spindles and Golgi tendon organs) intended to make any necessary corrections (routes 3 and 4 in Figures 2 and 3, and route 6 in Figure 3).

2.3.2. Reciprocal inhibition (driven by Ia INs)

During a voluntary movement, agonist muscles (e.g. biceps brachii during elbow flexion, or erector spinae during trunk extension) contribute to such a motion while antagonist muscles (e.g. triceps brachii during elbow flexion, or rectus abdominis during

trunk extension) resist the same motion. Although co-contraction of agonist and antagonist muscles occurs under a wide range of circumstances (Enoka, 1994), there have been debates in the area of neurophysiology on whether such co-contraction really exists for over a century.

Near the end of the 19th century, two French neurophysiologists, Beaunis (1889) and Demeny (1890), concluded independently that antagonist muscles co-contract to some extent in most movements. Unfortunately, their work very soon was overshadowed by Sherrington's influential groundwork for the theory of reciprocal inhibition, in which he showed the relaxation of antagonist muscles during activation of their agonist counterparts (Sherrington, 1909). Such a phenomenon occurs because agonist muscle contraction activates agonist Ia interneurons (Ia INs) which inhibit antagonist alpha MNs, which in turn inhibit antagonist muscle contraction (Figure 2). Such logic underlies the principle of reciprocal inhibition which claims this phenomenon to be the only law that rules motor control. According to Smith (1981), Sherrington's influence was so powerful that reciprocal inhibition had been considered the only reflex model underlying voluntary movements, and the theory had kept many researchers away from investigating co-contraction of antagonist muscles for decades. It is interesting, however, to note that Tilney and Pike (1925) recognized the existence of antagonist co-contraction and suggested that the cerebellum plays an important role in activating such co-contraction. Unfortunately, their hypothesis was given little attention until almost a half century later, when it gained support from experimental results. Terzuolo et al. (1973a, 1973b) conducted experiments on monkeys and Hallett et al. (1975) worked with humans. Both of their work showed that lesions in the cerebellum disturb and diminish the agonist-antagonist reciprocity (Deluca and Mambrito, 1987).

For the past several decades, more attention has been given to the investigation of muscle co-contraction (Nielsen, 1998), which will be discussed in more detail in the following sections.

2.3.3. Physiology of muscle co-contraction (Renshaw cells)

Agonist and antagonist muscles co-contract to increase joint stiffness and stabilize moving or posture holding body segments (Enoka, 1994; Humphrey and Reed, 1983). A great number of empirical studies have shown that such phenomena are widely evident in static (Lavender et al., 1992; Marras and Granata, 1997) and dynamic (Granata and Marras, 1995b; McGill, 1991, 1992) conditions. More specifically, antagonist trunk muscle co-contraction was found to increase during dynamic, asymmetric (Marras and Mirka, 1990, 1992), lateral (Marras and Granata, 1997), and twisting (Marras and Granata, 1995) exertions. It is noted that antagonist trunk muscles refer to those trunk muscles that make no contributions to the moment required to balance any external loading present in the task.

A major mechanism that was found to promote agonist-antagonist co-contraction is the discharging of Renshaw cells. Renshaw cells are inhibitory interneurons located in the spinal cord horn and driven in part by motoneurons. As stated in Hultborn et al. (1979), muscle force, as the output of the motoneuronal system, can be approximated as the product of number of recruited motoneurons and firing frequency. The regulation of Renshaw cells determines the input-output relation (or gain) of this motoneuronal system (Figure 4). Inhibition of Renshaw cells results in a larger gain which usually corresponds with strong and crude movements, while facilitation of Renshaw cells leads to smaller gain which is present during weak and finely tuned movements. Hultborn et al. (1971) showed evidence

supporting that excitation of Renshaw cells can depress inhibitory Ia INs and thus facilitate antagonist muscle co-contractions.

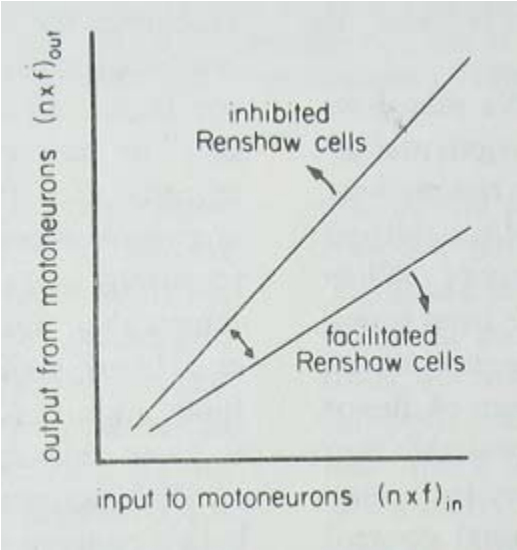

Figure 4 Relationship between input and output of MNs affected by facilitation or inhibition of Renshaw cells. (From Hultborn et al. (1979))

Nielsen (1998) suggested that the human brain selectively activates Renshaw cells during co-contractions. According to Brooks (1986), forces exerted by agonist and antagonist muscles, during practically all movements, are planned before the onset of the movement. Therefore, skilled motor programs must contain information on the degree of either facilitation or inhibition on Renshaw cells, with such facilitation promoting co-contraction and such inhibition yielding reciprocal inhibition (Figure 5). Therefore, Renshaw cells can be viewed as the switch utilized by higher command levels to adjust the level of agonist and antagonist co-contractions.

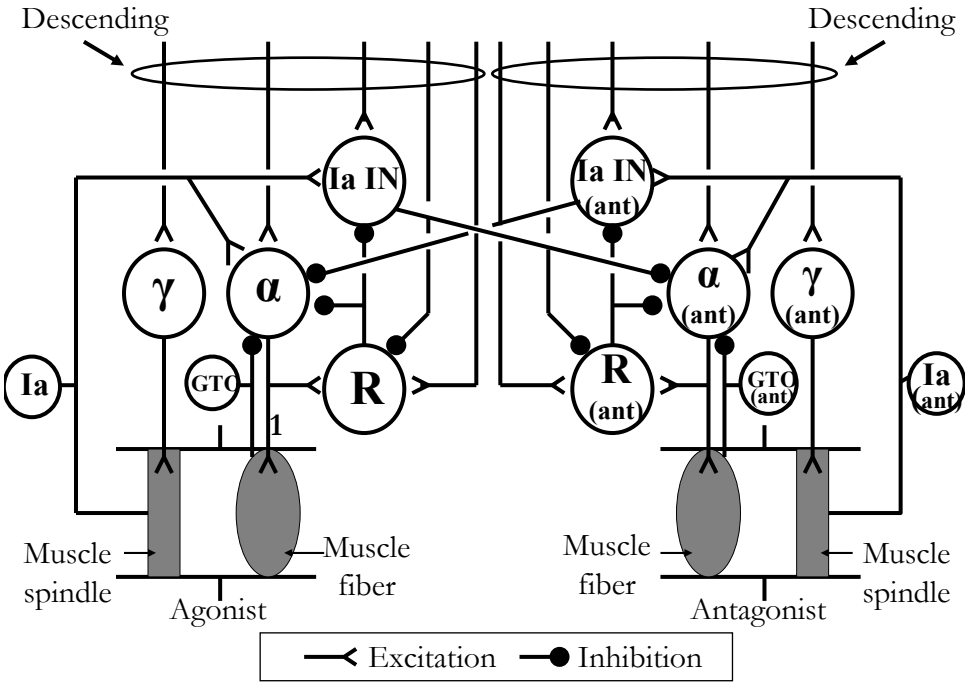

Figure 5 Diagram of descending (central command) paths to alpha and gamma MNs, Ia IN, and Renshaw cells of a pair of agonist and antagonist muscles. (α: alpha MN, γ: gamma MN, Ia: Ia fiber, R: Renshaw cell) (Modified from (Hultborn et al., 1976; Hultborn et al., 1979))

The literature review finds that the relationship between activation of Renshaw cells and external kinematics remains unclear to researchers (Nielsen, 1998). However, there are a few task related factors that may affect the level of co-contraction, such as load magnitude, velocity (rate of muscle length change), joint angle, and skill level. Higher load magnitude corresponds to increased tension in agonist muscles. This is detected by Golgi tendon organs, which function to inhibit the alpha MNs and subsequently tone down the increasing of agonist muscle exertions. It was found that heavy loads raise exertions from antagonist muscles (Schultz et al., 1987), and therefore may help bring the exertions of most muscles in the system closer to each other. However, the trend in the difference between the torque generated by agonist muscles and the torque generated by antagonist muscles is unclear.

Velocity corresponds to the rate of length change of all muscles crossing the joint, while joint angle corresponds to lengths of all such muscles. Both measures are sensed by the muscles spindles embedded in those muscles. Empirical evidence shows increased joint velocity produces higher level of co-contraction (Suzuki *et al.*, 2001). Joint angle may also affect the level of co-contraction, in that an extended elbow can produce a less stable posture around the elbow (Milner, 2002) which will result in higher level of co-contraction. Less skilled movements evoke greater co-contraction than well learned ones (Brooks, 1986). In the case of arm movement, the dominant arm of an individual usually has practiced a wide variety of movements more often than the nondominant arm has. Therefore, when acting out the same movement, the nondominant arm normally engages a higher level of co-contraction than the dominant arm does.

2.3.4. Equilibrium Point Hypothesis (the λ Model)

The Equilibrium Point Hypothesis (EPH) is a motor control theory that was developed and advocated by the group of researchers led by Feldman (1993). The idea of the EPH theory can be demonstrated with a pair of curves in a coordinate system where the abscissa (x-axis) represents joint angle (e.g. elbow extension angle with 0° meaning full flexion) and the ordinate (y-axis) represents torque (Figure 6). Note that the curve in the upper half of the coordinate represents the torque-angle relationship for flexors, and the curve in the lower half represents the torque-angle relationship for extensors. The x-intercepts for the two curves, denoted as λ_f and λ_e for flexors and extensors respectively, are named the threshold angles for recruitment of the flexors and extensors. This means that flexors get

activated when joint (extension) angle is greater than λ_f, and extensors become activated when joint (extension) angle is smaller than λ_e.

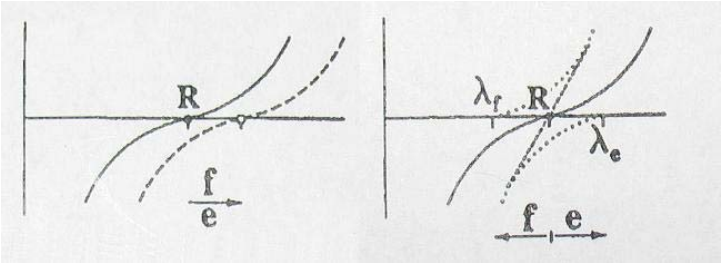

Figure 6 A scenario in Equilibrium Point Hypothesis where the external torque is zero and R is the equilibrium point (abscissa – joint (extension) angle; ordinate – torque). Left coordinate demonstrates reciprocal inhibition command and right coordinate shows co-contraction command. Solid curves are used to represent curves before shifting, and dashed curves after shifting (f – flexors; e – extensors). λ_f and λ_e are the threshold angles for recruitment of the flexors and extensors (from Feldman (1993))

The equilibrium point (EP) is the point on the abscissa (angle) where the torque generated by muscle forces (i.e. the sum of the torques from both curves corresponding to this point) matches the external torque. Therefore, EP represents the real-time joint angle. Figure 6 in fact shows a scenario where there is no external torque, and thus R is the EP. The essential idea of EPH is that the reciprocal inhibition command shifts both curves (and EP subsequently) in the same direction at the same pace along abscissa (left coordinate in Figure 6), and the co-contraction command shifts the two curves in the opposite direction without shifting the EP (right coordinate in Figure 6). Therefore, only the reciprocal inhibition command is responsible for producing voluntary movement, while the co-contraction command increases net joint stiffness and never initiates movement (Feldman, 1993). EPH owes its root to neurophysiology, and works well with the phenomenon of agonist and

antagonist co-contraction. The theory provides a basis for the model of weighted central commands to be discussed in the next section.

2.3.5. Separation of reciprocal inhibition and co-contraction commands

Recently, a number of researchers discovered evidence to support the existence of an independent neuronal system that generates antagonist co-contraction. Humphrey and Reed (1983) found evidence to suggest the existence of two separate central nervous systems for the generation of the two major patterns of agonist-antagonist activities: reciprocal inhibition and co-contraction. These two systems send out signals that converge onto common elements at the level of the motoneuron pool (Deluca and Mambrito, 1987). Based on the Equilibrium Point Hypothesis (EPH) theory, Feldman (1993) proposed a model of weighted combination of independent reciprocal inhibition and co-contraction commands.

As will be discussed in Chapter 3, a close analogy can be made between Feldman's model and the optimization-based model proposed by this dissertation. Therefore, the model developed by Feldman (1993) serves as the conceptual basis for the proposed model in the current study.

2.4. Entropy

Since its birth, entropy as a scientific measure has been applied to the areas of classical thermodynamics, statistical thermodynamics, and information theory, with distinct but related definitions. Entropy originated from thermodynamics in 1860s, introduced by thermodynamicist Rudolf Clausius, used to measure the amount of energy in a thermodynamic system relative to the temperature and the heat that enters (or exits) the

system (Perrot, 1998). In this sense, entropy denoted by S, is quantitatively defined by the following differential quantity:

$$dS = \delta Q / T \tag{2-28}$$

where dS is the change in entropy, δQ is the amount of heat absorbed in a reversible process wherein the system goes from one state to another, and T is the absolute temperature (Perrot, 1998). Therefore, the SI unit of entropy under this definition is joule per kelvin ($J \bullet K^{-1}$).

In the 1870s, Ludwig Boltzmann developed the statistical definition of entropy to be applied in statistical thermodynamics. Under this definition, entropy describes the number of possible microscopic configurations of a thermodynamic system. This is shown as follows:

$$S = k_B \ln \Omega \tag{2-29}$$

where Ω is the number of microscopic configurations, and k_B is the Boltzmann's constant which has the same unit as the entropy in classical thermodynamics ($J \bullet K^{-1}$). This constant bears the relation between temperature and energy. The above quantitative definition can also be expressed as:

$$S = -k_B \sum_i p_i \ln p_i \tag{2-30}$$

where k_B is the Boltzmann's constant, and p_i is the probability of the system staying in the i-th microstate during the fluctuations of the system. The statistical definition of entropy introduced the idea of amount of uncertainty to the meaning of entropy, which leads to other important properties of entropy as well as adaptation of entropy in other fields including information theory.

In late 1940s, information theorist Claude Shannon, who was working at Bell Laboratories at that time, took a suggestion from his colleague at Princeton, John Von

Neumann, and extended the use of the term "entropy" to the field of information theory. John von Neumann said to Claude Shannon in a milestone setting conversation, "Nobody knows what entropy really is, so in a debate you will always have the advantage" (Tribus and McIrvine, 1971). Having that in mind, Shannon removed the Boltzmann's constant from the entropy definition in statistical thermodynamics, and defined the information entropy (or Shannon's entropy) as a "measure of uncertainty" and a unitless quantity as follows:

$$E = -\sum_i p_i \log p_i \tag{2-31}$$

$$= \sum_i p_i \log \frac{1}{p_i} \qquad (i = 1,2,...,n) \tag{2-32}$$

where p_i is the probability of a discrete random variable having the *i*-th outcome, and n is the number of total outcomes. Therefore, $\sum_{i=1}^{n} p_i = 1$. The greater the uncertainty of the system, the greater the uniformity of p_i's, the greater the value of *E* (Guisau, 1977; Kapur and Kesavav, 1992; Fang *et al.*, 1997;). That is *E* is maximized when $p_1 = p_2 = ... = p_n = \frac{1}{n}$, where any state is equally likely. Vice versa.

The entropy applied in the current study takes the form of the information entropy, i.e. $-\sum_i p_i \log p_i$, although it has a less strict definition (e.g. $\sum_{i=1}^{n} p_i \neq 1$). Thus, the name "pseudo entropy" would better suit this term. However, for simplicity purposes, the one-word term "entropy" will be the used for the rest of this research. A detailed description of the entropy used in the current study will be illustrated in the next chapter.

3. PROPOSED ENTROPY-ASSISTED OPTIMIZATION MODEL (EASOM)

The shortcomings of current optimization methods for modeling muscle coactivation strategies and their underlying neurophysiology call for new approaches in optimization models that will not only generate accurate predictions of antagonist muscle exertions but also bear strong physiological meaning. As was illustrated in the Section 2.4, entropy as a scientific measure has wide applications in many fields due to its flexible definition. It is realized that when formulated properly, entropy can be introduced into the objective function of an optimization model where it takes on the role of the co-contraction command that was outlined in neurophysiology literature (Feldman, 1993). As a result, such a model will be able to predict antagonist muscle contractions and have physiological meaning. The formulation of *co-contraction entropy* applied in the current dissertation is described as $-\sum_{i=1}^{n}\frac{x_i}{\sigma_0}\log\frac{x_i}{\sigma_0}$ ($i=1,2,...,n$), where n is the number of muscles in the system, x_i is the muscle stress of muscle i, σ_0 is the muscle stress limit. It is noted that $\frac{x_i}{\sigma_0}$ represents the utilization of muscle i, and its value is between 0 and 1. Therefore, according to the property of information entropy, the larger the value of $-\sum_{i=1}^{n}\frac{x_i}{\sigma_0}\log\frac{x_i}{\sigma_0}$, the more uniform muscle stresses are, in other words there is a higher degree of co-contraction. Maximizing co-contraction then would be equivalent to maximizing $-\sum_{i=1}^{n}\frac{x_i}{\sigma_0}\log\frac{x_i}{\sigma_0}$ or minimizing $\sum_{i=1}^{n}\frac{x_i}{\sigma_0}\log\frac{x_i}{\sigma_0}$.

Based on the concept of Feldman's weighted central command model (1993), we

apply an optimization model where the objective function is a weighted combination of two functions that represent the two central neuronal systems. The first function is a classical objective function $\sum_{i=1}^{n}(\frac{F_i}{C_i})^p$ which induces reciprocal inhibition (agonist muscle only contraction), and the second one is the co-contraction entropy $-\sum_{i=1}^{n}\frac{x_i}{\sigma_0}\log\frac{x_i}{\sigma_0}$ which encourages agonist and antagonist muscle co-contraction. A general formulation of this optimization model is as follows.

$$\textit{Minimize}\quad (1-W)\sum_{i=1}^{n}(\frac{x_i * PCSA_i}{C_i})^p + W\sum_{i=1}^{n}\frac{x_i}{\sigma_0}\log\frac{x_i}{\sigma_0} \qquad (3\text{-}1)$$

$$\textit{Subject to}\ \sum_{i=1}^{n}(r_i^k \times F_i) = M_{ext}^k \quad (k = x, y, z) \qquad \text{(Joint moment equilibrium)} \qquad (3\text{-}2)$$

$$0 \le x_i \le \sigma_0 \quad (i = 1,\ldots,n) \qquad \text{(Muscle stress limit)} \qquad (3\text{-}3)$$

where

W is called the *co-contraction weight factor*;

n is the number of muscles in the model;

x_i is the muscle stress of muscle i;

$PCSA_i$ is the physiological cross sectional area of muscle i;

F_i is the force generated by muscle i (note that $F_i = x_i * PCSA_i$);

C_i is a constant associated with muscle i;

p is a positive integer and, along with C_i determine the physiological meaning of the first term in the objective function (i.e. $\sum_{i=1}^{n}(\frac{x_i * PCSA_i}{C_i})^p$);

σ_0 is the upper bound for muscle stress, or muscle stress limit;

r_i^k is the moment arm for muscle *i* about the *k* axis through the joint;

M_{ext}^k is the torque generated by external loads and mass of body segments around the *k* axis through the joint.

The use of the co-contraction weight factor W will enable us to quantify the level of muscle co-contraction relative to different task variables and help better understand the relationship between reciprocal inhibition and co-contraction.

4. PILOT STUDY

4.1. Subject

One right-handed subject with no history of upper extremity injury was recruited for the pilot study.

4.2. Apparatus

4.2.1. Experimental task

A set of dumbbells of different weights (10, 20, 30 and 40 lbs) were used as handheld loads during isometric and isokinetic trials. The Kin-Com 125e Dynamometer (Chattecx Corporation, TN) was utilized in the current pilot study to control forearm movement. The dynamometer allowed for isometric (static) mode, which provided static resistance during maximum voluntary isometric contractions (MVICs) (Figure 7) as well as angular guidance during isometric trials. The Kin-Com Dynamometer was also able to run passively with constant angular velocity within a preset range of angle, therefore providing guidance to the subject during isokinetic trials (Figure 8). The system comes with graphical visual feedback on the real-time level of torque exertion.

4.2.2. Data collection

Eight pairs of surface Ag-AgCl electrodes (Model E22x, In-Vivo Metric) and the Myopac system (RUN Technologies, CA) were used to measure electromyography (EMG) of sampled muscles. The EMG signals were pre-amplified (1000x) before filtered (band-pass filter of 10-1000 Hz) by the Myopac system. The output from Myopac was recorded by the Global Lab software (Data Translation Inc., MA).

4.3. Experimental Design

4.3.1. Independent (task) variables

The independent (task) variables included load magnitude (L) (10, 20, 30, and 40 lbs), angular velocity (V) (0°/s, 20°/s, 30°/s, and 40°/s), and elbow flexion angle (A) (45°, 90°, and 135° with 0° meaning full elbow extension).

4.3.2. Dependent variables

The dependent variables included the co-contraction weight factor *W* and a ratio (Ratio) obtained by dividing the moment resulting from antagonist muscles with the moment generated by agonist muscles. The value of Ratio represented the level of antagonist muscle co-contraction associated with the empirical EMG data. EMG muscle activities were collected on the elbow flexors (biceps short head, biceps long head, brachialis, and brachioradialis) and elbow extensors (anconeus, triceps lateral head, triceps long head, and triceps medial head). Table 10.9 and Figure 10.14 in Marieb (2001) were referred to for the electrode placement locations of the sampled muscles. For all muscles except brachialis, surface electrodes were placed on the belly of corresponding muscles. The window for collecting brachialis activity was located distal to the humerus on the medial side and slightly to the anterior. The distance between the centers of electrodes within each pair was 1.5 cm for all muscles except brachialis where the distance was 2 cm. In order to reduce muscle cross-talk to a minimal level, the electrode placement locations were chosen to maximize the contribution from the corresponding muscle based on the relative cross-sectional areas of the

muscles in the region. All muscle activities were collected on the dominant (right) arm of the subject.

The co-contraction weight factor (W) was derived from comparing the EMG generated muscle forces (or actual forces F_{act}) at a certain task condition (a combination of L, V and A) with an array of muscle forces predicted by EASOM (F_{pred}) corresponding to a series of co-contraction weight factor (W) values (from 0 to 1 with an interval of 0.01). Among all 101 W values, the co-contraction weight factor for the given task condition was picked such that it yielded the least sum of squared error between F_{act} and F_{pred}.

4.4. Procedures

The experiment began with a period of stretching and warm-up. Anthropometric data were gathered, including forearm length, hand length and body weight. This was followed by placement of surface electrodes. Once these were placed and signals verified, the subject performed a series of maximum voluntary isometric contraction (MVIC) exertions specifically designed to isolate the muscle of interest during the contraction. Before the measurement started, the dynamometer was adjusted so that its center of rotation was at the subject's elbow height and the distance between the center of rotation and the handle matches the distance between the subject's elbow joint and knuckle. To measure the MVICs of elbow flexors, the subject firmly held the attachment on the dynamometer arm with his dominant hand (in supination position), with forearm parallel to the dynamometer arm and upper arm close and in line with his trunk (Figure 7). The subject was asked to flex his elbow against the static resistance from the dynamometer set in isometric model. MVICs were measured at

elbow angles of 45°, 90°, and 135° on the dynamometer, where 0° corresponded with full extension of the arm. MVICs of elbow extensors were also measured. Due to the difficulty in obtaining true maximum elbow extensions, three different approaches were attempted. For the first method, the subject was asked to simply utilize the dynamometer and adopt the arm position assumed during maximum flexion exertions except the palm is in a pronation posture. In the second approach, the same procedure was followed as in the first one, plus a static resistance was applied on the elbow to prevent it from moving forward during elbow extension. The third approach asked the subject to perform a pushup motion against the resistance of a chair. As in the maximum flexion exertions, the maximum elbow extensions were measured at elbow angles of 45°, 90°, and 135° (with 0° meaning full elbow extension). For each elbow extensor at each elbow angle, the largest EMG value across the three methods was used as the maximum value. The EMG values generated during these MVIC flexions and exertions were used in data processing to normalize the EMG data from the following trials. A one-minute break was provided between maximum exertions. All maximum exertions were collected during five-second sessions although the subject was only asked to reach maximum in about three seconds. Rest break was given after these exertions. After completing the MVIC exertions, subjects began the experimental phase of the study. Before trials began, the subject underwent training for the isokinetic trials.

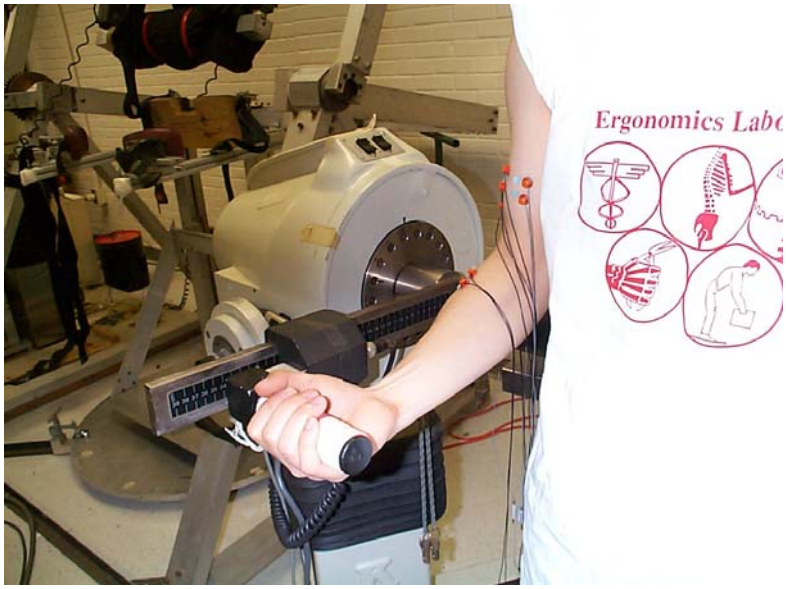

Figure 7 Measurement of elbow flexor MVIC

During an isokinetic trial, the dynamometer was preset to run passively under a designated angular velocity within the angle range between 30° and 150°. With the visual guidance from the moving arm of the dynamometer, the subject was instructed to run his forearm as parallel as possible to the moving dynamometer arm while holding the load and keeping upper arm still and close to torso (Figure 8). The training session lasted until the subject felt comfortable with the execution of the technique. The subject then performed a total of 48 trials, among which 24 were isometric (static) trials (combinations of four levels of load, three levels of angle, and two repetitions) and 24 were isokinetic (dynamic) trials (combinations of four levels of load, three levels of velocity, and two repetitions). The order of all trials (regardless of isometric or isokinetic) was completely randomized. During each isometric trial, the subject was first to reach a stable state when holding the load at a designated angle, and then the EMG was collected for five seconds. During each dynamic trial, the subject was asked to follow moving dynamometer arm. Data collection began near

full extension (0°) and continued until the end of the concentric exertion (full flexion at near 150°). Sufficient rest breaks were provided between trials to prevent fatigue from the subject.

Figure 8 Elbow flexion motion with forearm guided by the dynamometer arm during an isokinetic trial

4.5. Data Processing

4.5.1. EMG-assisted model

The muscles considered in both the EMG-assisted biomechanical model and EASOM are biceps short head (BIC(S)), biceps long head (BIC(L)), brachialis (BRA), brachioradialis (BRD), anconeus (ANC), triceps lateral head (TRI(Lt)), triceps long head (TRI(Lg)), and triceps medial head (TRI(Md)). For the above mentioned muscles, Pigeon et al. (1996) provide regression functions for estimating the moment arms relative to elbow flexion angles. In the current pilot study, these values were scaled (multiplied) by the ratio between the mid-upper arm circumference (flexed at 90°) of the subject and the median value obtained from

military personnel anthropometry data (DOD-HDBK-743A, 1991). Such a ratio, when squared, was also used to scale (multiply) the physiological cross sectional areas data present in An (1984).

The formulas for calculating force-length and force-velocity factors were taken from Benoit and Dowling (2006) and modified for use in the current elbow EMG-assisted model. as shown below. Figure 9 shows the force-angle factor as a function of elbow flexion angle, and Figure 10 depicts the force-velocity factor as a function of angular velocity.

$$f_{ag}(\theta) = 1 \Big/ \left(e^{\left((1-105/(105+|75-\theta|))/1.2\right)^2} \right) \tag{4-1}$$

$$f_{ant}(\theta) = 1 \Big/ \left(e^{\left((1-105/(105+|105-\theta|))/1.2\right)^2} \right) \tag{4-2}$$

$$f_{ag}(\omega) = 1 - 0.005 \times \omega \tag{4-3}$$

$$f_{ant}(\omega) = 1 + 0.008 \times \omega \tag{4-4}$$

where

θ is the elbow flexion angle (°);

$f_{ag}(\theta)$ is the force-angle factor for agonist (elbow flexor) muscles;

$f_{ant}(\theta)$ is the force-angle factor for antagonist (elbow extensor) muscles;

ω is the angular velocity (°/s);

$f_{ag}(\omega)$ is the force-velocity factor for agonist (elbow flexor) muscles;

$f_{ant}(\omega)$ is the force-velocity factor for antagonist (elbow extensor) muscles.

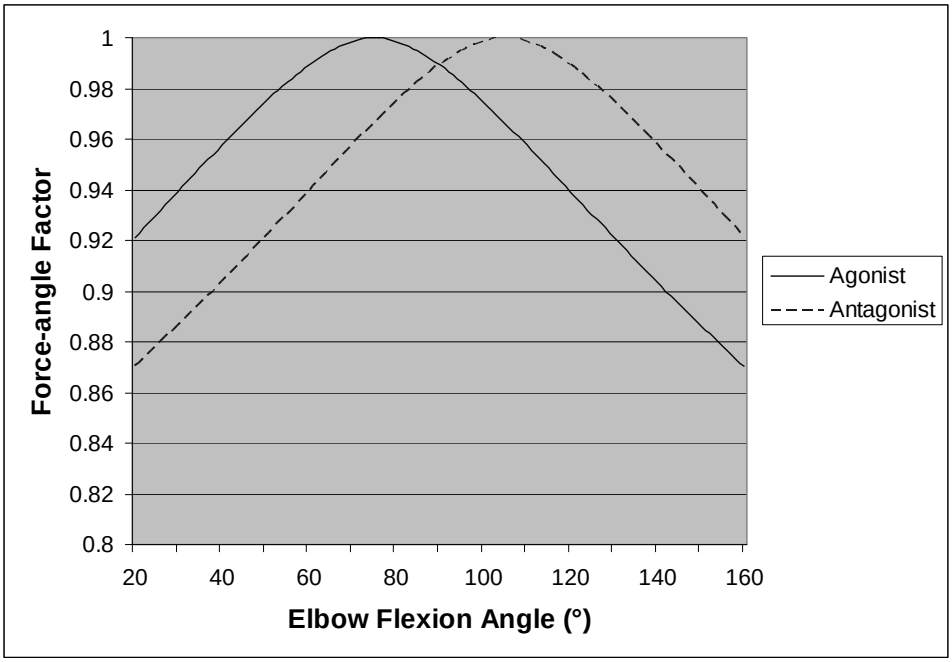

Figure 9 Relationship between force-angle factor and elbow flexion angle for both agonist and antagonist muscles

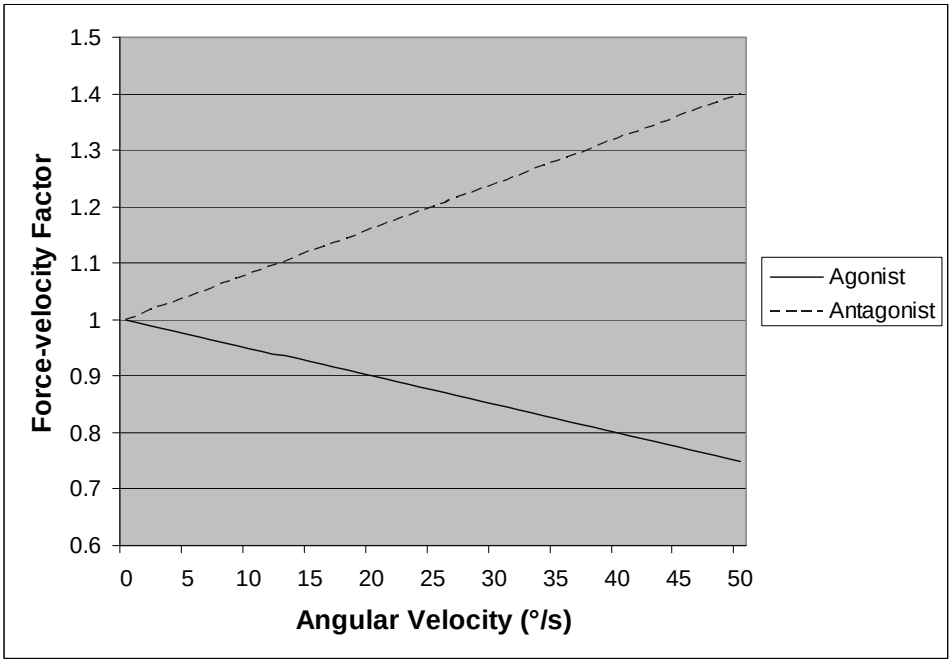

Figure 10 Relationship between force-velocity factor and angular velocity for both agonist and antagonist muscles

The raw EMG data were filtered in MatLab using a 15 - 500 Hz pass filter as well as a notch filter that eliminated 60 Hz and its aliases. Once filtered these signals were rectified (full-wave). This processing occurred in both the data collected during the experimental trials as well as the maximum voluntary contractions. The EMG data collected during the maximum exertions were partitioned into 1/8 second windows and the maximum of the 40 windows (5 second collection period) for each muscle in each posture for either flexors or extensors were identified and were used as the denominator in the process of normalizing the trial data. The EMG data for each isometric trial were averaged across its collecting period. For each of dynamic trials, the data for angle ranges of 45°±1°, 90°±1°, and 135°±1° were extracted, and averaged for each angle range to be used as the data point for that angle level.

EMG-assisted model was used to convert the empirical EMG data into muscle forces (F_i). It can be expressed as follows (Marras and Sommerich, 1991; McGill and Norman, 1986).

$$F_i = \frac{EMG_i(t)}{EMG_{i,\max}} \times f(\theta) \times f(\omega) \times PCSA_i \times gain \qquad (4\text{-}5)$$

where

F_i is the force generated by muscle *i*;

$EMG_i(t)$ is the raw EMG signal for muscle *i* at time *t*;

$EMG_{i,\max}$ denotes the maximum EMG for muscle *i* at the current elbow flexion angle;

θ is the current elbow flexion angle (°);

$f(\theta)$ is the force-angle factor for muscle *i* at the current elbow flexion angle (θ);

ω is the current angular velocity (°/s);

$f(\omega)$ is the force-velocity factor for muscle *i* at the current angular velocity (ω);

$PCSA_i$ denotes the physiological cross sectional area of muscle *i*;

gain is a constant across all muscles for an individual and shows that person's force generating potential. It represents the maximum force that can be produced per muscle cross sectional area (N/cm^2).

As Equation (4-5) shows, the raw EMG signal ($EMG_i(t)$) was first normalized to maximum EMG ($EMG_{i,\max}$). Force-angle ($f(\theta)$) and force-velocity ($f(\omega)$) factors for the muscle were then taken into consideration since all muscles have different force-generating capabilities under different lengths (corresponding to different elbow flexion angles) or velocities. The value of the last component *gain* was adjusted until the torque generated by EMG-based muscle forces matches the measured torque from the experiment (Granata and Marras, 1995a). In the pilot study, the *gain* for each experimental condition was determined using the data from that specific condition equilibrium between the external moment and the internal moment were equal. This value of gain was allowed to vary across subjects and across conditions, but was constant across muscles. We let $\widetilde{F}_{act}$ denote the vector that represents the outcome from the EMG-assisted model and consists of eight elements each of which corresponds with the EMG generated muscle force for each of the eight muscles involved.

After muscle forces were calculated using the EMG-assisted model, the ratio (Ratio) of moment generated by antagonist muscle forces over moment generated by agonist muscles forces was obtained for each experimental condition. This value provided a measure for the level of muscle co-contraction associated with the empirical EMG data.

4.5.2. Optimization model (EASOM)

The general form of EASOM displayed in Chapter 3 (equations (3-1) to (3-3)) was reformulated for the pilot study, as shown below in equations (4-6) to (4-8).

$$Minimize \quad (1-W)\sum_{i=1}^{8} x_i^{\,3} + 10^5 * W * \sum_{i=1}^{8}\left(\frac{x_i}{\sigma_0}\log\frac{x_i}{\sigma_0}\right) \tag{4-6}$$

$$Subject\ to \quad \sum_{i=1}^{8} r_i * PCSA_i * x_i = T \tag{4-7}$$

$$0 \le x_i \le \sigma_0 \qquad (i = 1,2,\ldots,8) \tag{4-8}$$

where

W is the *co-contraction weight factor*;

x_i is the muscle stress of muscle i;

σ_0 is the muscle stress limit;

r_i is the moment arm for muscle i;

$PCSA_i$ is the physiological cross sectional area of muscle i;

T is the torque generated by the handheld load and the masses of forearm and hand.

As mentioned earlier, there were eight muscles in this elbow model. As shown in the objective function (4-6), the sum of cubed muscle stresses ($\sum_{i=1}^{8} x_i^{\,3}$) was utilized to represent the command for reciprocal inhibition (agonist only contraction). It is noted that the magnitude of $\sum_{i=1}^{8} x_i^{\,3}$ is normally in the order of 10^6, while the magnitude of the entropy term ($\sum_i \frac{x_i}{\sigma_0}\log\frac{x_i}{\sigma_0}$) is usually less than 1. Therefore, a scaling factor of 10^5 was applied to the

entropy term (equation (4-6)) to help balance the difference in magnitude between the two components of the objective function (4-6). Since we treated the elbow as a single-plane model (flexion in sagittal plane), there was only one equation of the joint moment equilibrium condition (equation (4-7)). The approaches to calculating moment arms (r_i) and physiological cross sectional areas ($PCSA_i$) were the same as described in Section 4.5.1 for the EMG-assisted model. In the pilot study, the value of muscle stress limit for each task condition (i.e. combination of task variables) was set to equal the *gain* value obtained in the EMG-assisted model for that condition. (Note that the EASOM predicted muscle force (e.g. for muscle *i*) is equal to $PCSA_i * x_i$.)

The implementation of EASOM was carried out using the Sequential Quadratic Programming algorithms within the optimization toolbox in MatLab 7. The output from a single run of this MatLab program was in fact a vector of eight elements, each corresponding with the predicted muscle force for each of the eight muscles involved in the model. We denote such an output as $\widetilde{F}_{pred}$.

4.5.3. Generation of condition-specific co-contraction weight factor *W*

For a given task condition (a combination of all task variables), the corresponding co-contraction weight factor *W* was obtained using the approach that follows. The *W* was first assigned with values from 0 to 1 with an interval of 0.01. These 101 *W* values then resulted in 101 corresponding EASOM predicted muscle force vectors ($\widetilde{F}_{pred}$). We compared each of these vectors ($\widetilde{F}_{pred}$) with the EMG generated muscle force vector ($\widetilde{F}_{act}$) and calculated the

sum of squared error between $\widetilde{F}_{act}$ and $\widetilde{F}_{pred}$. Among all the W values assigned, the co-contraction weight factor W for the given condition was chosen such that it yielded the least sum of squared error between $\widetilde{F}_{act}$ and $\widetilde{F}_{pred}$.

4.5.4. Simple linear regression for W

For this pilot study, data from load magnitude levels of 10, 20, and 40 lbs were used to generate co-contraction weight factors for establishing the simple linear regression equation associating the co-contraction weight factor (W) with load magnitude L (lbs), angular velocity V (°/s) and elbow flexion angle A (°). Data from the load magnitude level of 30 lbs were later used to validate the model. With the condition related co-contraction weight factors obtained from the previous step for all conditions, the regression equation associating W with task variables (L, V and A) was established using PROC REG in SAS 9.

4.5.5. Model validation

Recall that the data under conditions with 30 lbs load magnitude were used for validation, and the number of such conditions was 12 (combination of one level of magnitude, four levels of angular velocity and three levels of elbow flexion angle). With the regression equation for W in place, each of the 12 combinations of task variables was input into the regression equation to generate the W value corresponding to that particular condition. Using the resulting values of W along with task variables, EASOM was able to predict the muscle force vector ($\widetilde{F}_{pred}$) associated with each of the 12 conditions. The quality of the EASOM predicted muscle forces was evaluated by comparing these predictions with the muscle forces

found through the EMG-assisted modeling technique. This comparison considered the following measures: (1) percent error (per muscle per condition), (2) average absolute percent error (per muscle), and (3) coefficient of determination (R^2) (per muscle). The equations for calculating percent error and average absolute percent error are shown in equations (4-9) and (4-10). The coefficient of determination was found by squaring the correlation coefficient between F_{pred} and F_{act}.

$$(Percent\ Error)^{i,j} = \frac{F_{pred}^{i,j} - F_{act}^{i,j}}{F_{act}^{i,j}} \times 100\% \qquad (i = 1,\ldots,8;\ j = 1,\ldots,12) \qquad (4\text{-}9)$$

$$(Average\ Absolute\ Percent\ Error)^{i} = \frac{\sum_{j=1}^{12} \left| (Percent\ Error)^{i,j} \right|}{12} \qquad (i = 1,\ldots,8) \qquad (4\text{-}10)$$

where

$(Percent\ Error)^{i,j}$ is the percent error for muscle i under condition j;

$F_{pred}^{i,j}$ is the EASOM predicted muscle force for muscle i under condition j;

$F_{act}^{i,j}$ is the EMG generated muscle force for muscle i under condition j;

$(Average\ Absolute\ Percent\ Error)^{i}$ is the average absolute percent error for muscle i.

4.6. Results

4.6.1. Ratio (derived from empirical EMG data)

Recall that Ratio means the ratio of torque generated by antagonist muscles over torque generated from agonist muscles, and the muscle forces used in the calculation was obtained from the EMG-assisted model. As the load magnitude increases from 10 lbs to 40 lbs, Ratio drops by 43.1% (from 0.36 to 0.21) (Figure 11). Figure 12 shows that Ratio rises by

72.1% (from 0.18 to 0.31) when angular velocity increases from 0 to 40°/s. As its relationship with of elbow flexion angle, Ratio is 0.40 at 45°, compared with 0.19 at both 90° and 135° (Figure 13).

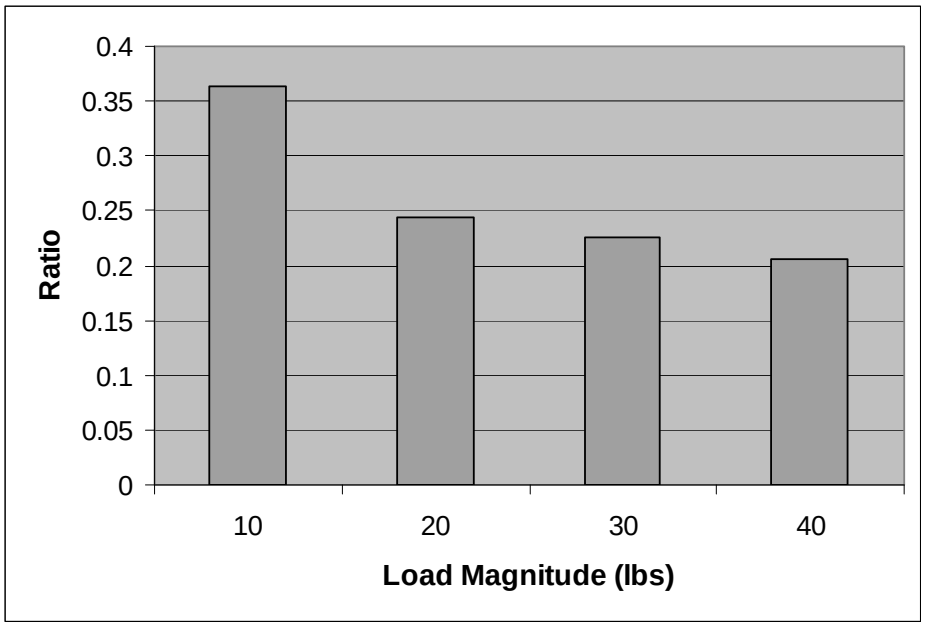

Figure 11 Relationship between Ratio and load magnitude (each bar represents the averaged Ratio across all values of Ratio under that level of load magnitude).

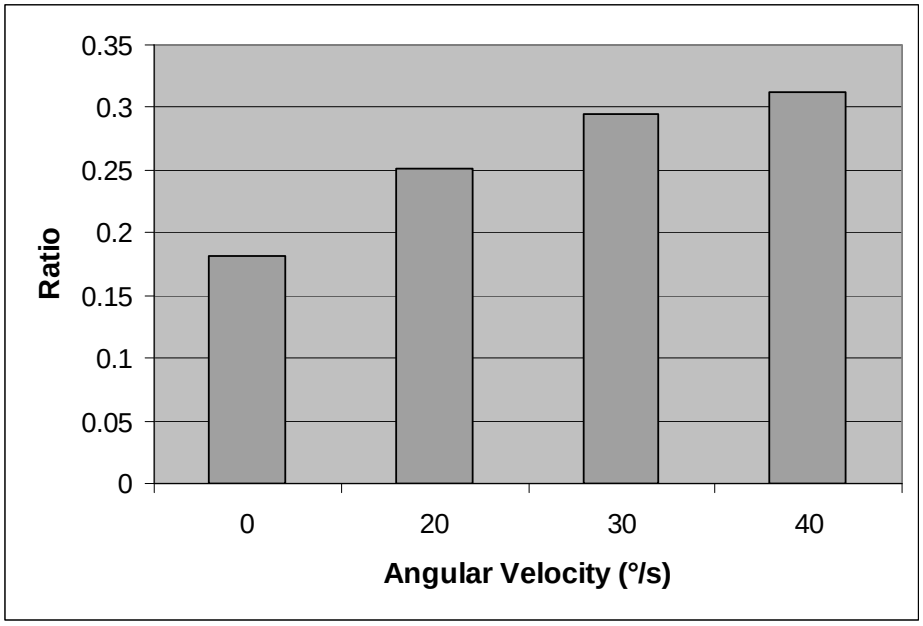

Figure 12 Relationship between Ratio and angular velocity (each bar represents the averaged Ratio across all values of Ratio under that level of angular velocity).

Figure 13 Relationship between Ratio and elbow flexion angle (each bar represents the averaged Ratio across all values of Ratio under that level of elbow flexion angle).

4.6.2. Co-contraction weight factor (W)

The simple linear regression equation relating W to magnitude load (L), angular velocity (V) and elbow flexion angle (A) was obtained as shown below.

$$W = (77.396 + 1.066 \times L + 0.399 \times V - 0.469 \times A) \times 10^{-2} \quad (4\text{-}11)$$

From the values of coefficients associated with all three task variable, it is apparent that the value of W rises with increased load magnitude (Figure 14) or increased angular velocity (Figure 15) and drops with greater elbow flexion angle (Figure 16). Although both Ratio and co-contraction weight factor W can be used to represent the level of muscle co-contraction, it is noted that the trend of W relative to load magnitude (Figure 14) contradicts the trend of Ratio relative to the same task variable (Figure 11). Exploration of possible cause for this contradiction will be discussed later in Section 4.7.

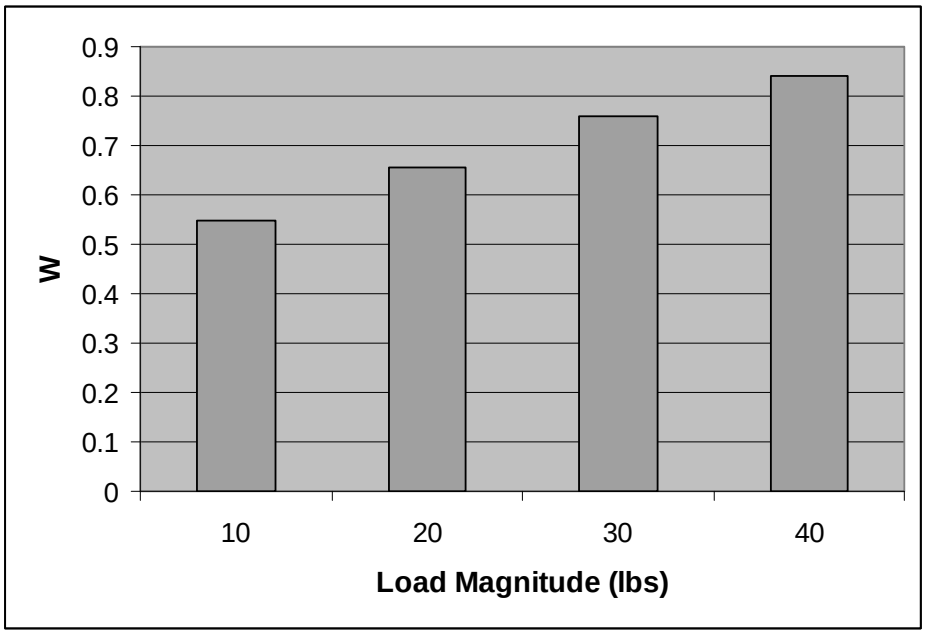

Figure 14 Relationship between co-contraction weight factor (W) and load magnitude (each bar represents the averaged W across all W values under that level of load magnitude).

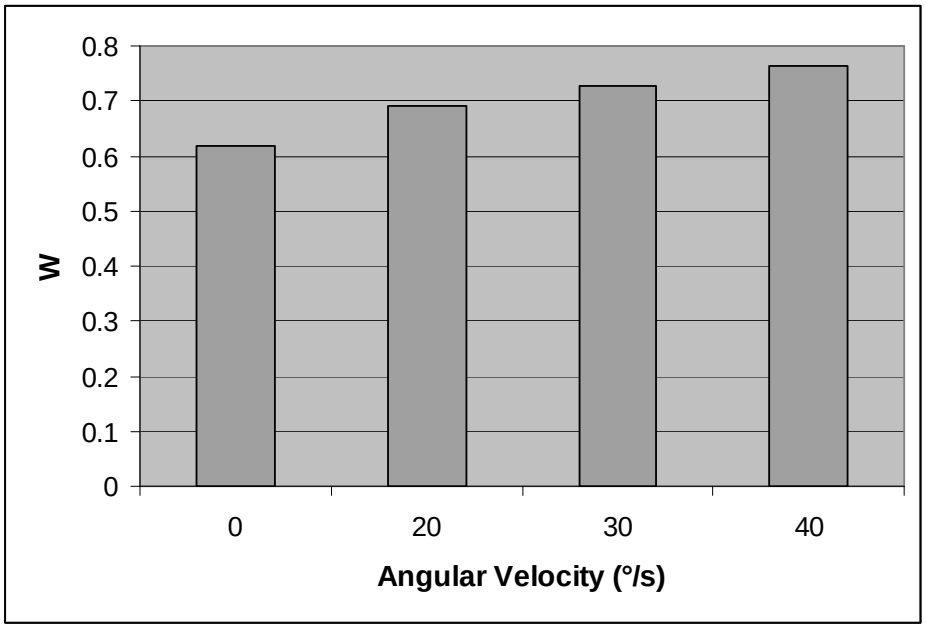

Figure 15 Relationship between co-contraction weight factor (*W*) and angular velocity (each bar represents the averaged *W* across all *W* values under that level of angular velocity).

Figure 16 Relationship between co-contraction weight factor (*W*) and elbow flexion angle (each bar represents the averaged *W* across all *W* values under that level of elbow flexion angle).

4.6.3. Model validation

The regression equation for *W* obtained from the previous section enabled EASOM to predict muscle forces under different conditions. With the predicted muscle forces along with empirical EMG data under 30 lbs conditions, we were able to obtain the percent errors (per muscle per condition) (Figure 17) , average absolute percent errors (per muscle) and R^2 (per muscle) (Table 1) between the EASOM predicted and EMG generated muscle forces. As Table 1 shows, the average absolute percent error ranges from 28.6% (BIC(S)) to 99.3% (TRI(Lg)) with an averaged value of 59.6%. The value of R^2 ranges from 0.002 (BIC(L) and ANC) to 0.737 (TRI(Lt)) with an averaged value of 0.468 (Table 1).

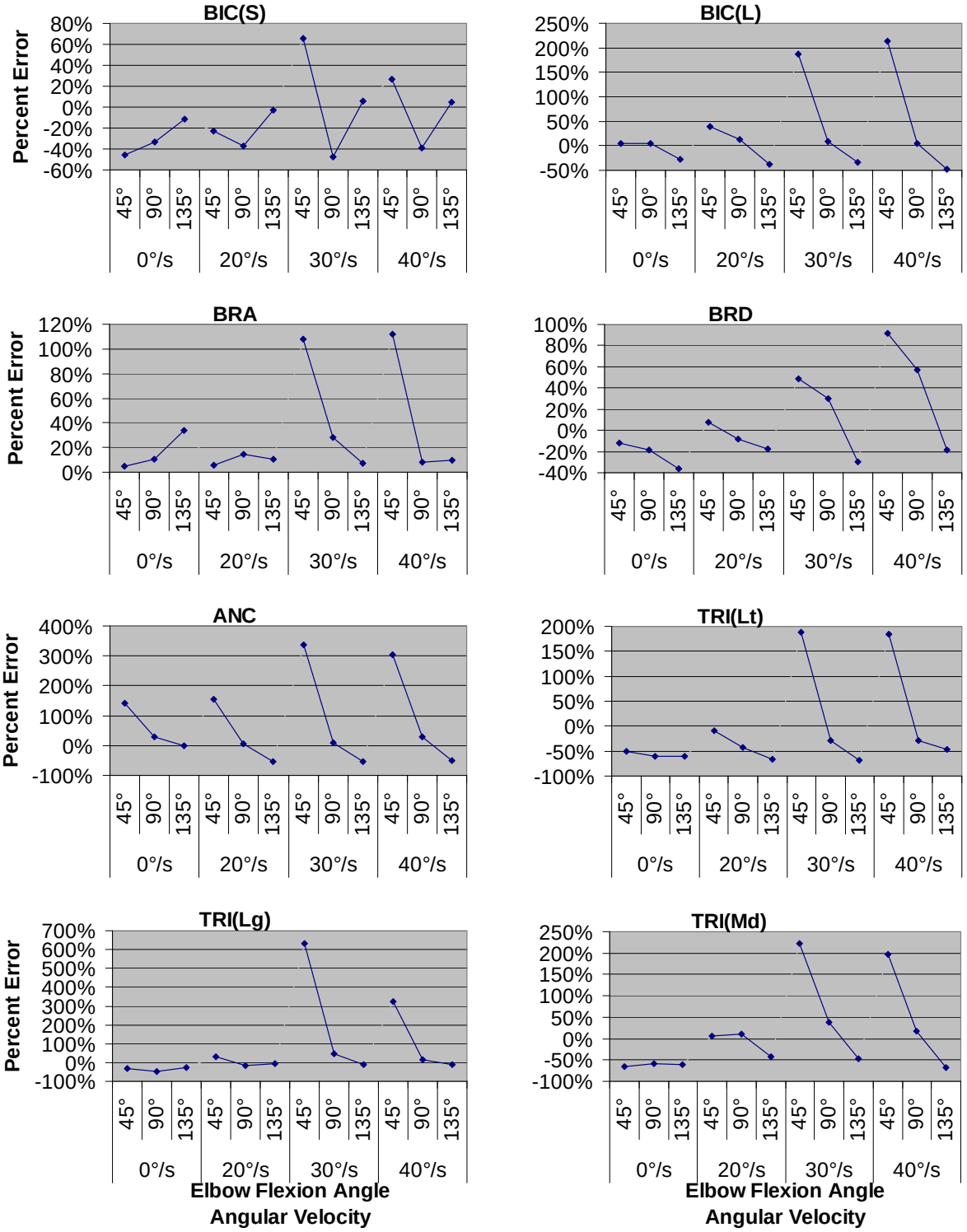

Figure 17 Percent errors for muscle force prediction under 30 lbs conditions. (BIC(S) – biceps short head; BIC(L) – biceps long head; BRA – brachialis; BRD – brachioradialis; ANC – anconeus; TRI(Lt) – triceps lateral head; TRI(Lg) – triceps long head; TRI(Md) – triceps medial head)

Table 1 Average absolute percent errors (AAPEs) and R^2 between EASOM predicted and EMG generated muscle forces under 30 lbs (BIC(S) – biceps short head; BIC(L) – biceps long head; BRA – brachialis; BRD – brachioradialis; ANC – anconeus; TRI(Lt) – triceps lateral head; TRI(Lg) – triceps long head; TRI(Md) – triceps medial head)

	BIC(S)	BIC(L)	BRA	BRD	ANC	TRI(Lt)	TRI(Lg)	TRI(Md)
AAPE	28.60%	51.90%	29.50%	31.30%	97.20%	69.60%	99.30%	69.70%
R^2	0.504	0.002	0.706	0.689	0.002	0.737	0.556	0.534

4.7. Discussion and Lessons Learned

Prior to the pilot study, it was expected that co-contraction level would increase with higher angular velocity and greater extension of the elbow. These hypotheses were confirmed by the results of Ratio (Figures 12 and 13) and *W* (Figures 15 and 16). It was hypothesized that greater load magnitude should bring up exertion levels of more muscles, thus contribute to better balance among muscle exertions (higer *W* value). This was confirmed by the Figure 14. However, the hypothesis on the trend of Ratio with regard to load magnitude was never clear. The result showed a decreased Ratio as load magnitude increased, which showed opposite trend than *W*. The EMG generated muscle force results showed that muscle forces from brachialis, one of the flexors (agonist muscles), increased at a much faster rate with increasing load than any other muscles. This may explain the drop of Ratio with higher load magnitude. This shows that it is necessary to make different interpretations of Ratio and *W* in terms of muscle co-contraction level.

In order for Ratio to work, a clear understanding is necessary on whether muscles are agonist or antagonist. This shows no problem in circumstances where the roles of muscles are clear, such as elbow flexion in the sagittal plane as in the current study. However, under situations where muscle functions are not as clear (e.g. asymmetric trunk motions), using Ratio as an index for level of muscle co-contraction can face great challenges. These are the

circumstances where *W* has an apparent advantage. The application of the co-contraction weight factor *W* requires no distinction between agonist and antagonist muscle groups since the entropy component in EASOM encourages exertions from all muscles. Because of this advantage of *W* in quantifying co-contraction, for the next stage of the experiment, we would only focus on the co-contraction weight factor *W* as indicator of level of muscle co-contraction. It was hypothesized that *W* increases with higher load magnitude, and with increased velocity. Also, *W* tends to be higher with greater elbow extension. *W* was also hypothesized to be lower at dominant arm than in the non-dominant arm.

In addition, there were a number of lessons that had been learned from the pilot study and will help refine the experimental protocols used for future experiments. These are detailed as follows.

4.7.1. Experimental design

4.7.1.1. Type of dynamic trials: free vs. controlled

The free dynamic trials that were adopted during the pilot study have greater advantage over controlled isokinetic trials using the dynamometer, in that free dynamic approach yields natural arm movement and prevents extra muscle exertions used to compensate for the attempt to maintain a certain torque level on the dynamometer during controlled dynamic trials. Thus, free dynamic trials should be able to produce muscle exertion patterns that are closer to those from real world voluntary elbow flexion motions. This can also help reduce the fatigue caused by overexertion. Such free dynamic trials would be adopted in future experiments.

4.7.1.2.MVIC measurement of elbow extensors

In terms of proper ways of collecting MVICs of elbow extensors, from the subjective feedback and experimental results, the involvement of the dynamometer as the only apparatus had trouble obtaining the true maximum EMG. Therefore, assistive device needs to be involved firmly secure the elbow to overcome this problem.

4.7.1.3.Levels of load magnitude and angular velocity

Despite the choice of levels of weight (10, 20, 30, and 40 lbs) for the dumbbells used in the pilot study, the distinction of levels according to percent of maximum capacity should work better in that it has physiologically similar effects on each subject (thus yielding similar overall normalized EMG at the same load level) and can avoid complication of results due to different perceived exertions from subjects with different strength capacity. Therefore, data collected in the dissertation experiment will be relative to the subject's individual elbow flexion strength capacity.

Since the results from pilot study show a monotonic trend for Ratio as well as W in higher velocity range, the range of velocity levels will be expanded from 0, 20, 30, and 40˚/s to 0, 20, 40, and 60˚/s in order to have better representation of real world situations, especially at the higher end of the angular velocity spectrum.

4.7.1.4.Dexterity as a task variable

Recall that only data from the dominant arm were collected during the pilot study. However, dexterity (e.g. dominant arm vs. non-dominant arm) is closely related to level of experience, data from the non-dominant arm would be collected in future experiments. The

results in this regard may help show the effect of training on level of co-contraction and generate implications that might benefit real word problems. However, considering the length of the experiment and its physical demand on each subject, it is wise to only collect data from one arm during a single experiment session. The experimental procedure applied to the dominant elbow can be duplicated on the non-dominant elbow.

4.7.2. EMG-assisted model for the elbow joint

The results showed largest errors at 45 degree angle (Figure 17), which was very likely due to the difficulty experienced by the EMG-assisted elbow model in generating accurate muscle forces at that elbow flexion angle. The strength and accuracy of the EMG-assisted model are critical to the quality of EASOM since establishment of EASOM is based on the use of the results from the EMG-assisted model. Therefore, for the next stage of the study we would need a more robust EMG-assisted model for the elbow joint. Potential improvement included more accurate modeling of force-angle factor and consideration of the contribution from passive elastic muscle component. Detailed description will be presented in Section 6.7.2.

4.7.3. EASOM

4.7.3.1. Muscle stress limit

For the EASOM model applied in the pilot study, muscle stress limit was allowed to vary across different conditions and its value was set to match the *gain* value obtained from the EMG-assisted model for the same condition. However, in the real world, EASOM needs to be utilized without any assistance from the EMG-assisted model. Therefore, in order for

EASOM to be an independent model, a fixed value for the muscle stress limit is necessary. According to Langenderfer et al. (2005), this muscle stress limit is set to 500 N/cm^2.

4.7.3.2.Range of the co-contraction weight factor *W*

In the pilot study, the value of *W* was allowed to range from 0 to 1. However, it was observed from the results of muscle force prediction, when the value of W was close to 0 (especially between 0 and 0.1), the predicted muscle forces for antagonist muscles were mostly zero. Since muscle co-contraction always exists (Granata and Marras, 1995b; Lavender et al., 1992; Marras and Granata, 1997; McGill, 1991), it makes sense to raise the lower bound for *W* above zero. Therefore, we would have *W* to range from 0.1 to 1.

4.7.3.3.Neural network vs. polynomial regression

One of the critical components in establishing the EASOM model (especially its parameters) is to obtain the relationship between the co-contraction weight factor (*W*) and the task variables with the processed experimental data. One solution would be through linear regression which was the solution to the pilot study. However, robustness of such an approach would be rather limited considering almost all real world problems are non-linear. In light of this issue, for future experiments, polynomial regression would be utilized in place of linear approach. In addition, a backpropagation neural network would be applied as an alternative to model such a relationship. Such a neural network model has the advantage of being able to approximate a target function (linear or non-linear) as closely as possible regardless of the nature of such a function in reality (Smith, 1993). The detail for the neural network will be discussed in Section 6.7.3.3.

5. RESEARCH OBJECTIVES

There is a need for an optimization-based biomechanical model that can predict antagonist muscle forces which is supported by basic neurophysiological principles. The goal of this research is the development and validation of an entropy-assisted optimization model (EASOM). Chapter 4 displayed the course of a pilot study where a preliminary formulation of such a model was applied to the elbow joint (a single-plane model) in one subject. The goal of this experiment was to refine and validate the EASOM modeling approach for the elbow joint. Applying EASOM to a simple anatomical structure such as the elbow joint facilitates the procedure of familiarization of the functioning and working mechanics of EASOM, and furthermore clears the way for future application of EASOM on more complicated anatomical structures (e.g. the lumbar region of the torso).

6. METHODS

6.1. Subjects

A total of twelve male subjects were recruited for this study. Only subjects who had predominant handedness were recruited. None of the subjects were ambidextrous (with both hands being equally adept in common activities) or mixed-handed (with both hands being adept in different tasks). Only data from one arm (either dominant or non-dominant) were collected during a single experiment session. Based on the arm involved in EMG data collection, subjects were separated into dominant (D) and non-dominant (ND) groups. Among all the subjects, eight agreed to participate in both experiment sessions (on both arms), thus they belonged to both subject groups. The two sessions for the same subject were separated by at least one day. The remaining four subjects were evenly split into the two groups. Therefore, both D and ND groups consisted of ten subjects. The average ages (and standard deviations) for the D and ND groups are 27.5 (2.84) and 28.1 (2.47), respectively. All subjects were right-handed although handedness was not used as a criterion in subject screening. All subjects had no history of upper extremity injury and gave informed consent at the time of participation. Anthropometric characteristics of the participants are shown in Table 2.

During processing of the empirical EMG data, it was found that both D and ND groups each had one subject for whom a large portion (over 10%) of his EMG data generated physiologically unrealistic muscle force results. Therefore, these two subjects' EMG data were removed from subsequent data processing and analysis. Each of the resulting D and ND groups consisted of nine subjects, among whom seven belonged to both groups. Anthropometric characteristics of the remaining participants are shown in Table 3. It is

noted that seven subjects belonged to both D and ND groups. There was also one subject in each group for whom a small portion (less than 10%) of the EMG data generated the same kind of questionable results. For these two subjects, only those problematic EMG data were eliminated from subsequent data processing and analysis procedures.

Table 2 Subjects' anthropometric data

Subject #	Overall			Dominant (D)			Non-dominant (ND)		
	Age (years)	Weight (kg)	Stature (m)	Age (years)	Weight (kg)	Stature (m)	Age (years)	Weight (kg)	Stature (m)
1	26	70.1	1.772	26	70.1	1.772	-	-	-
2	26	74.8	1.756	26	74.8	1.756	26	74.8	1.756
3	27	68.9	1.800	27	68.9	1.800	27	68.9	1.800
4	33	77.6	1.687	33	77.6	1.687	33	77.6	1.687
5	31	65.8	1.664	31	65.8	1.664	31	65.8	1.664
6	28	68.0	1.687	-	-	-	28	68.0	1.687
7	24	102.5	1.830	24	102.5	1.830	-	-	-
8	24	61.2	1.750	24	61.2	1.750	24	61.2	1.750
9	28	59.4	1.672	-	-	-	28	59.4	1.672
10	28	103.9	1.790	28	103.9	1.790	28	103.9	1.790
11	28	65.8	1.747	28	65.8	1.747	28	65.8	1.747
12	28	72.6	1.735	28	72.6	1.735	28	72.6	1.735
Mean	**27.6**	**74.2**	**1.741**	**27.5**	**76.3**	**1.753**	**28.1**	**71.8**	**1.729**
SD	**2.57**	**14.5**	**0.0537**	**2.84**	**14.9**	**0.0500**	**2.47**	**12.6**	**0.0486**

Table 3 Subjects' anthropometric data (after removal of one subject from each group as described in Section 6.1)

Subject #	Overall			Dominant (D)			Non-dominant (ND)		
	Age (years)	Weight (kg)	Stature (m)	Age (years)	Weight (kg)	Stature (m)	Age (years)	Weight (kg)	Stature (m)
1	26	74.8	1.756	26	74.8	1.756	26	74.8	1.756
2	27	68.9	1.800	27	68.9	1.800	27	68.9	1.800
3	33	77.6	1.687	33	77.6	1.687	-	-	-
4	31	65.8	1.664	31	65.8	1.664	31	65.8	1.664
5	28	68.0	1.687	-	-	-	28	68.0	1.687
6	24	102.5	1.830	24	102.5	1.830	-	-	-
7	24	61.2	1.750	24	61.2	1.750	24	61.2	1.750
8	28	59.4	1.672	-	-	-	28	59.4	1.672
9	28	103.9	1.790	28	103.9	1.790	28	103.9	1.790
10	28	65.8	1.747	28	65.8	1.747	28	65.8	1.747
11	28	72.6	1.735	28	72.6	1.735	28	72.6	1.735
Mean	**27.7**	**74.6**	**1.738**	**27.7**	**77.0**	**1.751**	**27.6**	**71.2**	**1.733**
SD	**2.65**	**15.1**	**0.0553**	**2.96**	**15.7**	**0.0526**	**1.88**	**13.2**	**0.0492**

6.2. Apparatus

6.2.1. Experimental task

Three sets of dumbbells of adjustable weight were used as the handheld load during the experiment. The mass of the handles (everything except the plates) for the three dumbbells were 1.700, 1.725 and 1.750 kg. The minimum load increment (mass of the smallest pair of plates) for all dumbbells was fixed at 1.14 kg.

The Kin-Com 125e dynamometer (Chattecx Corporation, TN) was utilized to provide static resistance during measurement of maximum voluntary isometric contraction (MVIC) (Figures 18 and 19). The dynamometer was also able to run passively back and forth within a preset angle range at a pre-designated angular velocity, and therefore was able to provide guidance for forearm motion during isokinetic (dynamics) elbow flexion trials (Figure 20, right).

6.2.2. Data collection

Sixteen pairs of surface Ag-AgCl electrodes (Model E22x, In-Vivo Metric) and the Myopac EMG collection system (RUN Technologies, CA) were used to measure electromyographic (EMG) muscle activity of sampled muscles. The EMG signals were pre-amplified (1000x) before filtering (band-pass filter of 10-1000 Hz) by the Myopac system. The output from Myopac was recorded by the QuickDAQ software (Data Translation Inc., MA) at a rate of 1024 Hz.

6.3. Task Variables

The task variables included load magnitude (L) (20%, 35%, and 50% of maximum elbow flexion capacity at 90° elbow flexion), angular velocity (V) (0°/s, 20°/s, 40°/s, and 60°/s), elbow flexion angle (A) (45°, 90°, and 135° with 0° meaning full elbow extension), and dexterity (dominant (D) and non-dominant (ND)). Since the smallest weight increment on the dumbbells was fixed, it was impossible to obtain the exact weights corresponding to the three levels of the load magnitude. Therefore, for a weight associated with a level of L, the closest weight available was used.

During processing of the EMG data, it was found that most of the data associated with conditions at 135º flexion generated physiologically unrealistic muscle force results. Therefore, all EMG data (across all subjects) at the level of 135º flexion were removed from subsequent data processing and analysis.

6.4. Experimental Procedures

6.4.1. Preparation

The subject was first introduced to the experimental protocol which had been approved by the Internal Review Board of North Carolina State University. If the subject agreed to participate in the experiment, he would then provide informed consent in written form. Before the experiment started, a number of anthropometric measures were taken. These included body mass, distance between elbow joint and base of palm ($d_{e,bp}$), distance between elbow joint and knuckle ($d_{e,k}$), and the mid-upper arm circumference (MUAC) at 90° elbow flexion. The subject was then given a stretching and warm-up session to prevent potential discomfort or injury that might occur during the experiment. This was followed by

placement of surface electrodes. On the arm (either D or ND) chosen for the experiment session, EMG muscle activity was collected on four elbow flexors (biceps short head (BIC(S)), biceps long head (BIC(L)), brachialis (BRA), and brachioradialis (BRD)) and four elbow extensors (anconeus (ANC), triceps lateral head (TRI(Lt)), triceps long head (TRI(Lg)), and triceps medial head (TRI(Md))) on one arm. Table 10.9 and Figure 10.14 in Marieb (2001) were referred to for the locations of the sampled muscles. For all muscles except BRA, surface electrodes were placed on the belly of corresponding muscles. The window for collecting BRA activity was located distal to the humerus on the medial side and slightly to the anterior. The distance between the centers of electrodes within each pair was 1.5 cm for all muscles except BRA where the distance was 2 cm. In order to reduce muscle cross-talk to a minimal level, the electrode placement locations were chosen to maximize the contribution from the corresponding muscle based on the relative cross-sectional areas of the muscles in the region. It is recognized, however, that it is impossible to isolate a specific muscle in this region of the body. These positions were chosen to maximize the contribution of the named muscle to the signal collected.

6.4.2. MVIC measurement

Once the surface electrodes were placed and signals verified, the subjects performed a series of MVIC exertions specifically designed to isolate the muscle group of interest during the contraction. Prior to the measurement, the height of the dynamometer was adjusted so that the center of rotation of the metal arm was at the same height as the subject's elbow (Figure 18). Before measuring MVIC, the dynamometer was preset to isometric mode and set to a designated angle (45°, 90°, or 135°)

Figure 18 Maximum voluntary isometric contraction of elbow flexors

To measure the MVIC of elbow flexors, a handle was attached to the load cell mounted on the metal arm. The relative location of the load cell to the metal arm was adjusted such that the distance between the center of rotation and the handle matched the distance between the subject's elbow joint and base of palm (Figure 18). The subject was then instructed to put his hand underneath the handle in supination position and have the base of the palm lined-up with the handle. In the meantime, the subject was also allowed to adjust his stance so that his forearm would run parallel to the metal arm and upper arm would be kept close and in line with his trunk (with zero shoulder flexion/extension and abduction). (Such an adjustment of foot stance was also encouraged before the start of an MVIC exertion of the extensors, as well as before the start of each trial during the trial phase of the experiment.) During the MVIC of elbow flexors, the subject was verbally encouraged to flex his elbow and resist (using base of palm) against the static resistance (handle) as hard as possible. During MVIC at 90° elbow flexion, the maximum force exerted on the handle was also recorded (by reading from the screen attached to the dynamometer). This number was then input into a biomechanical model to calculate the weight of the handheld load

corresponding to the maximum capacity at 90° elbow flexion angle. This value was then multiplied by 20%, 35% and 50% to determine the levels of load magnitude.

To measure MVIC of elbow extensors, the subject was asked to put his hand above the handle in pronation position and have the base of the palm lined-up with the handle. During the MVIC of elbow extensors, the subject was verbally encouraged to extend his elbow against the static resistance as hard as possible. Two kinds of attachment were used to provide the static resistance. The first attachment was the handle that was also used for MVIC of flexors. The subject was asked to push (using base of palm) against the static resistance (handle) as hard as possible (Figure 19, left). The second attachment was a U-shaped metal bar (Figure 19, right). One side of the bar could be fixed to the metal arm of the dynamometer, while the other side provided a platform on which the subject was instructed to lay his forearm. In order to use this attachment, the height of the dynamometer was first lowered until there was no contact between the metal bar and the forearm. The dynamometer was then raised until the bar made contact with the forearm. At the same time, the subject was asked to adjust his foot stance so that the elbow was a couple of inches off the edge of the base of the metal bar to clear the electrodes for anconeus. Care was taken to ensure that there was no shoulder flexion/extension or abduction at the end of the adjustment. With the forearm on the metal bar, the subject was instructed to hold his fist (halfway between supination and pronation) and press down on the bar as hard as possible. After finishing all tasks using the U-shaped metal bar, the height of the dynamometer was adjusted again the same way as described at the beginning of this section. During MVIC of elbow extensors, the subject kept the elbow stationary.

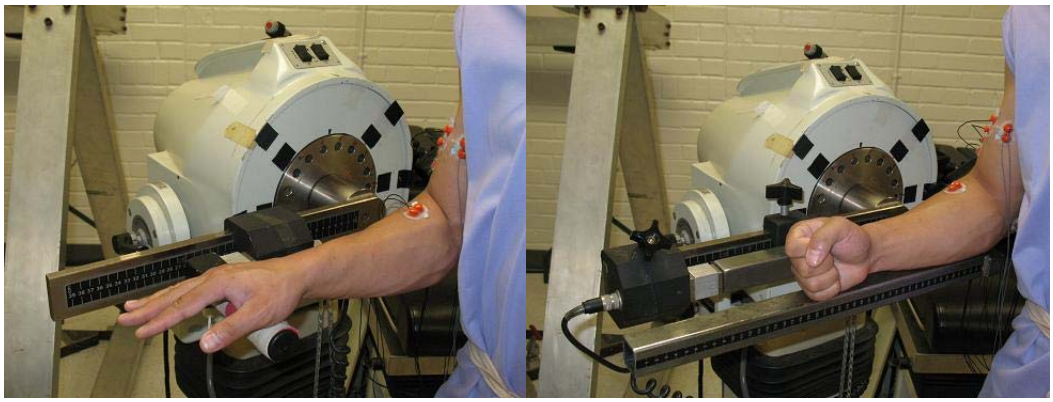

Figure 19 Maximum voluntary isometric contraction of elbow extensors with different attachments provided as static resistance (Left: handle; Right: U-shaped metal bar)

MVIC for both flexors and extensors were measured at elbow flexion angles of 45°, 90°, and 135°, where 0° corresponded with full elbow extension. During each MVIC task, the subject was instructed to reach his maximum capacity in three seconds, and data were collected for five seconds. A one-minute rest break was provided between two consecutive MVIC exertions. A five-minute break was given after all MVIC exertions. An MVIC exertion (either flexion or extension) at a certain angle was carried out twice (each of the two attachments for MVIC of extension was utilized once at each flexion angle). Therefore, there were a total of twelve MVIC sessions, four at each flexion angle. Between the two attempts to exert maximum flexion at 90° elbow flexion, the larger maximum force recorded was entered into the model to calculate the sub-maximal loads in the experimental trials. Among the four maximum EMG values (two from flexion and two from extension) collected for each muscle at a certain elbow flexion angle, the largest value was chosen as the maximum EMG for that muscle at that very flexion angle. The angle-specific maximum EMG data later were used to normalize the EMG activity collected during trials. The normalized data would then enter the EMG-assisted biomechanical model to calculate individual muscle forces. The

details are discussed in Section 6.7.1.

During MVIC exertions at 45° and 135°, the subject was advised to split his feet slightly in the sagittal plane (front-back) to stabilize the whole body and prevent it from leaning forwards or backwards due to the horizontal reaction force from the handle or the U-shaped attachment.

6.4.3. Trials

After the completion of MVIC exertions, the trial phase of the experiment began. Before data collection started, subjects underwent a short training session designed to familiarize the subject with the drill of the isokinetic (dynamic) trials. The training session lasted until subjects felt comfortable with the execution of the techniques (typically between five and ten minutes). Subjects then performed a total of 36 trials, among which 18 were isometric (static) trials (combinations of three levels of load magnitude, three levels of angle, and two repetitions) and 18 were isokinetic (dynamic) trials (combinations of three levels of load, three levels of velocity, and two repetitions). The order of the 36 trials was completely randomized. Three dumbbells were set up that corresponded (approximately) to all three levels of load magnitude. They were laid out side by side at approximately waist height about one foot in front of the subject during trials. The subject would be instructed to pick up a specific dumbbell at the start of each trial and return it to its original spot after finishing the trial. For convenience purposes, three wooden bars were attached to the front of the dynamometer using Velcro tapes, which simulated the metal arm at 45°, 90° and 135° (Figure 20, left). This was done to eliminate the need to reset the angle range for isokinetic trials after completion of an isometric trial.

During an isometric trial, the subject picked up a specific dumbbell as instructed and lined up the dumbbell and forearm with the wooden bar corresponding to the designated angle for that trial (Figure 20, left). After his dumbbell holding arm had reached a stable state (2-3 seconds), the subject informed the experimenter verbally that he was "ready". The data collection then began and lasted for three seconds. During an isokinetic trial, the dynamometer was preset to run passively back and forth under a designated angular velocity within an angle range of 30° to 150° (again with 0° meaning full elbow extension). With the visual guidance from the moving metal arm of the dynamometer, the subject was instructed to keep his forearm parallel to the moving dynamometer arm while holding the dumbbell and keeping upper arm still (with zero shoulder flexion/extension and abduction) (Figure 20, right). For each isokinetic trial, data were collected during a concentric bout (30° to 150° elbow flexion). Rest breaks were given between trials to prevent fatigue from the subject.

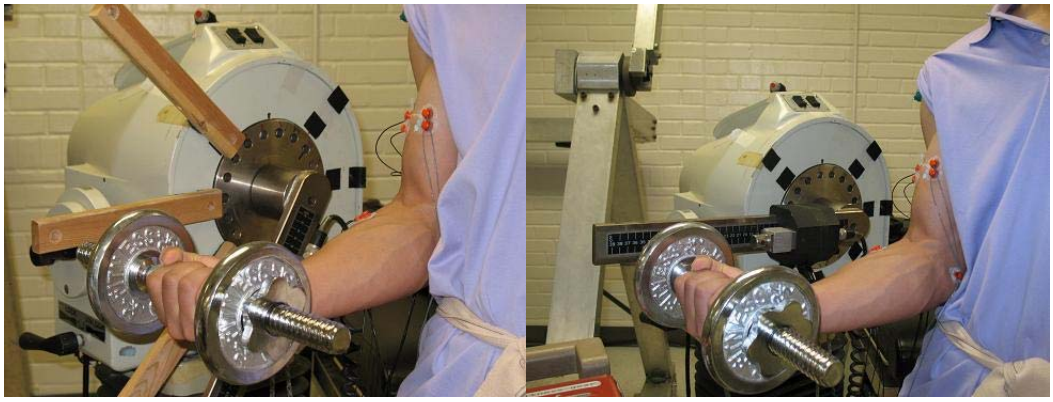

Figure 20 Trail phase of the experiment (Left: isometric trial; Right: isokinetic trial)

6.5. Biomechanical Model

6.5.1. Anthropometric an physiological considerations

The estimates for the mass and center of mass for hand and forearm were taken from Pheasant and Haslegrave (2005) and McConville et al. (1980). The equations for calculating muscle physiological cross sectional areas and moment arms are shown below.

$$PCSA_i = PCSA_i^{AN} \times \left(\frac{MUAC_{90}}{32.30} \right)^2 \tag{6-1}$$

$$r_i = r_i^{Pigeon} \times \frac{MUAC_{90}}{32.30} \tag{6-2}$$

where

$PCSA_i$ is the physiological cross sectional area (PCSA) for muscle *i*;

$PCSA_i^{AN}$ is the PCSA data for muscle *i* taken from An et al. (1981);

$MUAC_{90}$ is the mid-upper arm circumference (MUAC) at 90° elbow flexion;

r_i is the moment arm for muscle *i*;

r_i^{Pigeon} is the moment arm data for muscle *i* taken from Pigeon et al. (1996);

We considered $PCSA_i^{AN}$ and r_i^{Pigeon} as the average values for PCSA and moment arm for muscle *i* I among the general population. Therefore, for an individual subject, we needed to scale his PCSA and moment arm according to the size of his arm. Such a size was measured by $MUAC_{90}$. The population average for $MUAC_{90}$ was obtained (32.20 (cm) as in equations (6-1) and (6-2)) according to military personal anthropometry data (DOD-HDBK-743A, 1991). Therefore, for each subject, the ratio between $MUAC_{90}$ and this average value

was calculated. The squared value of this ratio was used to scale PCSA (in (6-1)). The ratio itself was also used to scale muscle moment arms (in (6-2)). These data were used in both the EMG-assisted model and the EASOM models.

6.5.2. A simplified anatomical model for the elbow

A single-plane (sagittal) anatomical elbow model was established and muscle line of action data were taken from Seireg and Arvikar (1989) to enable calculation of elbow joint reaction forces. We denote the two components of elbow joint reaction force on the humerus as R_x and R_y, where R_x is perpendicular to the axis of humerus and R_y is along the axis of humerus, both in the sagittal plane. It is noted that R_x and R_y are equivalent to a shear and a compression force, respectively, to the humerus. In this model, all muscles were modeled as strings connecting muscle origins and insertions. The geometric locations of the origin and insertion for each muscle relative to the elbow joint at different elbow flexion angles were calculated from data in Seireg and Arvikar (1989). With these location data, the orientation of line of action (in the sagittal plane) for each muscle was obtained. (Appendix i contains the detailed data).

6.6. EASOM Formulation

The elbow joint in this study was assumed to be a single-plane (sagittal) model with single degree of freedom, where four flexors and four extensors were involved in the model. The entropy assisted optimization model (EASOM) used in this study then took on the following form:

$$Minimize \quad (1-W)\sum_{i=1}^{8} x_i^{\,3} + 10^5 * W * \sum_{i=1}^{8}\left[\left(\frac{x_i}{500}\log\frac{x_i}{500}\right) * PCSA_i\right] \tag{6-3}$$

$$Subject\ to \quad \sum_{i=1}^{8} r_i * PCSA_i * x_i = T \tag{6-4}$$

$$0 \le x_i \le 500 \qquad (i = 1,2,\ldots,8) \tag{6-5}$$

where

W is the co-contraction weight factor;

x_i is the muscle stress of muscle i;

$PCSA_i$ is the physiological cross sectional area of muscle i;

r_i is the moment arm for muscle i about the elbow joint in the sagittal plane, and its value is positive if muscle i is agonist and negative if muscle i is antagonist;

T is the torque generated by the handheld load and the mass of forearm and hand around the elbow joint in the sagittal plane.

Compared with the EASOM formulation applied in the pilot study ((4-6) to (4-8)), there are a couple of changes that occurred in the above formulation. First, $PCSA_i$ was added to the entropy term in (6-3), in order to increase the realism of muscle force prediction. Second, the muscle stress limit was replaced with a fixed value of 500 N/cm^2 (as in (6-3) and (6-5)). Such a value was chosen according to Langenderfer et al. (2005). Since this is a single-plane model, only one moment equilibrium equation (6-4) was needed.

6.7. Data processing

6.7.1. EMG signal processing

The raw EMG data were filtered in MatLab using a 15 - 500 Hz pass filter as well as a notch filter that eliminated 60 Hz and its aliases. Once filtered, these signals were rectified (full-wave). This processing applied to the data collected during the experimental trials as well as the maximum voluntary isometric contractions. The EMG data collected during a MVIC exertion were partitioned into 1/8 second windows and the maximum of the 40 windows (5 second collecting period) for each muscle was identified as the maximum EMG value for that muscle during this exertion. For each muscle, the maximum among all four MVIC exertions at a certain flexion angle was picked and used as the denominator in the process of normalizing the trial data corresponding to the same muscle and angle. The EMG data for each isometric trial were averaged across its collecting period. For each of the dynamic trials, the data for angle ranges of 45°±1°, 90°±1°, and 135°±1° were extracted, and averaged for each angle range to be used as the EMG data for that angle level during that trial condition. The normalized EMG data from two replicates for the same task condition were averaged and treated as the single data point for the same condition.

The EASOM was implemented using the Sequential Quadratic Programming algorithms within the optimization toolbox in MatLab 7. The output from a single run of the MatLab program was a vector of eight elements, each corresponding to the predicted muscle force for each of the eight muscles involved. Such an muscle force vector output was denoted as $\widetilde{F}_{pred}$.

6.7.2. EMG-assisted model

An EMG-assisted model was used to convert the empirical EMG data into muscle forces. The equation for the model used for this stage of the study is shown below (Marras and Sommerich, 1991; McGill and Norman, 1986).

$$F_i = \left(\frac{EMG_i(t)}{EMG_{i,\max}} \times f_i(\theta) + f_{i,pe}(\theta) \right) \times f_i(\omega) \times PCSA_i \times gain \qquad (6\text{-}6)$$

where

F_i is the force generated by muscle *i*;

$EMG_i(t)$ denotes the raw EMG signal for muscle *i* at time *t*;

$EMG_{i,\max}$ is the maximum EMG for muscle *i* at the current elbow flexion angle;

θ is the current elbow flexion angle (°);

$f_i(\theta)$ is the force-angle factor for muscle *i* at the current elbow flexion angle (θ);

$f_{i,pe}(\theta)$ is a factor resulting from passive elastic muscle component, for muscle *i* at the current elbow flexion angle (θ);

ω is the current angular velocity (°/s);

$f_i(\omega)$ is the force-velocity factor for muscle *i* at the current angular velocity (ω);

$PCSA_i$ denotes the physiological cross sectional area of muscle *i*.

gain is a constant across all muscles for an individual and shows that person's force generating potential. It represents the maximum force that can be produced per muscle cross sectional area (N/cm^2).

The raw EMG signal muscle *i* ($EMG_i(t)$) was normalized by the maximum EMG ($EMG_{i,\max}$). This first step helped eliminate possible analytical errors resulting from electrode placement, skin abrasion, flesh resistance, muscle fiber density and depth, and electronic channel differences (Mirka, 1991). The force-angle ($f_i(\theta)$) and force-velocity ($f_i(\omega)$) factors were then taken into consideration since all muscles had different force-generating capabilities under different lengths or velocities. The passive elastic component of a muscle could also come into play, in the form of a factor $f_{i,pe}(\theta)$, when the muscle length at current flexion angle was greater than the resting length of the muscle (Chang *et al.*, 1999). It is also noted that the value *gain* was allowed to vary across conditions within a subject (see Discussion for detailed discussion on this issue). The approach to calculate the force-angle factor ($f_i(\theta)$) and the passive elastic component factor (($f_{i,pe}(\theta)$)) was adapted from Chang et al. (1999) (see Appendix ii for detail). The equations used to calculate the force-velocity factors for agonist muscles ($f_{ag}(\omega)$) and antagonist muscles ($f_{ant}(\omega)$) were taken from Benoit and Dowling (2006), shown as follows.

$$f_{ag}(\omega) = 1 - 0.005 \times \omega \qquad (6\text{-}7)$$

$$f_{ant}(\omega) = 1 + 0.008 \times \omega \qquad (6\text{-}8)$$

where

ω is the angular velocity (°/s);

$f_{ag}(\omega)$ is the force-velocity factor for agonist (elbow flexor) muscles;

$f_{ant}(\omega)$ is the force-velocity factor for antagonist (elbow extensor) muscles.

We let $\widetilde{F}_{act}$ denote the actual muscle force vector, which consists of the eight elements each corresponds to the EMG generated muscle force for each of the eight muscles involved in the model.

6.7.3. Modeling the co-contraction weight factor *W*

The modeling of the co-contraction weight factor *W* consisted of two steps. The first step generated condition-specific *W* values using empirical EMG data (Section 6.7.3.1), and the second step established a statistical model that was able to predict *W* value by task variables. The statistical modeling of *W* in terms of task variables could be achieved by both polynomial regression (Section 6.7.3.2) and neural network (Section 6.7.3.3).

6.7.3.1. Generation of condition-specific co-contraction weight factor *W*

The co-contraction weight factor *W* associated with a given task condition was obtained using the empirical EMG data along with the EMG-assisted model. For the given condition, we compared the EMG generated muscle force vector ($\widetilde{F}_{act}$) with a series of EASOM predicted muscle force vectors ($\widetilde{F}_{pred}$) corresponding to a series of co-contraction weight factor values (*W* assigned with values from 0.1 to 1 with an interval of 0.01). Among all 91 *W* values assigned, the co-contraction weight factor for the given condition was chosen such that it yielded the least sum of squared error between $\widetilde{F}_{act}$ and $\widetilde{F}_{pred}$. (Note that both $\widetilde{F}_{act}$ and $\widetilde{F}_{pred}$ were eight-element vectors.)

6.7.3.2. Polynomial regression for *W*

With the condition related co-contraction weight factors (*W*'s) obtained from the previous step for all conditions, the polynomial regression equation associating *W* with load magnitude L (% of capacity), angular velocity V (°/s) and elbow flexion angle A (°) was obtained using stepwise polynomial regression with PROC REG in SAS 9. The variables that were allowed in the regression equation include L, V, A, and their squared terms, where the significance level for each variable to enter and stay in the equation was set at $p<0.05$. Separate equations were established for D and ND. *W* values predicted by this equation were later used in the EASOM model for predicting individual muscle forces.

6.7.3.3.Neural network (backpropagation) modeling of *W*

A backpropagation neural network was considered as an alternative to the regression model described above. As illustrated in Smith (1993), a three-layer (i.e. input, hidden, and output layers) back-propagation neural network was applied to model the relationship between co-contraction weight factor (*W*) and the task variables (L (load), A (angle), V (velocity)). Separate modeling was carried out for dominant and non-dominant elbows. All three task variables were continuous-valued. There were no direct connections from inputs to the output node. The logistic function was used as the mapping function for all nodes, and the adaptive learning rates with momentum was chosen to be the learning law.

According to the guidelines laid out in Masters (1993), we chose to use one layer of hidden neurons. The size of the hidden layer (number of hidden nodes) was selected so that model training can be accomplished within a reasonable time frame and the overfiting issue

could also be avoided (Masters, 1993). The geometric pyramid rule as advocated in Masters (1993) was followed, shown below.

$$hids = \sqrt{ins \times outs} \tag{6-9}$$

where *hids*, *ins* and *outs* denote the numbers of hidden, input and output neurons respectively.

The training paradigm is as follows (according to Masters (1993) and Smith (1993)). With the given training data set, different initial weights were randomly generated and the back propagation model was trained until the point when (1) improvement of the average absolute percent error between the target *W* values associated with the training set and the predicted *W* values is negligible, and (2) the average absolute percent error between the target *W* values associated with the test samples and the predicted *W* is about to creep up (which means overfiting is starting to occur). It should be noted that every time the neural network runs, it starts with randomly generated initial weights. Therefore, for a certain epoch count, the model needs to be run multiple times to quantify the errors associated with the same epoch number.

While the neural network approach was considered in this study, it should be noted that the results of a comparison of the neural network predictions and those of the polynomial regression approach outlined above showed no consistent differences in predictive ability. Therefore, the remainder of this work will present the results of the EASOM model's utilization of the values of W predicted using the polynomial regression approach.

6.8. EASOM Model Evaluation

6.8.1. Comparison with other optimization models

To evaluate the relative performance of the EASOM, a comparison with other established biomechanical optimization models was performed. Unfortunately, many of the optimization models that introduced the concept of stability (either through the objective function or the constraints) are so body region specific (typically spinal models) that it was impossible to develop a straightforward analogue to these models. Our comparison therefore was limited to the linear programming, double-linear programming and non-linear programming (sum of cubed muscle stresses) approaches previously outlined. The adaptations of each of these approaches for the elbow joint are outlined below. In each of these models, n=8 and refers to the same eight muscles used in the EASOM approach.

6.8.1.1. Linear programming (LP)

The formulation of the LP-based model developed for the elbow joint is shown below.

$$Minimize \quad \sum_{i=1}^{8} F_i \tag{6-10}$$

$$Subject\ to \quad \sum_{i=1}^{8} (r_i \times F_i) = M_{ext} \tag{6-11}$$

$$0 \le \frac{F_i}{PCSA_i} \le \sigma_0 \qquad (i = 1,\ldots,n) \tag{6-12}$$

where

F_i is the force generated by muscle *i*;

r_i is the moment arm for muscle *i* about the elbow joint in the sagittal plane;

M_{ext} is the torque generated by external loads and mass of hand and forearm around the elbow joint in the sagittal plane;

$PCSA_i$ is the physiological cross sectional area of muscle *i*;

σ_0 is the upper bound for muscle stress, or muscle stress limit.

6.8.1.2.Double linear programming (DLP)

The DLP-based model formulation is shown as follows.

Stage one:

$$\textit{Minimize} \quad \sigma_0 \tag{6-13}$$

$$\textit{Subject to} \quad \sum_{i=1}^{8}(r_i \times F_i) = M_{ext} \tag{6-14}$$

$$0 \le \frac{F_i}{PCSA_i} \le \sigma_0 \qquad (i = 1,\ldots,n) \tag{6-15}$$

Stage two:

$$\textit{Minimize} \quad \sum_{i=1}^{8} F_i \tag{6-16}$$

$$\textit{Subject to} \quad \sum_{i=1}^{8}(r_i \times F_i) = M_{ext} \tag{6-17}$$

$$0 \le \frac{F_i}{PCSA_i} \le \sigma_0^* \qquad (i = 1,\ldots,n) \tag{6-18}$$

where

σ_0 is the upper bound for muscle stress, or muscle stress limit;

r_i is the moment arm for muscle *i* about the elbow joint in the sagittal plane;

F_i is the force generated by muscle *i*;

M_{ext} is the torque generated by external loads and mass of hand and forearm around the elbow joint in the sagittal plane;

$PCSA_i$ is the physiological cross sectional area of muscle *i*;

σ_0^* is the minimum value of σ_0 obtained from stage one.

6.8.1.3.Non-linear programming – sum of cubed muscle stresses (SCS)

The formulation of the SCS model applied to the elbow joint is shown below.

$$Minimize \quad \sum_{i=1}^{8}\left(\frac{F_i}{PCSA_i}\right)^3 \tag{6-19}$$

$$Subject\ to \quad \sum_{i=1}^{8}(r_i \times F_i) = M_{ext} \tag{6-20}$$

$$0 \le \frac{F_i}{PCSA_i} \le \sigma_0 \qquad (i = 1,\ldots,n) \tag{6-21}$$

where

F_i is the force generated by muscle *i*;

$PCSA_i$ is the physiological cross sectional area of muscle *i*;

r_i is the moment arm for muscle *i* about the elbow joint in the sagittal plane;

M_{ext} is the torque generated by external loads and mass of hand and forearm around the elbow joint in the sagittal plane;

σ_0 is the upper bound for muscle stress, or muscle stress limit.

6.8.2. Measures

In evaluating the quality of predictions of the EASOM modeling approach we considered not only the predictions of the individual muscle forces, but also the overall biomechanical effects through the predicted joint reaction forces. It should be noted here that the muscle values calculated using the EMG-assisted model are considered the "gold-standard" that all predictions are compared against. Therefore, unless otherwise mentioned, any error or R^2 for an optimization approach means the error or R^2 between that optimization approach and the EMG derived results.

6.8.2.1. Muscle force prediction

A preliminary evalution was achieved by calculating the averaged predicited muscle force across all subjects for each muscle and comparing the results among the different modeling approaches (i.e. LP, DLP, SCS, EASOM, and EMG). The quality of the EASOM muscle force predictions was then evaluated by the following measures: (1) average absolute error (per muscle), (2) R^2 (per muscle), and (3) a parital R^2 measure i.e. $R^2_{(EMG)(EASOM),(SCS)}$ (per each agonist muscle). $R^2_{(EMG)(EASOM),(SCS)}$ represents the additional contribution of EASOM on top of SCS. (Recall that SCS constitutes the first component of the objective function of EASOM.) In other words, $R^2_{(EMG)(EASOM),(SCS)}$ shows statistically the contribution of the entropy term. It should be noted that all the above measures were calculated for D and ND groups separately. The equations for calculating the average absolute error and $R^2_{(EMG)(EASOM),(SCS)}$ are shown in (6-22) and (6-23). R^2 values were obtained using MatLab 7. As equation (6-23) shows, calculation of $R^2_{(EMG)(EASOM),(SCS)}$ requires the values of correlation coefficient and R^2 between EMG and SCS. Since SCS approach is unable to predict

antagonist muscle activity, such a correlation coefficient and R^2 do not exist for antagonist muscles. Therefore, we calculated $R^2_{(EMG)(EASOM),(SCS)}$ for the agonist muscles only.

$$(Average\ Absolute\ Error)_i = \frac{\sum_{j=1}^{d} \left| F_{pred}^{i,j} - F_{act}^{i,j} \right|}{d} \qquad (i = 1,\ldots,8) \qquad (6\text{-}22)$$

where

$(Average\ Absolute\ Error)_i$ is the average absolute error for muscle i;

$F_{pred}^{i,j}$ is the EASOM predicted muscle force for muscle i under condition j;

$F_{act}^{i,j}$ is the EMG generated muscle force for muscle i under condition j;

d is the number of all conditions across all subjects in a group (either D or ND).

$$R^2_{(EMG)(EASOM),(SCS)}\Big|_i = \left[\frac{R_{(EMG)(EASOM)}\Big|_i - R_{(EMG)(SCS)}\Big|_i * R_{(EASOM)(SCS)}\Big|_i}{\sqrt{1 - R^2_{(EMG)(SCS)}\Big|_i}\sqrt{1 - R^2_{(EASOM)(SCS)}\Big|_i}} \right]^2 \quad (i = 1,\ldots,4) \qquad (6\text{-}23)$$

where

$R^2_{(EMG)(EASOM),(SCS)}\Big|_i$ is the partial R^2 measure $R^2_{(EMG)(EASOM),(SCS)}$ for agonist muscle i;

$R_{(EMG)(EASOM)}\Big|_i$ is the correlation coefficient between forces for agonist muscle i generated from EMG and EASOM;

$R_{(EMG)(SCS)}\Big|_i$ is the correlation coefficient between forces for agonist muscle i generated from EMG and SCS;

$R_{(EASOM)(SCS)}\Big|_i$ is the correlation coefficient between forces for agonist muscle i generated from EASOM and SCS;

$R^2_{(EMG)(SCS)}\big|_i$ is the R^2 measure between forces for agonist muscle *i* generated from EMG and SCS;

$R^2_{(EASOM)(SCS)}\big|_i$ is the R^2 measure between forces for agonist muscle *i* generated from EASOM and SCS.

6.8.2.2. Joint reaction force prediction

A two-part preliminary evalution was first carried out to examine and compare the trends of averaged estimated R_y (compression force imposed on the humerus) with regard to load magnitude and task kinematics (i.e. static vs. dynamic) among the different modeling approaches (i.e. LP, DLP, SCS, EASOM, and EMG). We only concentrated the preliminary evaluation on the compression force because the majority of the existing literature in the same area focuses on joint compression forces (especially the spinal compression force). Comparisons will be made in this dissertation between the findings from this study and those from the literature (Chapter 8). The first part of the evaluation consisted of calculation of the averaged estimation for R_y (across all subjects) for each level of load magnitude from each of the five different modeling approaches. The average value (across all subjects) for contributions from antagonist muscles to R_y estimations was also derived for each load magnitude level and each modeling approach. Such a contribution was calculated as $(R_y^{ant} / R_y) \times 100\%$, where R_y^{ant} is the estimated compression force imposed on the humerus resulting only from the predicted antagonist muscle forces. The second part of the preliminary evaluation was to obtain the averaged R_y estimations (across all subjects) separately for static and dynamic tasks corresponding to each of the modeling approaches.

The quality of the predictions of the EASOM model for joint loading estimation was then evaluated by (1) average absolute error (for R_x and R_y), (2) average absolute percent error (for R_x and R_y), (3) R^2 (for R_x and R_y), and (4) a parital R^2 measure i.e. $R^2_{(EMG)(EASOM),(SCS)}$ (for R_x and R_y). It should be noted that all the above measures were calculated for D and ND groups separately. The equations for calculating the average absolute error, the average absolute percent error, and $R^2_{(EMG)(EASOM),(SCS)}$ are shown in (6-24), (6-25) and (6-26). R^2 values were attained using MatLab 7.

$$(Average\ Absolute\ Error)_k = \frac{\sum_{j=1}^{d} \left| R_{k,j}^{est} - R_{k,j}^{act} \right|}{d} \qquad (k = x, y) \tag{6-24}$$

$$(Average\ Absolute\ Percent\ Error)_k = \frac{\sum_{j=1}^{d} \left| \frac{R_{k,j}^{est} - R_{k,j}^{act}}{R_{k,j}^{act}} \times 100\% \right|}{d} \quad (k = x, y) \tag{6-25}$$

where

$(Average\ Absolute\ Error)_k$ is the average absolute error for R_k;

$(Average\ Absolute\ Percent\ Error)_k$ is the average absolute percent error for R_k;

$R_{k,j}^{est}$ is the estimated R_k (from EASOM predicted muscle forces) under condition j;

$R_{k,j}^{act}$ is the R_k calculated from EMG generated muscle forces under condition j;

d is the number of all conditions across all subjects in a group (either D or ND).

$$R^2_{(EMG)(EASOM),(SCS)}\Big|_k = \left[\frac{R_{(EMG)(EASOM)}\Big|_k - R_{(EMG)(SCS)}\Big|_k * R_{(EASOM)(SCS)}\Big|_k}{\sqrt{1 - R^2_{(EMG)(SCS)}\Big|_k}\sqrt{1 - R^2_{(EASOM)(SCS)}\Big|_k}} \right]^2 \quad (k = x, y) \tag{6-26}$$

where

$R^2_{(EMG)(EASOM),(SCS)}\big|_k$ is the partial R^2 measure $R^2_{(EMG)(EASOM),(SCS)}$ for the joint reaction force R_k;

$R_{(EMG)(EASOM)}\big|_k$ is the correlation coefficient between joint reaction forces R_k generated from EMG and EASOM;

$R_{(EMG)(SCS)}\big|_k$ is the correlation coefficient between joint reaction forces R_k generated from EMG and SCS;

$R_{(EASOM)(SCS)}\big|_k$ is the correlation coefficient between joint reaction forces R_k generated from EASOM and SCS;

$R^2_{(EMG)(SCS)}\big|_k$ is the R^2 measure between joint reaction forces R_k generated from EMG and SCS;

$R^2_{(EASOM)(SCS)}\big|_k$ is the R^2 measure between joint reaction forces R_k generated from EASOM and SCS.

6.9. Sensitivity Analysis

A twofold sensitivity analysis was performed to test the robustness of the model. Recall that nine subjects went through complete data processing within each group of D and ND, and among those seven belonged to both groups. The first part of the analysis examined how the difference in subject composition between D and ND groups might affect the form of the regression equations for the co-contraction weight factor W (i.e. W_D and W_{ND}), i.e. how the results might differ from those generated from D and ND groups that consisted of exactly the same subjects. To achieve this, only data from the seven overlapping subjects (from both D and ND groups) were used to generate the regression equations for W_D and W_{ND}, and the

results were compared with the regression equations obtained from the full data set (i.e. data from nine subjects each for D and ND groups).

The goal of the second part of the sensitivity analysis was to understand whether and how model performance might be affected by assigning different groups of subjects for model training and model evaluation. Within each group (D or ND), seven subjects were randomly picked. Within the data from each of these chosen subjects, three quarters of the conditions were again randomly selected. These data from the seven subjects were used for model training (development of regression equations for the prediction of *W*), thus made up the *training sample*. The remaining data from these seven subjects formed the *same-group test sample*. All data from the remaining subjects within that group constituted the *independent test sample*. To ensure the quality of model training and fairness during model assessment, such a selection approach might need to be repeated until all levels of each task characteristic (load magnitude, angular velocity and elbow flexion angle) were represented within every subject in each of the three samples. The above procedure is called a *sample draw*. During sensitivity analysis, nine sample draws were carrier out (25% of all possible draws). To maximize the generalizability of the sample draws, each subject needed to serve in the independent test sample exactly twice. For each draw, model performance was evaluated where the measures included average absolute error and R^2 for muscle force prediction and joint loading estimation, as well as average absolute percent error for joint loading estimation only.

Data from same-group test sample shared some common traits as those in the training sample because both data were drawn from the same group of subjects. Unlike the same-group test sample, subjects in the independent test sample were totally different from the

group of subjects from which training data were drawn. Therefore, it would be interesting to evaluate EASOM with both same-group and independent test samples to find out whether the model performance deteriorated from the former to the latter. If so, we wanted to know how much deterioration occurred, and whether different sample draws could change this trend. The predictions of muscle forces and joint reaction forces from each of these sample (training group sample, same-group test sample and independent test sample) were evaluated by comparing these predictions with those of the other optimization models as done with the full sample and outlined in Section 6.8.

7. RESULTS

In this chapter, we first show in Section 7.1 the regression equations (separately for dominant D and non-dominant ND groups) for the co-contraction weight factor *W*, and its relationships with each of the task variables are then presented in graphs in Section 7.2. In Section 7.3, model performance of EASOM is compared with those optimization-based models as shown explicitly in Section 6.8.2. Finally, we will present the results from sensitivity analysis in Section 7.4.

7.1. Polynomial Regression Equations for *W*

Recall that three of the task variables (i.e. load magnitude (L), angular velocity (V), and elbow flexion angle (A)) and their squared terms were allowed to enter the polynomial regression in a stepwise manner (using PROC REG in SAS). Recall that the significance level for each variable to enter and stay in the regression equation was set at $p<0.05$. For the fourth task variable, i.e. dexterity, two different regression equations were established separately for dominant (D) and non-dominant (ND) groups. The resulting regression equations are shown below.

$$W_D = -0.279 + 4.002 \times L - 3.659 \times L^2 + 0.00561 \times V - 0.0000545 \times V^2 \quad (7\text{-}1)$$

$$W_{ND} = -0.289 + 3.790 \times L - 3.273 \times L^2 + 0.00555 \times V - 0.0000627 \times V^2 \quad (7\text{-}2)$$

where

W_D is the co-contraction weight factor for the dominant (D) group;

W_{ND} the co-contraction weight factor for the non-dominant (ND) group;

L is the load magnitude (in percent, e.g. 25.6% or 0.256);

V is the angular velocity (°/s).

The model R^2 values for W_D regression equation (7-1) and W_{ND} regression equation (7-2) are 0.641 and 0.602, respectively. The partial R^2 (i.e. contributions to the model R^2) and p values for the regressor variables for W_D and W_{ND} are shown respectively in Tables 4 and 5 (in descending order of partial R^2 values).

Table 4 Partial R^2 and p values for the regressor variables for W_D

	Partial R^2	p
L	0.535	<0.0001
V	0.063	<0.0001
L^2	0.032	<0.0001
V^2	0.011	0.0121

Table 5 Partial R^2 and p values for the regressor variables for W_{ND}

	Partial R^2	p
L	0.534	<0.0001
V	0.034	<0.0001
L^2	0.021	0.0014
V^2	0.013	0.0083

The regression equations (7-1) and (7-2) show that at the significance level of $p<0.05$, the co-contraction weight factors for both the dominant group (W_D) and the non-dominant group (W_{ND}) respond to load magnitude (L), angular velocity (V) and their squared terms without showing relationship with either elbow flexion angle (A) or its squared term (Equations 7-1 and 7-2). The relationship between W and each individual task variable will be presented in the next section.

7.2. Response of W to Task Variables

Recall that there were a total of 24 task conditions (combinations of three levels of load magnitude L (i.e. 20%, 35% and 50%), four levels of angular velocity V (0°/s, 20°/s, 40°/s and 60°/s), and two levels of elbow flexion angle A (45° and 90°)). With regression equations (7-1) and (7-2), we were able to generate the W values (both W_D and W_{ND}) associated with each task condition.

In order to show the trend of W relative to each individual task variable, for each level of a task variable (L, V or A), average was taken across W (W_D or W_{ND}) values for all conditions at that level and then used to represent the W_D or W_{ND} value at the same level for the corresponding task variable. Taking this approach, we were able to obtain the relationship between W (W_D and W_{ND}) and each task variable which is illustrated in Figures 21, 22 and 23 for load magnitude (L), angular velocity (V) and elbow flexion angle (A) respectively. Figure 21 shows that both W_D and W_{ND} increase (by 92.5% for W_D and 107.9% for W_{ND}) when load magnitude increases from 20% to 50%.

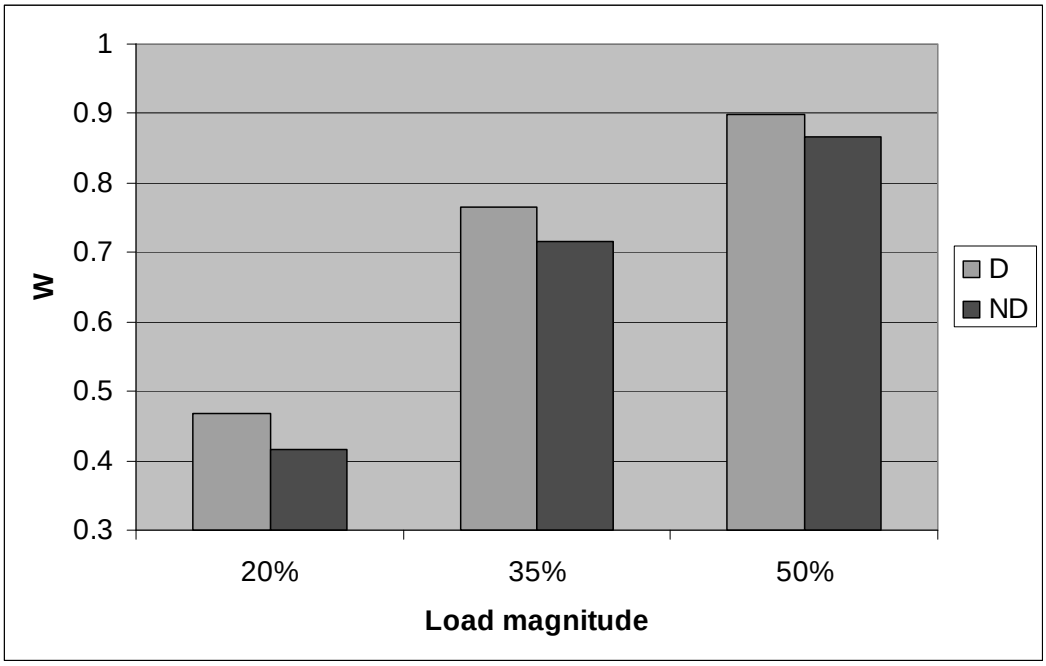

Figure 21 Relationship between *W* and load magnitude (L). (D – dominant, ND – non-dominant)

In Figure 22, W_D increases (by 22.7%) as angular velocity goes from 0°/s up to 60°/s although the increasing slows down between 40°/s and 60°/s. As the same figure displays, W_{ND} responds a bit differently to angular velocity (V) as W_{ND} rises (by 20.7%) with V increasing from 0°/s to 40°/s and decreases (by 2.0%) when V reaches 60°/s from 40°/s. Figure 23 shows that when elbow flexion angle increases from 45° to 90°, both W_D and W_{ND} remain at the same level. It is noted that all three figures show that W_D have overall higher values than W_{ND}. On average, W_D (0.71) is 6.6% higher than W_{ND} (0.67).

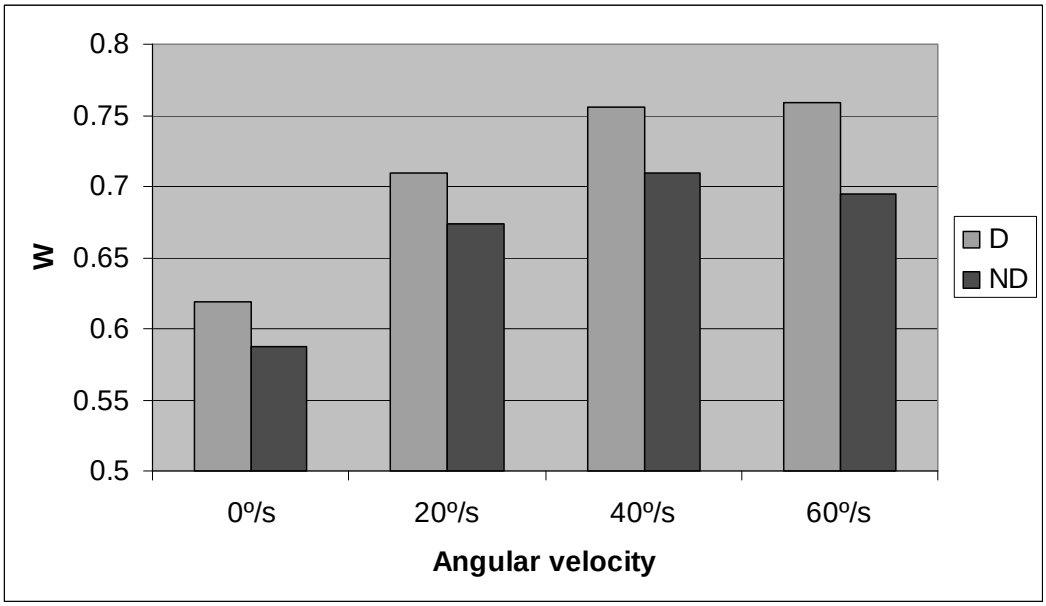

Figure 22 Relationship between *W* and elbow angular velocity (V) . (D – dominant, ND – non-dominant)

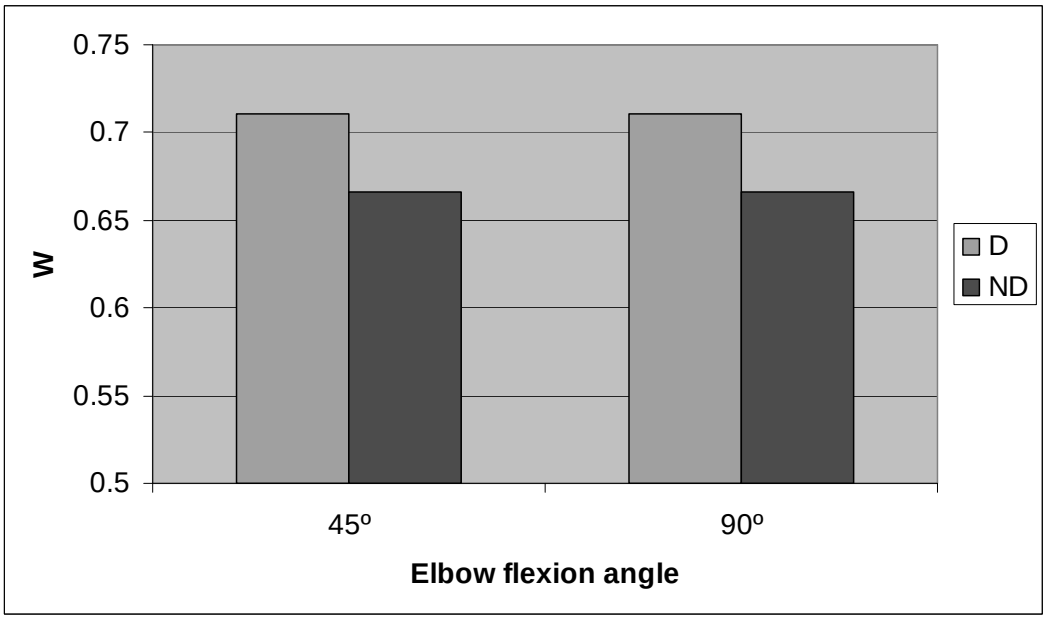

Figure 23 Relationship between *W* and elbow flexion angle (A) . (D – dominant, ND – non-dominant)

7.3. Model Validation

We assumed that the muscle forces generated from the EMG-assisted model (and the resulting joint reaction forces) were the gold standard and were used as baseline to calculate errors (average absolute or average absolute percent) and R^2. For each of these measures, the performance of EASOM was compared with those of LP, DLP and SCS (with formulations shown in Section 6.8.2). In this section, we first present results on the predicted muscle forces followed by the results on the estimated joint reaction forces.

7.3.1. Predicted muscle forces

Before displaying the results on the model evaluation measures in terms of muscle force prediction (as mentioned in Section 6.8.1.1), we first show the averages and standard deviations (across all trials and from subjects from both groups) of predicted muscle forces for all sampled muscles generated from LP, DLP, SCS, EASOM and EMG (Figure 24). Figure 24 demonstrates that LP was only able to predict muscle exertions from brachioradialis (BRD), and that all three approaches of LP, DLP and SCS were unable to generate muscle force predictions for antagonist elbow extensors (i.e. anconeus (ANC), triceps lateral head (TRI(Lt)), triceps long head (TRI(Lg)), and triceps medial head (TRI(Md))). It is also observed from Figure 24 that across all sampled muscles, the averages for muscle force prediction from EASOM were always closer to the averages from EMG than those from LP, DLP and SCS.

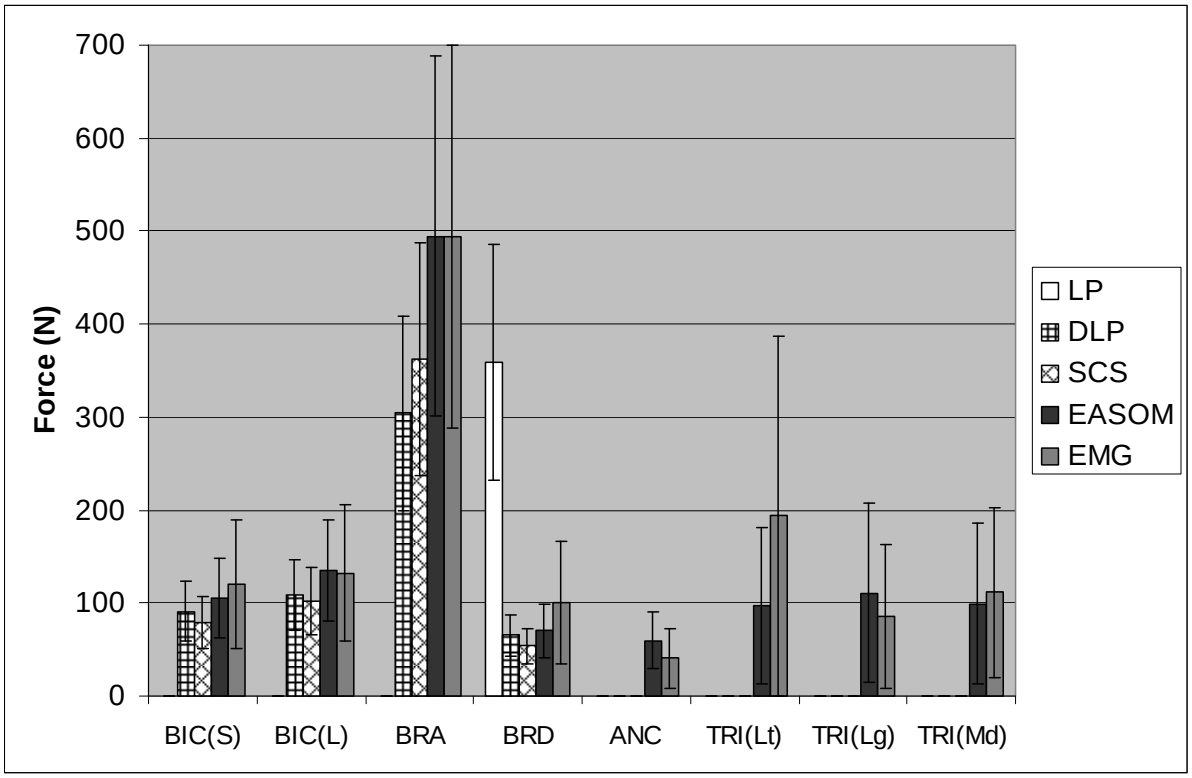

Figure 24 Averaged muscle forces generated from LP, DLP, SCS, EASOM, as well as the EMG-assisted model for each of the eight sampled elbow muscles. (Each error bar denotes one standard deviation.)

7.3.1.1.Average absolute error (AAE)

The results show that EASOM produced lower average absolute errors (AAEs) than LP, DLP, and SCS for all muscle force predictions, for both dominant D (Figure 25) and non-dominant ND (Figure 26) groups. For the D group, the range of AAEs (in N) in muscle force predictions across all muscles for EASOM was from 26.2 to 140.7, compared with 48.7 to 530.8 for LP, 40.4 to 251.7 for DLP, and 44.5 to 251.7 for SCS (Figure 25). For the ND group such a range for EASOM was from 26.8 to 100.7, compared with 32.7 to 456.8 for LP, 31.8 to 163.5 for DLP, and 32.7 to 136.4 for SCS (Figure 26).

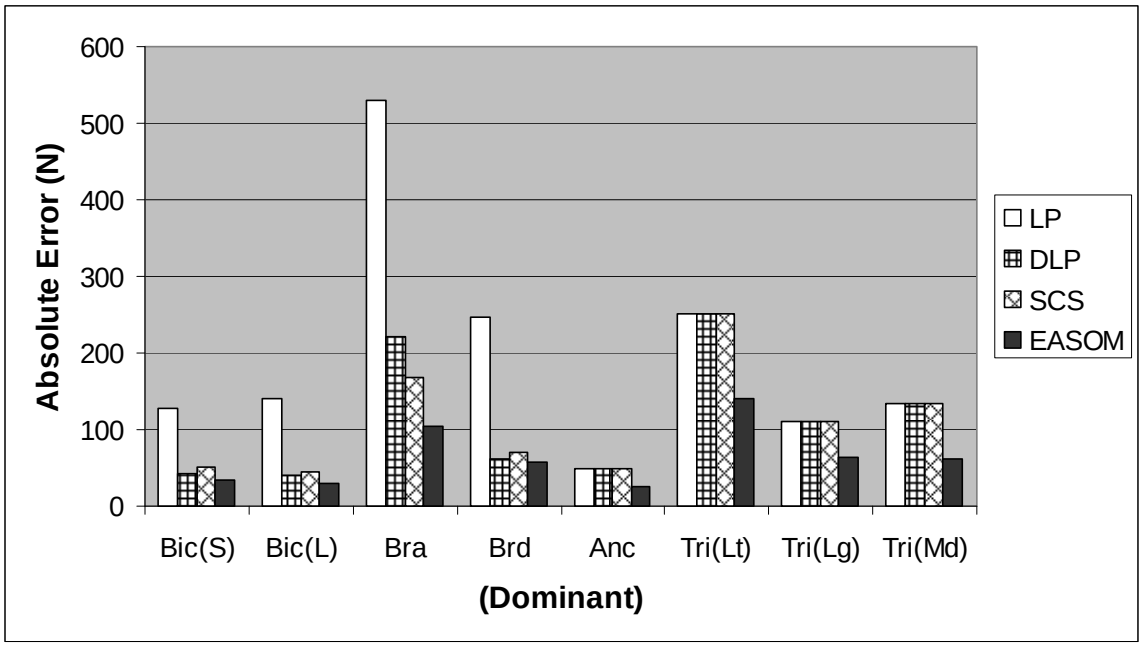

Figure 25 Average absolute error between muscles forces generated from optimization (shown in legend) and empirical EMG for the dominant elbow

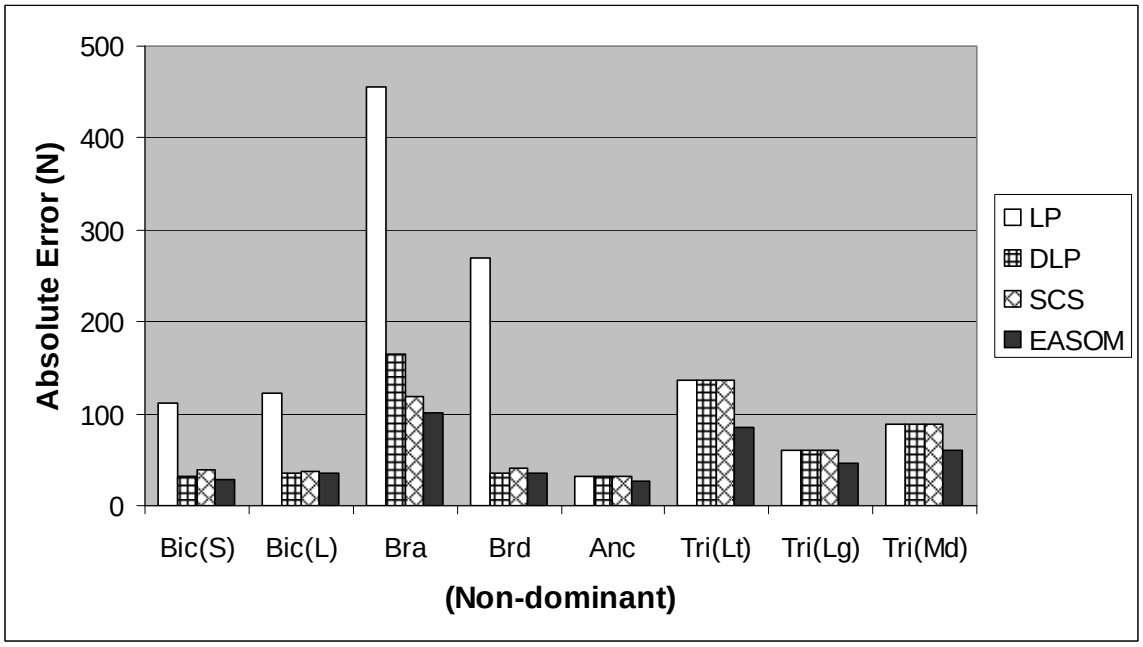

Figure 26 Average absolute error between muscles forces generated from optimization (shown in legend) and empirical EMG for the non-dominant elbow

7.3.1.2.R^2

Since all three optimization approaches of LP, DLP and SCS predicted muscle forces from antagonist elbow extensors to be zero, R^2 values could not be calculated for those muscles (i.e. anconeus (Anc), triceps lateral head (Tri(Lt)), triceps long head (Tri(Lg)), and triceps medial head (Tri(Md))) associated with LP, DLP and SCS (Figures 27 and 28). Therefore, only R^2 values for the agonist elbow flexors were compared among optimization models. Figure 27 shows that for the agonist elbow flexors in the D group, EASOM yielded higher R^2 values than all three approaches of LP, DLP and SCS for all except brachioradialis (Brd, with R^2 values from EASOM lower than LP and DLP). For the D group, the range of R^2 values across all agonist muscles for EASOM was from 0.18 to 0.73, compared with 0 to 0.26, 0.20 to 0.60, and 0.18 to 0.58 for LP, DLP and SCS respectively. It is also noted that R^2 values across all antagonist elbow extensors for EASOM ranged from 0.26 to 0.46. As shown in Figure 28, for the agonist elbow flexors in the ND group, R^2 values from EASOM were never higher than all of LP, DLP and SCS approaches. For all agonist (flexor) muscles (i.e. biceps short head (Bic(S)), biceps long head (Bic(L)), brachialis (Bra), and brachioradialis (Brd)), the R^2 value from EASOM was lower than DLP and SCS. For brachioradialis (Brd), EASOM yielded an R^2 value that was also lower than LP. For the ND group, the range of R^2 values across all agonist muscles for EASOM was from 0.11 to 0.56, compared with 0 to 0.18, 0.13 to 0.60, and 0.11 to 0.60 for LP, DLP and SCS respectively. It is also noted that R^2 values across all antagonist elbow extensors for EASOM ranged from 0.05 to 0.37 (Figure 28).

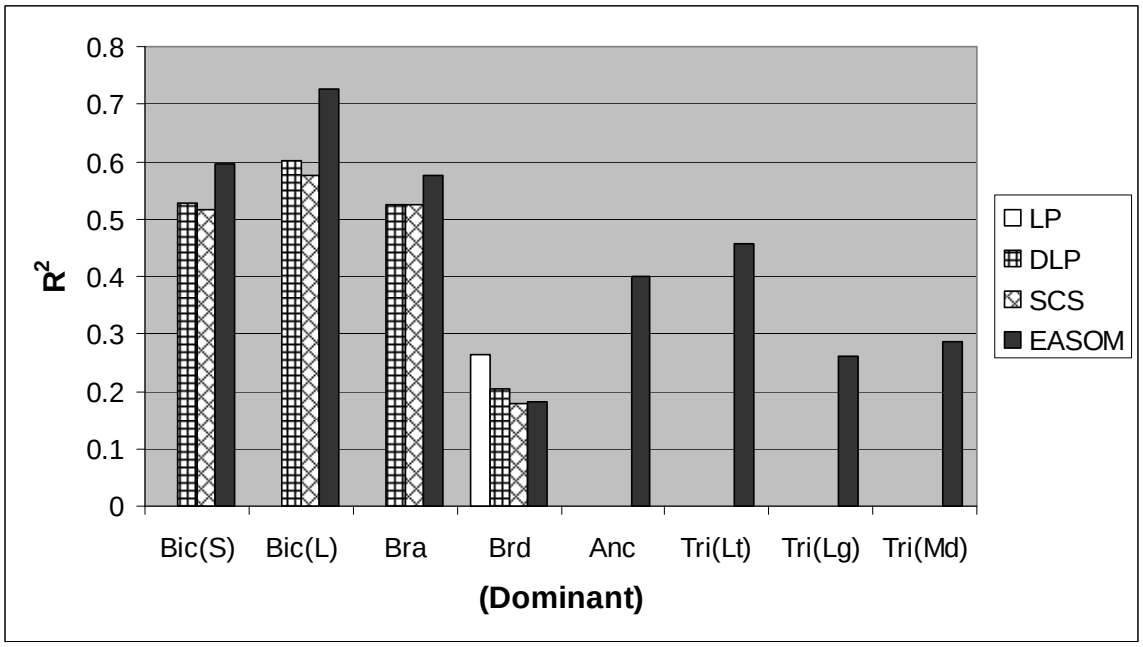

Figure 27 R^2 between muscles forces generated from optimization (shown in legend) and empirical EMG for the dominant elbow

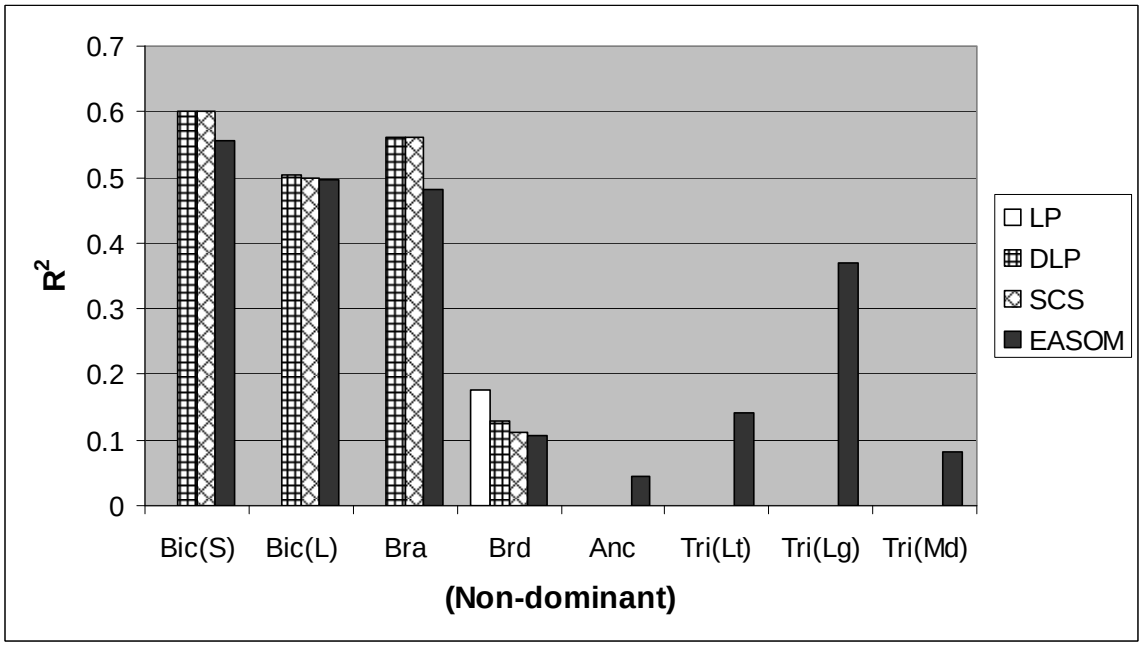

Figure 28 R^2 between muscles forces generated from optimization (shown in legend) and empirical EMG for the non-dominant elbow

7.3.1.3.Partial R^2 ($R^2_{(EMG)(EASOM),(SCS)}$)

Recall that values of $R^2_{(EMG)(EASOM),(SCS)}$ were only calculated for the agonist muscles (Section 6.8.2.1). As Table 6 shows, the value of $R^2_{(EMG)(EASOM),(SCS)}$ ranges from 0.0100 (brachioradialis) to 0.3616 (biceps long head) for the D groups and from 0.0001 (brachialis) to 0.0324 (biceps long head) for the ND group.

Table 6 Values of $R^2_{(EMG)(EASOM),(SCS)}$ for agonist muscle forces for each of the D and ND groups

	Biceps short head	Biceps long head	Brachialis	Brachioradialis
D	0.1753	0.3616	0.1143	0.0100
ND	0.0118	0.0324	0.0001	0.0016

7.3.2. Estimated joint reaction forces

In this section, we will present the results on model evaluation measures with regard to joint reaction force estimation (as described in Section 6.8.1.2). Before presentation of these results, we first show the averages and standard devations (across all trials and from subjects from both groups) for estimations of R_y (compression force imposed on the humerus) at all three levels of load magnitude generated from LP, DLP, SCS, EASOM and EMG (Figure 29). Figure 29 also shows at each load magnitude level and each modeling approach, the average for the contribution (in percent) from the antagonist muscles to R_y. Such a contribution was observed to be zero for LP, DLP and SCS at all load magnitude levels. For EASOM, the contributions were 29.8%, 29.5% and 30.7% for the increasing levels of load magnitude (i.e. 20%, 35% and 50% of miximum capacity respectively). For EMG, such contributions were 31.9%, 33.1% and 34.8% for 20%, 35% and 50% of miximum capacity respectively. In addition to the trend of R_y estimations relative to load magnitude (as shown

in Figure 29), we show in Figure 30 the averages and standard devations of R_y estimations for both static and dynamic trials generated from LP, DLP, SCS, EASOM and EMG. It is observed that R_y estimations from LP, DLP and SCS remain the same beween static and dynamic trials, while averaged R_y estimations from both EASOM and EMG increase from static trials to dynamic trials (Figure 30).

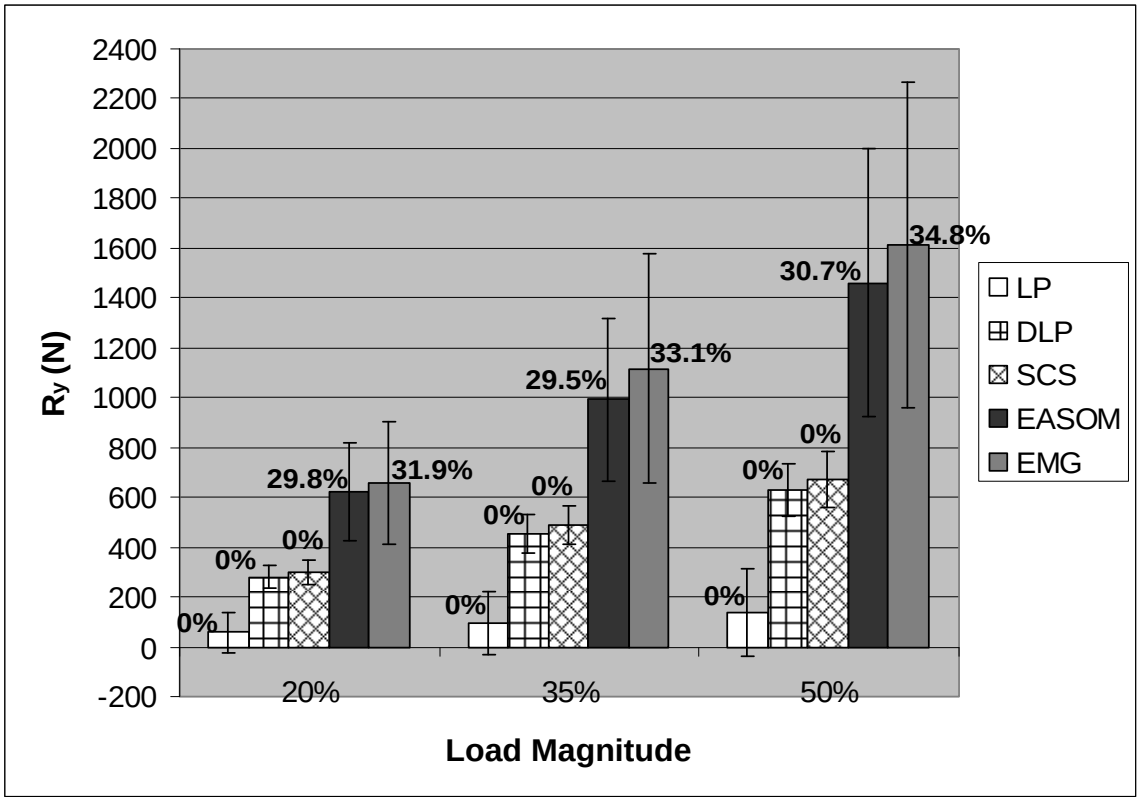

Figure 29 Averaged elbow joint compression (R_y) estimations from LP, DLP, SCS, EASOM, as well as the EMG-assisted model at each level of load magnitude. (Each error bar denotes one standard deviation.) The percent value above each bar represents the percent of the R_y estimation that is contributed by the antagonist muscles.

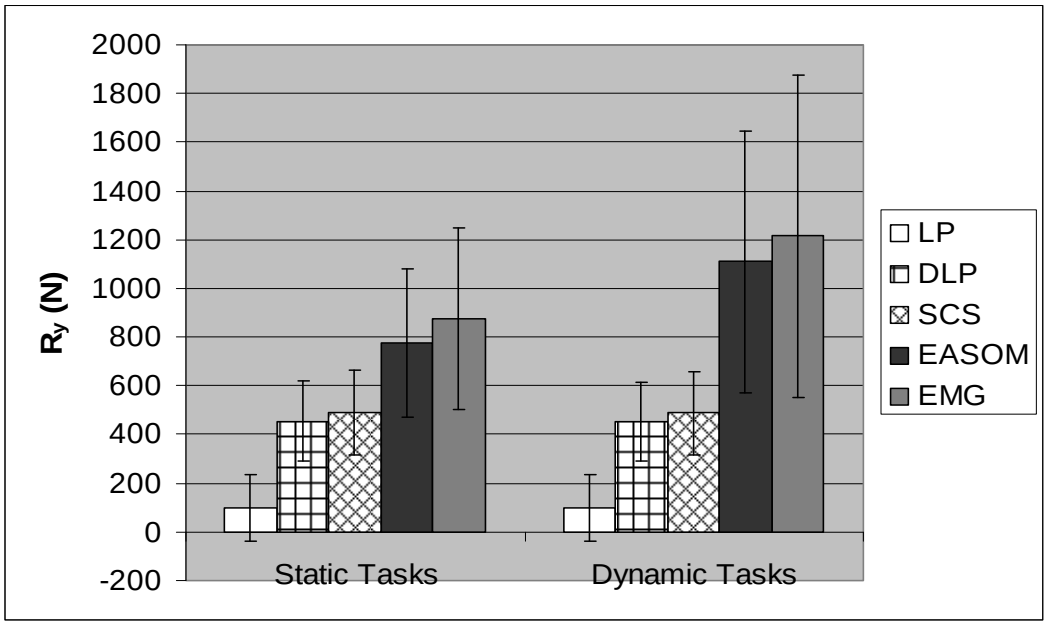

Figure 30 Averaged elbow joint compression (R_y) estimations from LP, DLP, SCS, EASOM, as well as the EMG-assisted model among all static task conditions and among all dynamic task conditions. (Each error bar denotes one standard deviation.)

7.3.2.1.Average absolute error

For estimation of both R_x and R_y in the dominant D group (as shown in Figure 31), EASOM generated lower average absolute errors (AAEs) than LP, DLP and SCS. The AAEs (in N) in estimation of R_x and R_y for EASOM is 34.9 and 345.8, compared with 121.3 and 1203.7, 56.8 and 837.7, and 59.8 and 804.1 for LP, DLP and SCS respectively (Figure 31).

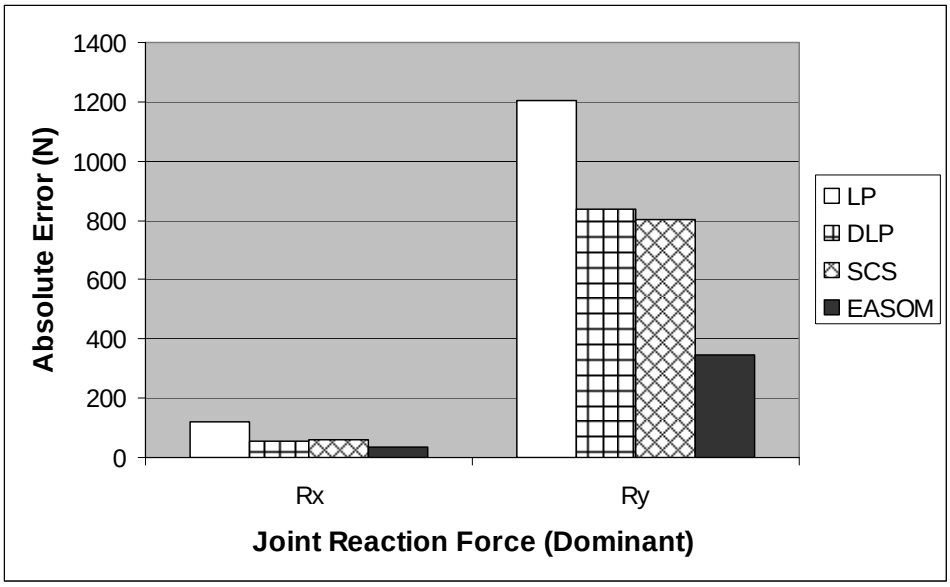

Figure 31 Average absolute error between joint reaction forces calculated from muscle forces predicted by optimization (shown in legends) and empirical EMG data for the dominant elbow

For the non-dominant ND group, the AAEs (in N) generated by EASOM in estimation of both R_x and R_y were lower than those resulting from LP, DLP and SCS (Figure 32). Such AAEs for EASOM were 29.4 and 262.5, compared with 140.8 and 863.2, 30.7 and 514.8, and 33.1 and 482.8 for LP, DLP and SCS respectively (Figure 32).

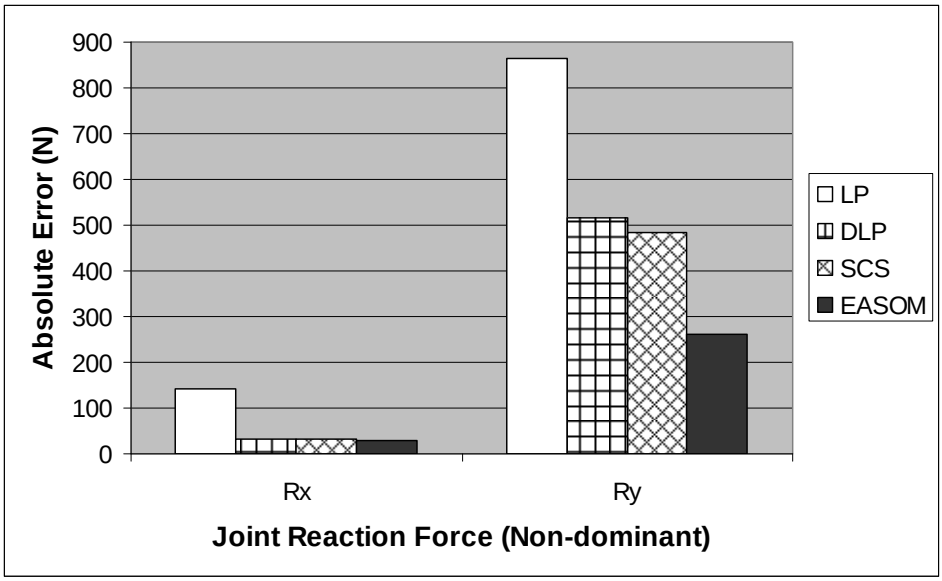

Figure 32 Average absolute error between joint reaction forces calculated from muscle forces predicted by optimization (shown in legends) and empirical EMG data for the non-dominant elbow

7.3.2.2.Average absolute percent error

For the dominant D group, the average absolute percent errors (AAPEs) in estimation of R_x and R_y for EASOM were 21.1% and 24.2%, compared with 78.0% and 90.8%, 31.3% and 58.9%, and 33.3% and 55.9% for LP, DLP and SCS respectively (Figure 33). Therefore, for the D group EASOM generated lower AAPEs in joint loading estimation than LP, DLP and SCS.

Figure 34 shows that for the non-dominant ND group, AAPEs in estimating R_x and R_y for EASOM were 21.6% and 25.9%, compared with 107.8% and 89.4%, 21.7% and 50.8%, and 23.7% and 47.3% for LP, DLP and SCS respectively. Thus, like in the D group, for the ND group EASOM yielded lower AAPEs in joint loading estimation than LP, DLP and SCS (Figure 34).

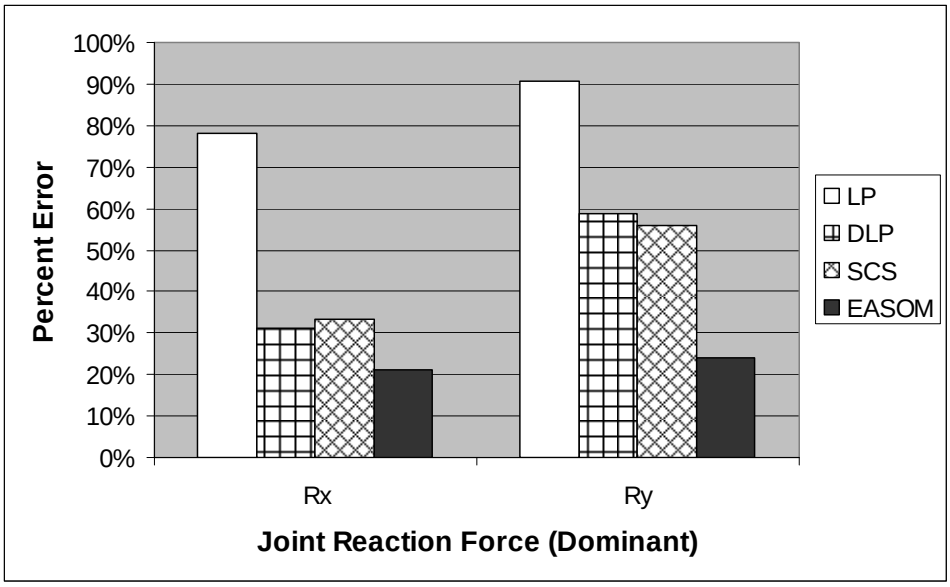

Figure 33 Average absolute percent error between joint reaction forces calculated from muscle forces predicted by optimization (shown in legends) and empirical EMG data for the dominant elbow

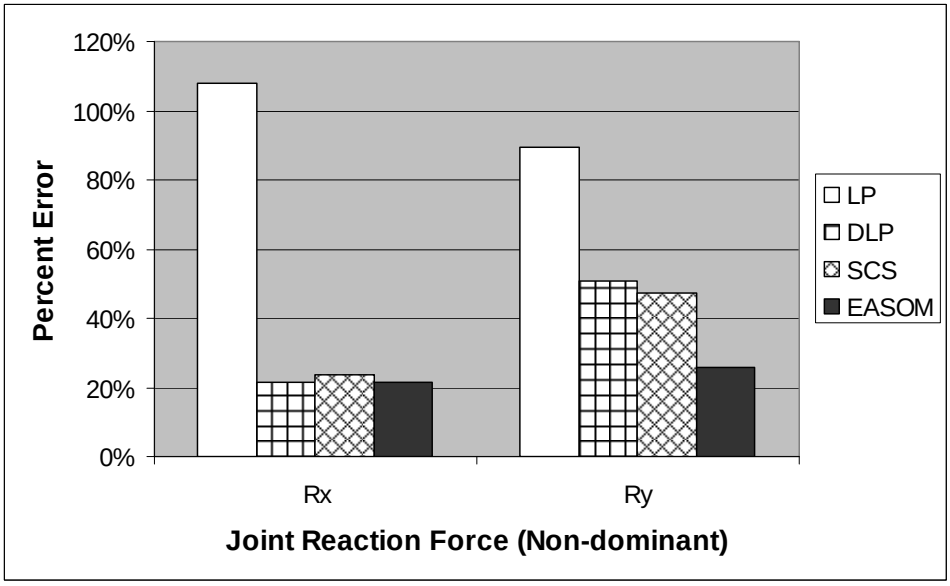

Figure 34 Average absolute percent error between joint reaction forces calculated from muscle forces predicted by optimization (shown in legends) and empirical EMG data for the non-dominant elbow

7.3.2.3.R^2

For the dominant D group, EASOM generated R^2 values in estimation of R_x and R_y that were higher than all three approaches of LP, DLP and SCS (Figure 35). The R^2 values in estimating R_x and R_y for EASOM were 0.72 and 0.49, compared with 0.66 and 0.01, 0.69 and 0.30, and 0.68 and 0.31 for LP, DLP and SCS respectively (Figure 35).

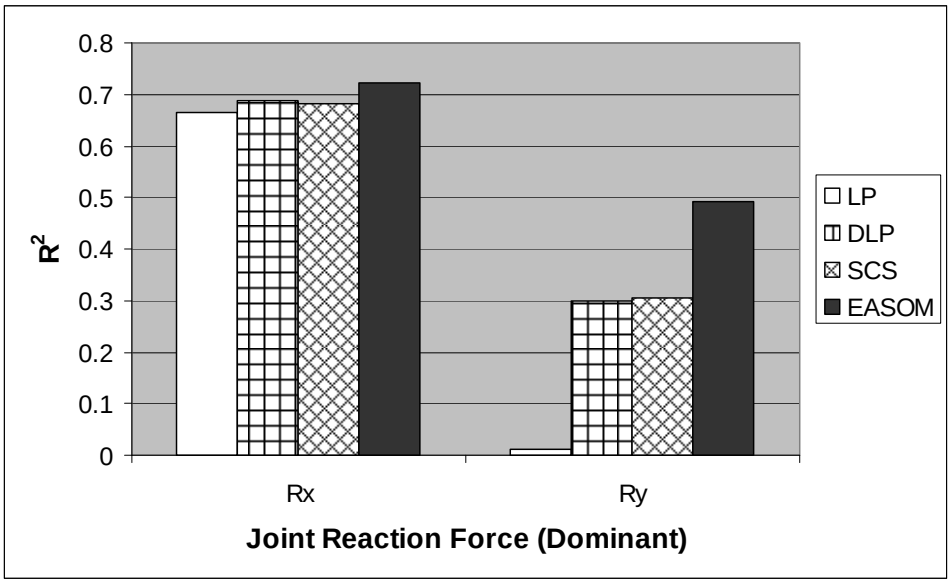

Figure 35 R^2 between joint reaction forces calculated from muscle forces predicted by optimization (shown in legends) and empirical EMG data for the dominant elbow

Figure 36 shows that for the non-dominant ND group, the R^2 values in estimation of R_x and R_y generated by EASOM were 0.76 and 0.38, compared with 0.73 and 0.05, 0.80 and 0.48, and 0.80 and 0.48 for LP, DLP and SCS respectively. Thus, for the ND group, the only occasions when EASOM generated a higher R^2 value in estimating R_x or R_y were when the R^2 values in estimation of R_x and R_y from EASOM (0.76 and 0.40 respectively) were higher than those from LP (0.73 and 0.05) (Figure 36).

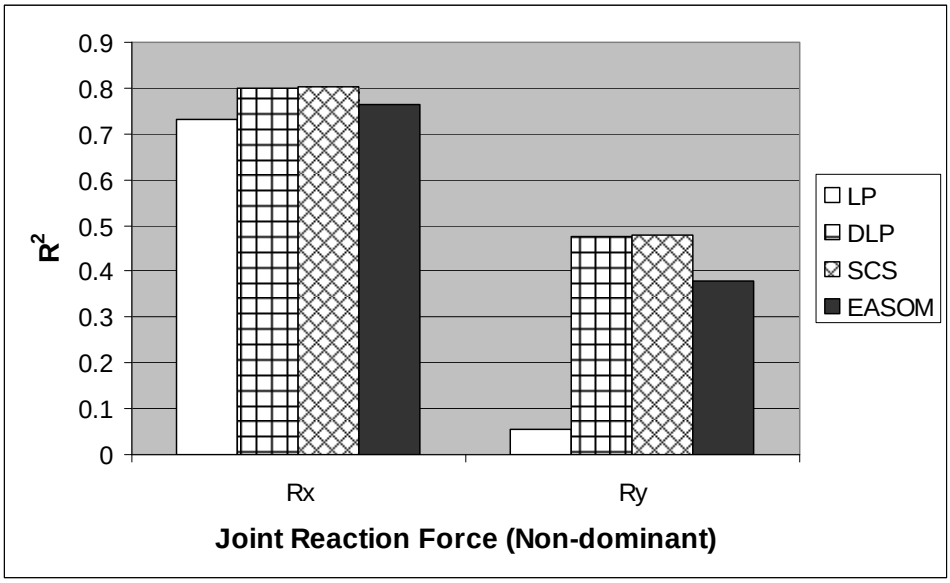

Figure 36 R^2 between joint reaction forces calculated from muscle forces predicted by optimization (shown in legends) and empirical EMG data for the non-dominant elbow

7.3.2.4.Partial R^2 ($R^2_{(EMG)(EASOM),(SCS)}$)

Table 7 shows that the values of $R^2_{(EMG)(EASOM),(SCS)}$ for R_x and R_y are 0.1235 and 0.2785 respectively for the D group and 0.0004 and 0.0578 respectively for the ND groups.

Table 7 Values of $R^2_{(EMG)(EASOM),(SCS)}$ for R_x and R_y for each of the D and ND groups

	R_x	R_y
D	0.1235	0.2785
ND	0.0004	0.0578

7.4. Sensitivity analysis

7.4.1. Regression equations for W (W_D and W_{ND})

Let the W regression equation assume the following general form:

$$W = C_0 + C_L \times L + C_{L^2} \times L^2 + C_V \times V + C_{V^2} \times V^2 + C_A \times A + C_{A^2} \times A^2 \qquad (7\text{-}3)$$

where

C_0, C_L, C_L^2, C_V, C_V^2, C_A, and C_A^2 are coefficients that define the form of the regression equation.

In the first part of the sensitivity analysis, the data from the seven overlapping subjects from D and ND groups were used to generate the regression equations for W_D and W_{ND}. The resulting values for the coefficients (along with those from the full data set within each group) are shown in Table 8. For the D group, the regression equations for W_D generated from both sets of data agree in form in that both consist of the following variables only: L, L^2, V, and V^2. For the ND group, the two regression equations for W_{ND} differ in that the equation generated from the overlapping subjects (within ND) allowed A^2 to enter while the one from the full data set did not. The *p* values for regressor variables and model R^2 values for the W_D and W_{ND} regression equations (along with those values associated with the full data set within each group) are shown in Table 9.

Table 8 Values for coefficients in *W* regression equations (both D and ND) generated from the seven overlapping subjects within each group as well as from the full data set (as obtained in Equations 7-1 and 7-2).

		C_0	C_L	C_L^2	C_V	C_V^2	C_A	C_A^2
D	**Overlapping Subjects**	**-0.271**	**4.249**	**-4.089**	**0.00463**	**-0.0000406**	**0**	**0**
	Full Data Set	-0.279	4.002	-3.659	0.00561	-0.0000545	0	0
ND	**Overlapping Subjects**	**-0.274**	**4.019**	**-3.586**	**0.00439**	**-0.0000441**	**0**	**-0.00000655**
	Full Data Set	-0.289	3.79	-3.273	0.00555	-0.0000627	0	0

Table 9 *p* values for regressor variables and model R^2 values for *W* regression equations (both D and ND) generated from the seven overlapping subjects as well as from the full data set

		p value						Model R^2
		L	L^2	V	V^2	A	A^2	
D	**Overlapping Subjects**	**<0.0001**	**<0.0001**	**<0.0001**	**0.0333**	**-**	**-**	**0.739**
	Full Data Set	<0.0001	<0.0001	<0.0001	0.0121	-	-	0.641
ND	**Overlapping Subjects**	**<0.0001**	**0.0002**	**<0.0001**	**0.0478**	**-**	**0.0271**	**0.700**
	Full Data Set	<0.0001	0.0014	<0.0001	0.0083	-	-	0.602

Recall that during the second part of the sensitivity analysis, nine sample draws were carried out for each of the dominant D and non-dominant ND groups. Within each group, the training sample obtained from a draw was used to establish a polynomial regression equation associating W (W_D or W_{ND}) with task variables. Tables 10 and 11 show the values for those coefficients resulting from the nine sample draws within the dominant D group and the non-dominant ND group, respectively. The average and standard deviation for each coefficient across the nine draws, along with the values for the coefficients generated from the full data set within each group (as in Equations (7-1) and (7-2)) are also displayed at the last row in each table.

Table 10 Values for coefficients in *W* regression equations (dominant) resulting from the nine sample draws, along with the average and standard deviation for each coefficient. The last row shows the coefficients generated from the full data set (as obtained in Equation (7-1).

Sample Draw Number	C_0	C_L	C_L^2	C_V	C_V^2	C_A	C_A^2
1	-0.302	4.144	-3.747	0.00247	0	0	0
2	-0.272	3.844	-3.445	0.00629	-0.0000592	0	0
3	-0.352	4.528	-4.393	0.00507	-0.0000453	0	0
4	-0.312	4.211	-3.866	0.00222	0	0	0
5	-0.214	3.862	-3.582	0.00240	0	0	0
6	-0.406	4.986	-5.024	0.00195	0	0	0
7	-0.301	3.758	-3.178	0.00641	-0.0000654	0	0
8	-0.262	4.216	-4.054	0.00567	-0.0000523	0	0
9	-0.323	4.296	-4.001	0.00234	0	0	0
Average	**-0.305**	**4.205**	**-3.921**	**0.00387**	**-0.0000250**	**0**	**0**
Standard Deviation	**0.055**	**0.383**	**0.547**	**0.00193**	**0.0000298**	**0**	**0**
Full Data Set (D)	***-0.279***	***4.002***	***-3.659***	***0.00561***	***-0.0000545***	***0***	***0***

Table 11 Values for coefficients in W regression equations (non-dominant) resulting from the nine sample draws, along with the average and standard deviation for each coefficient. The last row shows the coefficients generated from the full data set (as obtained in Equation (7-2).

Sample Draw Number	C_0	C_L	C_L^2	C_V	C_V^2	C_A	C_A^2
1	-0.356	4.804	-4.554	0.00156	0	-0.00125	0
2	0.064	1.458	0	0.00732	-0.0000881	0	0
3	-0.208	3.555	-3.037	0.00210	0	0	0
4	-0.270	4.051	-3.689	0.00117	0	0	0
5	-0.315	3.588	-2.813	0.00638	-0.0000791	0	0
6	-0.136	3.843	-3.511	0.00178	0	-0.00095	0
7	-0.459	5.019	-4.961	0.00200	0	0	0
8	-0.355	3.692	-2.966	0.00659	-0.0000727	0	0
9	0.064	1.407	0	0.00855	-0.0001040	0	0
Average	**-0.219**	**3.491**	**-2.837**	**0.00416**	**-0.0000380**	**-0.00024**	**0**
Standard Deviation	**0.185**	**1.276**	**1.760**	**0.00297**	**0.0000461**	**0.00049**	**0**
Full Data Set (ND)	***-0.289***	***3.790***	***-3.273***	***0.00555***	***-0.0000627***	***0***	***0***

Table 10 shows that for W_D, variables L, L^2 and V showed up in all equations from the nine sample draws, and the variable V^2 entered the equations four out of nine times. Neither A or A^2 appeared in any of the regression equations for W_D from the nine sample draws. Therefore, four out of the nine sample draws generated W_D regression equations that

contain exactly the same set of variables (i.e. L, L^2, V, and V^2) as what resulted from the full data set within the D group. For W_{ND} as Table 11 shows, L and V entered all nine regression equations, followed by L^2 (seven out of nine times), V^2 (four out of nine times) and A (two out of nine times). A^2 did not appear in any of the regression equations for W_{ND} from the nine sample draws. Only two out of the nine sample draws generated W_{ND} regression equations that contain exactly the same set of variables (i.e. L, L^2, V, and V^2) as the resulting resulting W_{ND} regression equation generated from the full data set for the ND group. It is also observed from Tables 10 and 11 that for both D and ND groups, the coefficients generated from full data set are all within one standard deviation from the average values from the nine sample draws. The *p* values for regressor variables and model R^2 values for the W_D and W_{ND} regression equations associated with each sample draw within D and ND groups are shown in Tables 12 and 13 respectively, along with those values associated with the full data set within each group (located at the last row in each table).

Table 12 *p* values for regressor variables and model R^2 values for W_D regression equations (dominant) resulting from the nine sample draws, along with those values associated with the full data set (D)

Sample Draw Number (D)	*p* value				Model R^2
	L	L^2	V	V^2	
1	<0.0001	0.0029	0.0001	-	0.602
2	<0.0001	0.0033	<0.0001	0.0474	0.623
3	<0.0001	<0.0001	<0.0001	0.0128	0.815
4	<0.0001	0.0003	<0.0001	-	0.660
5	<0.0001	0.0044	<0.0001	-	0.602
6	<0.0001	0.0002	0.0001	-	0.659
7	<0.0001	0.0047	<0.0001	0.0165	0.693
8	<0.0001	<0.0001	<0.0001	0.0096	0.766
9	<0.0001	0.0006	<0.0001	-	0.646
Full Data Set (D)	***<0.0001***	***<0.0001***	***<0.0001***	***0.0121***	***0.641***

Table 13 *p* values for regressor variables and model R^2 values for W_{ND} regression equations (non-dominant) resulting from the nine sample draws, along with those values associated with the full data set (ND)

Sample Draw Number (ND)	*p* value					Model R^2
	L	L^2	V	V^2	A	
1	<0.0001	<0.0001	0.0002	-	0.0023	0.770
2	<0.0001	-	0.0022	0.0162	-	0.530
3	<0.0001	0.0288	0.0007	-	-	0.554
4	<0.0001	0.0080	0.0332	-	-	0.567
5	<0.0001	0.0293	0.0039	0.0115	-	0.634
6	<0.0001	0.0015	0.0002	-	0.0268	0.682
7	<0.0001	0.0010	0.0010	-	-	0.576
8	<0.0001	0.0095	<0.0001	0.0069	-	0.712
9	<0.0001	-	0.0006	0.0040	-	0.543
Full Data Set (ND)	***<0.0001***	***0.0014***	***<0.0001***	***0.0083***	**-**	***0.602***

7.4.2. Model validation

During the second part of the sensitivity analysis, nine sample draws were carried out, which yielded nine training samples each for D and ND, nine same-group test samples each for both groups, as well as nine independent test samples each for D and ND. Recall that the measures used to evaluate model performance include average absolute error (AAE), average absolute percent error (AAPE), and R^2. In order to investigate the sensitivity of model performance in response to different sample draws, within each group of nine samples, average (and standard deviation) for each measure was calculated across the nine values (for that measure) resulting from the nine samples. In this section, we compare such average (and standard deviation) results from EASOM with those from LP, DLP and SCS, on the training sample data (Table 14 for dominant D and Table 15 for non-dominant ND), same-group test sample data (Table 16 for D and Table 17 for ND), and independent test sample data (Table 18 for D and Table 19 for ND).

7.4.2.1.Muscle force predictions

The results show that for all muscles in D group and all antagonist (extensor) muscles in ND group, EASOM always generated lower averaged AAE than LP, DLP and SCS, for all three types of samples (Tables 14 to 19). This however was not the case with some of the agonist (flexor) muscles in ND group. For the ND group, with training samples, averaged AAE for biceps long head (BIC(L)) from EASOM (36.19 N) was higher than DLP (34.93 N) and slightly higher than SCS (36.15 N), and averaged AAE for brachioradialis (BRD) from EASOM (35.03 N) was higher than DLP (34.75 N) (Table 15). With same-group test samples, the averaged AAE for BIC(L) from EASOM (38.56 N) was higher than both DLP (35.95 N) and SCS (37.08) (Table 17). With independent test samples, the averaged AAE for BIC(L) from EASOM (38.38 N) was higher than both DLP (35.14 N) and SCS (36.24), and the averaged AAE for BRD from EASOM (35.00 N) was higher than DLP (34.69 N) (Table 19).

7.4.2.2. Joint reaction force estimations

Within the dominant D group, for all of the training samples, same-group test samples and independent test samples, EASOM produced lower averaged AAEs and AAPEs in R_x and R_y than LP, DLP and SCS (Tables 14, 16 and 18).

Within the non-dominant ND group, EASOM produced lower averaged AAEs and AAPEs in R_y than LP, DLP and SCS for all of the training samples, same-group test samples and independent test samples. However, averaged AAE and AAPE in R_x for same-group test sample from EASOM (31.76 N and 22.18% respectively) were higher than those from DLP (30.81 N and 21.44%) (Table 17). For independent test sample (Table 19), EASOM

generated averaged AAE and AAPE in R_x (31.88 N and 23.13%) that were higher than those from DLP (30.71 N and 21.73%). For all other occasions within ND group, averaged AAEs and AAPEs from EASOM were lower than those from LP, DLP and SCS (Tables 15, 17 and 19).

Table 14 Comparison of model performance (in terms of validity of muscle force and joint reaction force predictions) for the *training sample (dominant)* between previous optimization-based models (i.e. LP, DLP, SCS) and EASOM. The measures include average absolute error, average absolute percent error, and R^2. Each cell contains the average (and standard deviation) for that particular measure across the nine resulting values from the training samples (dominant) associated with the nine sample draws.

Training Sample (Dominant)		**Muscle Forces**								**Joint Reaction Forces**	
		BIC(S)	**BIC(L)**	**BRA**	**BRD**	**ANC**	**TRI(Lt)**	**TRI(Lg)**	**TRI(Md)**	R_x	R_y
Average Absolute Error (N)	LP	128.38 (9.19)	140.36 (9.30)	524.23 (27.09)	246.98 (13.12)	47.41 (6.15)	245.84 (35.89)	109.29 (13.63)	130.27 (14.32)	121.07 (7.12)	1183.79 (105.83)
	DLP	42.72 (6.68)	39.98 (5.02)	215.62 (23.81)	60.86 (7.14)	47.41 (6.15)	245.84 (35.89)	109.29 (13.63)	130.27 (14.32)	55.34 (5.38)	822.75 (102.10)
	SCS	50.71 (7.73)	44.14 (5.63)	163.60 (21.93)	68.79 (7.62)	47.41 (6.15)	245.84 (35.89)	109.29 (13.63)	130.27 (14.32)	58.37 (5.40)	789.47 (101.85)
	EASOM	**35.26 (4.33)**	**29.06 (2.03)**	**106.11 (15.39)**	**56.29 (7.20)**	**27.62 (3.03)**	**136.61 (23.34)**	**68.96 (12.53)**	**65.68 (12.33)**	**35.22 (2.91)**	**343.97 (70.70)**
Average Absolute Percent Error	LP									79.72% (6.37%)	90.42% (0.89%)
	DLP									30.91% (2.29%)	58.52% (2.64%)
	SCS									32.95% (2.25%)	55.55% (2.82%)
	EASOM									**21.72% (1.27%)**	**24.33% (4.05%)**
R^2	LP	0.063 (0.040)	0.006 (0.006)	0.017 (0.019)	0.255 (0.057)	- -	- -	- -	- -	0.665 (0.041)	0.011 (0.010)
	DLP	0.546 (0.034)	0.611 (0.029)	0.528 (0.075)	0.194 (0.052)	- -	- -	- -	- -	0.691 (0.037)	0.314 (0.057)
	SCS	0.529 (0.032)	0.584 (0.030)	0.529 (0.075)	0.168 (0.049)	- -	- -	- -	- -	0.688 (0.036)	0.320 (0.058)
	EASOM	**0.597 (0.066)**	**0.717 (0.048)**	**0.566 (0.115)**	**0.172 (0.050)**	**0.385 (0.142)**	**0.445 (0.133)**	**0.311 (0.196)**	**0.305 (0.183)**	**0.725 (0.050)**	**0.505 (0.163)**

Table 15 Comparison of model performance (in terms of validity of muscle force and joint reaction force predictions) for the *training sample (non-dominant)* between previous optimization-based models (i.e. LP, DLP, SCS) and EASOM. The measures include average absolute error, average absolute percent error, and R^2. Each cell contains the average (and standard deviation) for that particular measure across the nine resulting values from the training samples (non-dominant) associated with the nine sample draws.

Training Sample (Non-dominant)		Muscle Forces								Joint Reaction Forces	
		BIC(S)	**BIC(L)**	**BRA**	**BRD**	**ANC**	**TRI(Lt)**	**TRI(Lg)**	**TRI(Md)**	R_x	R_y
Average Absolute Error (N)	LP	110.49 (6.84)	121.01 (9.92)	453.84 (13.49)	266.88 (14.68)	32.41 (3.18)	134.68 (9.15)	58.99 (4.58)	88.82 (13.59)	139.24 (8.79)	853.50 (36.23)
	DLP	30.53 (3.74)	34.93 (6.25)	163.34 (14.64)	34.75 (2.33)	32.41 (3.18)	134.68 (9.15)	58.99 (4.58)	88.82 (13.59)	30.62 (3.30)	509.64 (39.94)
	SCS	38.16 (4.55)	36.15 (6.73)	117.66 (13.24)	40.33 (2.51)	32.41 (3.18)	134.68 (9.15)	58.99 (4.58)	88.82 (13.59)	33.05 (3.45)	477.94 (40.39)
	EASOM	**28.69 (3.83)**	**36.19 (3.32)**	**101.36 (11.41)**	**35.03 (1.98)**	**26.67 (2.43)**	**85.55 (9.57)**	**46.01 (6.71)**	**58.52 (11.97)**	**28.91 (2.74)**	**264.18 (62.97)**
Average Absolute Percent Error	LP									108.10% (7.94%)	89.12% (0.61%)
	DLP									21.79% (2.19%)	50.64% (1.90%)
	SCS									23.81% (2.34%)	47.09% (2.03%)
	EASOM									**21.64% (2.05%)**	**26.17% (5.80%)**
R^2	LP	0.013 (0.013)	0.006 (0.007)	0.022 (0.024)	0.206 (0.110)	- -	- -	- -	- -	0.735 (0.046)	0.059 (0.011)
	DLP	0.605 (0.064)	0.516 (0.099)	0.571 (0.094)	0.156 (0.094)	- -	- -	- -	- -	0.800 (0.039)	0.488 (0.109)
	SCS	0.607 (0.066)	0.513 (0.108)	0.572 (0.099)	0.135 (0.087)	- -	- -	- -	- -	0.803 (0.037)	0.492 (0.110)
	EASOM	**0.561 (0.086)**	**0.511 (0.082)**	**0.487 (0.104)**	**0.133 (0.072)**	**0.090 (0.089)**	**0.147 (0.115)**	**0.378 (0.105)**	**0.129 (0.112)**	**0.757 (0.039)**	**0.401 (0.155)**

Table 16 Comparison of model performance (in terms of validity of muscle force and joint reaction force predictions) for the *same-group test sample (dominant)* between previous optimization-based models (i.e. LP, DLP, SCS) and EASOM. The measures include average absolute error, average absolute percent error, and R^2. Each cell contains the average (and standard deviation) for that particular measure across the nine resulting values from the same-group test samples (dominant) associated with the nine sample draws.

Same-group test Sample (Dominant)		**Muscle Forces**								**Joint Reaction Forces**	
		BIC(S)	**BIC(L)**	**BRA**	**BRD**	**ANC**	**TRI(Lt)**	**TRI(Lg)**	**TRI(Md)**	R_x	R_y
Average Absolute Error (N)	LP	131.90 (11.70)	143.49 (8.80)	541.04 (30.49)	254.88 (19.02)	48.80 (6.94)	251.31 (41.16)	111.24 (16.58)	137.64 (20.43)	126.26 (11.42)	1225.85 (117.84)
	DLP	44.86 (8.65)	40.64 (6.99)	224.38 (27.52)	60.65 (10.35)	48.80 (6.94)	251.31 (41.16)	111.24 (16.58)	137.64 (20.43)	56.15 (8.21)	846.52 (118.31)
	SCS	53.07 (9.53)	44.89 (7.00)	173.00 (24.35)	68.73 (11.27)	48.80 (6.94)	251.31 (41.16)	111.24 (16.58)	137.64 (20.43)	59.16 (8.21)	812.12 (118.40)
	EASOM	**37.20 (5.80)**	**30.82 (3.07)**	**114.24 (15.94)**	**55.44 (8.53)**	**27.77 (3.71)**	**143.93 (30.33)**	**73.60 (14.08)**	**67.60 (10.07)**	**35.44 (2.73)**	**373.97 (61.30)**
Average Absolute Percent Error	LP									78.54% (7.02%)	91.97% (1.44%)
	DLP									30.41% (2.94%)	59.42% (2.19%)
	SCS									32.35% (2.88%)	56.46% (2.36%)
	EASOM									**20.81% (1.87%)**	**25.82% (4.00%)**
R^2	LP	0.067 (0.074)	0.037 (0.059)	0.050 (0.087)	0.283 (0.060)	- -	- -	- -	- -	0.685 (0.040)	0.048 (0.043)
	DLP	0.545 (0.117)	0.623 (0.057)	0.521 (0.071)	0.214 (0.050)	- -	- -	- -	- -	0.698 (0.049)	0.328 (0.072)
	SCS	0.539 (0.111)	0.602 (0.054)	0.520 (0.070)	0.186 (0.046)	- -	- -	- -	- -	0.692 (0.052)	0.332 (0.073)
	EASOM	**0.573 (0.093)**	**0.697 (0.051)**	**0.543 (0.138)**	**0.187 (0.076)**	**0.378 (0.192)**	**0.319 (0.142)**	**0.208 (0.159)**	**0.257 (0.194)**	**0.706 (0.071)**	**0.434 (0.160)**

Table 17 Comparison of model performance (in terms of validity of muscle force and joint reaction force predictions) for the *same-group test sample (non-dominant)* between previous optimization-based models (i.e. LP, DLP, SCS) and EASOM. The measures include average absolute error, average absolute percent error, and R^2. Each cell contains the average (and standard deviation) for that particular measure across the nine resulting values from the same-group test samples (non-dominant) associated with the nine sample draws.

Same-group test Sample (Non-dominant)		**Muscle Forces**								**Joint Reaction Forces**	
		BIC(S)	**BIC(L)**	**BRA**	**BRD**	**ANC**	**TRI(Lt)**	**TRI(Lg)**	**TRI(Md)**	R_x	R_y
Average Absolute Error (N)	LP	116.14 (5.31)	126.13 (7.67)	464.87 (13.24)	275.64 (12.22)	32.85 (2.85)	142.68 (9.75)	64.10 (6.53)	91.30 (12.29)	145.60 (6.53)	893.00 (31.04)
	DLP	33.17 (4.84)	35.95 (5.47)	166.84 (10.40)	34.60 (6.88)	32.85 (2.85)	142.68 (9.75)	64.10 (6.53)	91.30 (12.29)	30.81 (3.61)	530.51 (32.11)
	SCS	41.65 (5.51)	37.08 (5.31)	120.06 (9.73)	39.98 (7.08)	32.85 (2.85)	142.68 (9.75)	64.10 (6.53)	91.30 (12.29)	33.22 (3.84)	497.62 (32.60)
	EASOM	**31.09 (5.51)**	**38.56 (6.28)**	**106.33 (14.73)**	**34.55 (6.59)**	**29.12 (5.12)**	**88.43 (9.98)**	**51.43 (14.00)**	**63.54 (14.62)**	**31.76 (5.42)**	**281.77 (71.44)**
Average Absolute Percent Error	LP									106.83% (7.66%)	90.34% (1.93%)
	DLP									21.44% (2.37%)	51.30% (1.88%)
	SCS									23.41% (2.46%)	47.76% (1.98%)
	EASOM									**22.18% (3.32%)**	**27.18% (5.79%)**
R^2	LP	0.019 (0.021)	0.031 (0.034)	0.029 (0.038)	0.201 (0.150)	- -	- -	- -	- -	0.742 (0.058)	0.052 (0.030)
	DLP	0.611 (0.102)	0.525 (0.098)	0.570 (0.061)	0.158 (0.134)	- -	- -	- -	- -	0.814 (0.033)	0.520 (0.110)
	SCS	0.608 (0.104)	0.526 (0.107)	0.572 (0.062)	0.140 (0.127)	- -	- -	- -	- -	0.818 (0.031)	0.524 (0.111)
	EASOM	**0.544 (0.123)**	**0.495 (0.095)**	**0.516 (0.085)**	**0.149 (0.133)**	**0.112 (0.122)**	**0.196 (0.100)**	**0.407 (0.145)**	**0.136 (0.134)**	**0.781 (0.069)**	**0.455 (0.144)**

Table 18 Comparison of model performance (in terms of validity of muscle force and joint reaction force predictions) for the *independent test sample (dominant)* between previous optimization-based models (i.e. LP, DLP, SCS) and EASOM. The measures include average absolute error, average absolute percent error, and R^2. Each cell contains the average (and standard deviation) for that particular measure across the nine resulting values from the independent test samples (dominant) associated with the nine sample draws.

Independent test Sample (Dominant)		**Muscle Forces**								**Joint Reaction Forces**	
		BIC(S)	**BIC(L)**	**BRA**	**BRD**	**ANC**	**TRI(Lt)**	**TRI(Lg)**	**TRI(Md)**	R_x	R_y
Average Absolute Error (N)	LP	130.21 (31.92)	143.51 (29.67)	539.07 (88.60)	246.21 (47.79)	52.69 (21.61)	264.50 (125.41)	113.92 (48.29)	136.62 (52.26)	117.60 (27.38)	1238.31 (361.96)
	DLP	43.79 (23.33)	42.01 (17.33)	226.72 (82.29)	64.38 (23.22)	52.69 (21.61)	264.50 (125.41)	113.92 (48.29)	136.62 (52.26)	61.21 (19.43)	870.73 (358.25)
	SCS	51.84 (26.91)	46.25 (18.99)	174.52 (76.87)	73.00 (25.28)	52.69 (21.61)	264.50 (125.41)	113.92 (48.29)	136.62 (52.26)	64.31 (19.38)	836.98 (358.01)
	EASOM	**36.82 (14.76)**	**31.94 (7.35)**	**118.72 (60.22)**	**59.18 (22.23)**	**27.36 (17.87)**	**157.85 (97.21)**	**77.01 (49.49)**	**72.49 (43.48)**	**35.91 (13.27)**	**418.00 (240.54)**
Average Absolute Percent Error	LP									72.93% (21.63%)	90.92% (1.69%)
	DLP									33.11% (8.16%)	59.36% (8.69%)
	SCS									35.11% (7.95%)	56.43% (9.32%)
	EASOM									**21.10% (7.02%)**	**28.88% (17.30%)**
R^2	LP	0.182 (0.143)	0.100 (0.099)	0.114 (0.109)	0.402 (0.166)	- -	- -	- -	- -	0.769 (0.130)	0.043 (0.054)
	DLP	0.635 (0.109)	0.665 (0.101)	0.631 (0.200)	0.322 (0.160)	- -	- -	- -	- -	0.777 (0.113)	0.489 (0.214)
	SCS	0.623 (0.114)	0.627 (0.104)	0.631 (0.200)	0.287 (0.155)	- -	- -	- -	- -	0.769 (0.111)	0.497 (0.215)
	EASOM	**0.630 (0.153)**	**0.699 (0.101)**	**0.639 (0.211)**	**0.290 (0.171)**	**0.532 (0.299)**	**0.503 (0.211)**	**0.420 (0.287)**	**0.437 (0.293)**	**0.791 (0.126)**	**0.612 (0.246)**

Table 19 Comparison of model performance (in terms of validity of muscle force and joint reaction force predictions) for the *independent test sample (non-dominant)* between previous optimization-based models (i.e. LP, DLP, SCS) and EASOM. The measures include average absolute error, average absolute percent error, and R^2. Each cell contains the average (and standard deviation) for that particular measure across the nine resulting values from the independent test samples (non-dominant) associated with the nine sample draws.

Independent test Sample (Non-dominant)		**Muscle Forces**								**Joint Reaction Forces**	
		BIC(S)	**BIC(L)**	**BRA**	**BRD**	**ANC**	**TRI(Lt)**	**TRI(Lg)**	**TRI(Md)**	R_x	R_y
Average Absolute Error (N)	LP	111.88 (20.48)	122.22 (32.02)	456.70 (42.16)	268.92 (48.42)	32.58 (10.29)	136.80 (29.93)	60.21 (16.72)	89.65 (45.28)	140.70 (28.35)	863.76 (113.34)
	DLP	31.19 (11.79)	35.14 (19.91)	164.42 (46.77)	34.69 (10.46)	32.58 (10.29)	136.80 (29.93)	60.21 (16.72)	89.65 (45.28)	30.71 (11.57)	515.40 (129.88)
	SCS	39.03 (14.57)	36.34 (21.26)	118.45 (40.18)	40.24 (10.74)	32.58 (10.29)	136.80 (29.93)	60.21 (16.72)	89.65 (45.28)	33.14 (12.08)	483.41 (131.69)
	EASOM	**30.40 (12.28)**	**38.38 (14.30)**	**113.07 (38.03)**	**35.00 (9.81)**	**30.22 (15.19)**	**88.59 (40.96)**	**55.05 (27.39)**	**69.06 (30.35)**	**31.88 (11.38)**	**315.08 (166.86)**
Average Absolute Percent Error	LP									107.70% (26.39%)	89.42% (1.29%)
	DLP									21.73% (7.73%)	50.84% (6.39%)
	SCS									23.74% (8.11%)	47.29% (6.85%)
	EASOM									**23.13% (8.44%)**	**31.31% (16.84%)**
R^2	LP	0.058 (0.069)	0.103 (0.128)	0.068 (0.061)	0.406 (0.225)	- -	- -	- -	- -	0.809 (0.054)	0.070 (0.030)
	DLP	0.672 (0.202)	0.585 (0.190)	0.668 (0.173)	0.332 (0.201)	- -	- -	- -	- -	0.864 (0.050)	0.644 (0.193)
	SCS	0.670 (0.208)	0.587 (0.215)	0.670 (0.182)	0.298 (0.188)	- -	- -	- -	- -	0.864 (0.050)	0.650 (0.196)
	EASOM	**0.634 (0.207)**	**0.599 (0.153)**	**0.621 (0.213)**	**0.282 (0.156)**	**0.376 (0.253)**	**0.430 (0.187)**	**0.414 (0.184)**	**0.391 (0.231)**	**0.841 (0.058)**	**0.654 (0.228)**

8. DISCUSSION

The current study addresses the issues associated with previous optimization-based biomechanical modeling approaches. Most of these kinds of models were unable to predict antagonist muscle exertions (e.g. LP in Schultz et al. (1982b); DLP in Bean et al. (1988); SCS in Crowninshield and Brand (1981)). Some succeeded in forcing antagonist muscle force predictions, however, the optimization models (especially the objective functions) they utilized bear little physiological meaning (e.g. Forster et al. (2004); Raikova (1999)). There were a few studies that involved physiological measures (such as spinal stability) in formulations of optimization models in order to predict muscle co-contraction. Unfortunately, such methods called for complex anatomical musculoskeletal models (e.g. 52-muscle model in Brown and Potvin (2005); 180-muscle model in Stokes and Gardner-Morse (2001)), which makes those sort of models too computationally costly for real world applications. More importantly, such models often generated unrealistic results (Stokes and Gardner-Morse (2001)).

Based on neurophysiological principles, this study establishes an optimization model in the elbow joint that predicts both agonist and antagonist muscle forces without the need for computationally costly anatomical models. The main neurophysiological theory (as the theoretical foundation for the current research) is the one proposed and advocated by Feldman (1993). It states that the central nervous system is a weighted combination of two independent command systems, where one produces reciprocal inhibition (agonist only muscle contraction) and the other induces muscle co-contraction. Studies also found mechanisms underlying these two components. That is activation of inhibitory Ia interneurons (Ia INs) is responsible for reciprocal inhibition (Sherrington, 1909) and

discharge of Renshaw cells cause muscle co-contraction (Hultborn et al., 1976; Hultborn et al., 1979). In order to apply Feldman's theory (1993) in an optimization formulation, the objective function would be a weighted combination of two components that mirror the functions of Ia INs (reciprocal inhibition) and Renshaw cells (agonist and antagonist muscle co-contraction). It is quite clear that those objective functions that only predict agonist muscle forces (e.g. LP, DLP and SCS) are all able to take on the role of Ia INs in an optimization formulation. For the counterpart of Renshaw cells in an objective function, we introduced the concept of entropy and created an entropy-related function that when minimized, encouraged uniform stress level among all muscles involved (i.e. muscle co-contraction). Therefore, for the current study we applied an objective function that is a weighted combination of (1) the sum of cubed muscle stresses (SCS) that induces agonist only contraction and (2) the entropy-related function that encourages muscle co-contraction. The entropy term applied in the objective function of EASOM requires exertions from all the muscles in the system. However, due to the nature of entropy (Guisau, 1977; Kapur and Kesavav, 1992; Fang *et al.*, 1997;), the muscles only need to exert collectively minimal effort (i.e. to produce as much forces as necessary as a group). The weight factor associated with the entropy-related component, called co-contraction weight factor (W), acts as a "dial" used by the central nervous system uses to adjust the weights between its two components. The larger the value of W, the more weight (the stronger command) that is imposed on muscle co-contraction. Therefore, it was hypothesized that W represents the level of muscle co-contraction and the quantified relationships between W and environmental task conditions (i.e. load magnitude, angular velocity, elbow flexion angle and dexterity) would support the physiology behind muscle co-contraction. By understanding the mechanisms behind W, we

might be able to obtain greater insight into the decision making process of central nervous system on the pattern of muscle co-contraction. It was also hypothesized that the entropy-assisted optimization model (EASOM) should provide realistic predictions for both agonist and antagonist muscle forces, which in turn would generate more satisfactory joint loading estimations, compared with models that cannot predict antagonist muscle exertions (e.g. LP, DLP and SCS).

The trend of *W* values reflects the relative strengths of the two command systems that correspond to inhibitory Ia INs (for reciprocal inhibition) and Renshaw cells (for agonist and antagonist co-contraction) and how they relate to various task condition variables, i.e. load magnitude, angular velocity, elbow flexion angle, and dexterity. As *W* value increases, the central nervous system (CNS) discharges more Renshaw cells, resulting in stronger co-contraction command. As the value of *W* decreases, CNS activates more Ia INs, which causes stronger reciprocal inhibition command. Based on the literature review, it was hypothesized in Section 4.7 that *W* value would increase with greater load magnitude (Schultz et al., 1987), higher angular velocity (Suzuki et al., 2001), greater elbow extension (Milner, 2002), and from D to ND (Brooks, 1986).

The results showed that *W* value increased with greater load magnitude for both D and ND groups (Figure 21), with angular velocity rising from 0°/s to 60°/s for the D group and from 0°/s up to 40°/s for the ND group (Figure 22). The above mentioned results all agree with the hypotheses as discussed in Section 4.7. However, there were exceptions. For the ND group, value of *W* decreased when angular velocity increased from 40°/s to 60°/s (Figure 22). This indicated that the ND elbow started getting more "comfortable" with the speed of the motion after a certain threshold between 40°/s to 60°/s, therefore lowering the

level of co-contraction. For both D and ND groups, *W* remained at the same level at 45° and 90° elbow flexion, i.e. elbow flexion angle did not play a role in determining the value of *W* (Figure 23). However, during the sensitivity analysis, the *W* regression equation for the overlapping subjects within the ND group contained A^2 as a regressor variable (Table 8), and the *W* regression equations for two sample draws within the ND group consisted of A as a regressor variable (Table 11). In those cases, *W* value increased with greater elbow extension (smaller elbow flexion angle), which agrees with the hypothesis. It is noted that none of the *W* regression equations for the D group generated during the sensitivity analysis contained A or A^2 as a regressor variable as for the full data set (Tables 8 and 10). This shows that the muscle co-contraction pattern in the dominant elbow, being more skilled than the non-dominant one, is less affected by elbow flexion angle. It is suspected that as the number of subjects increases, elbow flexion angle may start showing a significant effect for D group as well. Also contrary to the hypothesis, *W* value for the dominant elbow was higher than the non-dominant elbow. It was expected that the dominant arm, being more skilled, would have been more likely to achieve the necessary neuromuscular control utilizing only the agonist muscles while the non-dominant arm would have required more antagonist muscle co-contraction to maintain the necessary control of the movement. The data did not support this hypothesis, but all other hypothetical relationships between *W* and the task variables were supported by the data and therefore supported the expected physiology behind the muscle co-contraction.

The ability of quantifying the level of muscle co-contraction through the co-contraction weight factor *W* is one of the main strengths and contributions of EASOM. This weight factor focuses on the balance among exertions from all muscles and does not require a

definite categorization of muscles into agonist group and antagonist group. This may be especially helpful in investigating body regions (such as the low back) where muscles play roles (e.g. pure agonist vs. pure antagonist) that may not be clear during certain motions (e.g. asymmetric lifting).

During model validation, model performance of EASOM was compared with LP, DLP and SCS models. For the full data set, average absolute errors (AAEs) for predictions of muscle forces from EASOM were always lower than those from LP, DLP and SCS (Figures 25 and 26), confirming the hypothesis that EASOM generates more realistic muscle force predictions. The LP approach always activates muscles with larger moment arms prior to those with smaller moment arms (Bean *et al.*, 1988). In the current study, brachioradialis (BRD) has the largest moment arm among all agonist muscles. Besides, the muscle stress limit was set at 500 N/cm^2 and it turned out that BRD never had to reach that level in order to balance out external torques. Therefore, no other agonist muscles needed to be engaged, and BRD was the only muscle with non-zero muscle force predictions during the LP approach (Figure 24). As expected, DLP and SCS did a better job in distributing muscle exertions more evenly across the four agonist muscles than LP (Figure 24). Since SCS has slight preference in recruiting muscles with larger masses (van Dieen and Kingma, 2005) and brachialis (BRA) has the largest mass among all agonist muscles, muscle force predictions for BRA from SCS were higher than DLP in general (Figure 24). The results also confirmed that LP, DLP and SCS were unable to predict antagonist co-contraction (Brown and Potvin, 2005; Stokes and Gardner-Morse, 2001) as shown in Figure 24. EASOM not only predicted antagonist muscle activity, it also provided distinct improvement upon SCS in terms of

partial $R^2_{(EMG)(EASOM),(SCS)}$ in predicting agonist muscle forces, especially in the D group (Table 6).

Superiority of EASOM to LP, DLP and SCS was even more apparent in the results on joint loading estimations in terms of average absolute error (AAE) (Figures 31 and 32) and average absolute percent error (AAPE) (Figures 33 and 34), exhibiting agreement with the hypotheses. It should be noted that estimation of joint loading (especially in the spinal region) is often associated with intensity and injury risk of a physical task. Therefore, knowledge of model performance on estimating joint reaction forces is often more interesting than muscle force predictions. The results confirmed findings in the literature that models such as LP, DLP and SCS generate unrealistically low joint compression forces due to their inability to predict antagonist muscle forces (Cholewicki *et al.*, 1995) (Figure 29). Granata and Marras (1995b) found that antagonist trunk muscle co-contraction contribute to up to 45% of total spinal compression load. In the current study, the contribution to elbow joint compression (R_y) from antagonist muscles was up to 62.2% for the EMG-assisted model and 52.8% for EASOM. It should be noted that we are dealing with a different anatomical structure than in Granata and Marras study (1995b), therefore the results from both studies may not be comparable. Figure 29 also displays the averaged contributions from antagonist muscles (in percent values) to joint compression (R_y) for LP, DLP, SCS, EASOM and the EMG-assisted model at each level of load magnitude. Schultz et al. (1987) stress in their study that the lack of co-contraction prediction is especially undesirable during more strenuous tasks, where antagonist muscle contraction is widely evident. In the current study, we found that the contribution to joint compression from antagonist muscles increases slightly with load magnitude increased from 20% to 50% for both EASOM and EMG-assisted model (Figure

29), supporting Schultz et al.'s argument (1987). Since EASOM was able to consistently and systematically predict antagonist muscle forces according to the input of task variables, the predicted joint reaction forces tend to be closer to EMG generated results than the other three models.

For static tasks, the literature review indicates that DLP exhibits better performance than SCS when investigating a wide range of tasks (in all three planes) (Schultz et al., 1983) and/or utilizing a more realistic anatomical model (Brown and Potvin, 2005; Stokes and Gardner-Morse, 2001). SCS, on the other hand, has advantages in studying static tasks where loads are limited within the sagittal (flexion/extension) and transverse (twisting) planes (Hughes et al., 1994). These results are confirmed by the findings from this study where SCS performed slightly better than DLP (Figure 30) in a simplified single-plane (sagittal) elbow model. For dynamic tasks, Hughes (1995) found that DLP yielded much higher joint compression force than SCS during motions in the frontal (lateral bending) and transverse (twisting) planes. Hughes (2000) also discovered that for dynamic tasks limited within the sagittal (flexion/extension) plane, joint compression forces predicted by DLP and SCS should agree with each other. As Figure 30 indicates, although during dynamic tasks, estimation of joint compression force (R_y) from SCS was slightly higher than DLP, such difference was not significant, therefore supporting the findings from Hughes (2000). The same figure also shows that LP, DLP and SCS make predictions in the same way for static and dynamic tasks, while EASOM responds to dynamic tasks differently than to static ones in ways that are similar to the EMG generated responses.

For joint loading estimation and predictions for some muscle forces in the non-dominant ND group (Figures 28 and 36), EASOM had lower R^2 values than the other three

optimization models. This issue only occurred to the ND elbow probably because the level of experience in using one's non-dominant arm varied more among subjects than that of using the dominant arm. Therefore, muscle patterns among ND elbow muscles are expected to exhibit larger variability than D elbow muscles. The measure R^2 seems to be problematic here perhaps because LP, DLP and SCS were unable to predict antagonist muscle forces (and some of the agonist muscle forces for LP) and therefore predicted most muscle forces and joint loading to be at a consistently lower level than those calculated from empirical data. On the other hand, muscle force or joint loading predictions from EASOM were closer to (and often fluctuated around the level resulting from) the empirical data, which might have resulted in lower R^2 values than LP, DLP and SCS. Therefore, the fact that EASOM had lower R^2 values does not necessarily suggest inferior model performance. Further, the results on $R^2_{(EMG)(EASOM),(SCS)}$ provided evidence that EASOM has made distinct improvement upon SCS in estimating joint loading especially in the D group (Table 7).

Sensitivity analysis for model performance evaluation shows independent test sample yielded slightly larger AAEs and AAPEs (Tables 18 and 19) from EASOM than training sample (Tables 14 and 15) and same-group test sample (Tables 16 and 17). This is understandable since data from same-group sample may share common traits with data from training sample, while data from independent test sample were collected from subjects that were totally different from those in training or same-group test samples. In spite of this, the errors among independent test sample from EASOM were still lower in general than LP, DLP and SCS. Therefore, results from sensitivity analysis confirmed the finding from full data set that EASOM produced more realistic muscle force predictions and joint loading estimations than LP, DLP and SCS. It was even more impressive to see the results from

independent test sample since this data were collected from a group subjects that were totally different from those whose data were used to train the model. This indicated the great robustness of EASOM.

There are several limitations to this study associated with either the experiments or the modeling technique that should be mentioned. First, although the dynamic tasks in the experiment tried to simulate free dynamic motions, the requirement for each subject to closely follow the movement of dynamometer arm limited the freedom of the motion generated by the subject. A person might have tried to correct the speed of the motion and produced a somewhat different exertion pattern than during a true free motion, resulting in a somewhat biased response in terms of the co-activation patterns elicited. Second, the elbow model utilized in this dissertation is a simplified single-plane model, where all muscles were modeled as strings each connecting its origin and insertion (Seireg and Arvikar, 1989) and only motions in the sagittal plane were considered. This limits somewhat the generalizability of the results, but still provides some insight into the effectiveness of the modeling approach. Third, there were challenging methodological issues associated with the EMG-assisted models for two of our subjects. The basis for our model was from Langenderfer et al. (2005), where none of the antagonist muscles were involved in the model and the upper bound for muscle stress was set to 500 N/cm^2. While we advanced the model to include the antagonist muscle forces, we maintained the 500 N/cm^2 limit on the muscle stress. The results showed that one subject from each group wherein 10% of all conditions had gain values great than 500 N/cm^2 and, because of this, these two subjects' data were removed from data processing altogether. Finally, the EMG-assisted model used in the current study allowed gain value to vary within an individual so that the average torque generated from muscle forces exactly

matched the average of the measured torque value. This enabled the maintenance of consistency between muscle generated torque and external torque during optimization. Ideally, we would like to conform to the more physiologically appropriate approach and fix this value for a given subject across all conditions. However, given that this study is somewhat exploratory in its goals, we allowed this gain to vary across trials within a subject to ensure the feasibility of the mechanics of the optimization approach.

Despite the limitations and challenges associated with the modeling approach of EASOM, this dissertation contributes to the literature in that it provides an economical approach to predict muscle co-contraction based on neurophysiological theory, which generated more realistic muscle force predictions and especially joint loading estimations than conventional optimization-based models (such as LP, DLP and SCS). It also offers a new form of indicator that can quantify the level of muscle co-contraction relative to various task condition variables, which supports physiological evidence behind co-contraction. Although the EASOM approach was established and validated in the elbow joint, we believe that the regression equations for W obtained from this study will hold for other single-joint body segments (such as the knee joint) during simple flexion/extension movement, and EASOM will generate more accurate muscle force and joint loading predictions than LP, DLP and SCS when applied to these body regions.

9. CONCLUSIONS

This study established an entropy-assisted optimization model (EASOM) that addressed the issues associated with previous optimization-based biomechanical models. Unlike the previous models, EASOM can economically predict both agonist and antagonist muscle forces with clear connections to neurophysiology. In the current study, EASOM was developed and validated in the elbow joint.

The co-contraction weight factor (W), which was part of the objective function of EASOM, was quantified relative to task variables including load magnitude, angular velocity, elbow flexion angle, and dexterity. This allowed W to quantitatively represent level of muscle co-contraction and enabled EASOM to predict muscle forces associated with different task conditions. Results on W confirmed the physiological basis of EASOM. Further, the performance of EASOM was compared with three of the most often used optimization modeling approaches, i.e. linear programming (LP), double linear programming (DLP) and non-linear programming (NLP) formulations. It was found that EASOM produced consistently lower average absolute errors in individual muscle force predictions. For joint loading estimations, EASOM generated average absolute percent errors from 21.13% to 25.23%, compared with 77.99% to 107.79%, 21.70% to 58.87%, and 23.71% to 55.91% for LP, DLP and NLP respectively. Sensitivity analysis showed that the advantage of EASOM over LP, DLP and NLP remained despite using different subsets of the data for model training and testing, thus indicated the robustness in EASOM.

Future research may proceed in two directions. In this study, the entropy term used in the objective function of EASOM implies independence among exertions from different muscles. However, there might be correlation/covariance among muscle exertions since the

muscle co-contraction pattern in general is still unclear to biomechanists. Therefore, the first direction involves the application of cross entropy $-\sum_i p_i \log\left(\frac{p_i}{p_i^0}\right)$ in place of the entropy term $-\sum_i p_i \log p_i$, where p_i^0 is the *a priori* utilization level for muscle *i* that the model will make the prediction of p_i close to (Fang et al., 1997). By doing so, we can incorporate the idea of correlation/covariance into EASOM. Our goal then is to quantify such an *a priori* muscle utilization distribution $\boldsymbol{p^0}$ to assist in improving EASOM performance.

The other direction expands the application of EASOM to other parts of the body. Since back pain is such a serious issue as discussed in Section 2.1, application of EASOM in the lumbar region of torso is of most interest. In this region, there exists far more complicated anatomy than the elbow joint in that the lumbar region of the torso consists of multiple joints and thus is a complex multiple-degree-of-freedom system. However, the current study has built a solid foundation for this kind of exploration. For one, most of the task variables involved in this research may still be introduced in investigating the lumbar region. Such variables include load magnitude, angular velocity and (trunk) flexion/extension angle. A new task variable that may be of interest is the angle of asymmetry, which may share some common physiological traits as dexterity, one of the variables in this study. For the current study, there existed great difficulty in transforming stability-related optimization-based spinal models into the elbow joint. Therefore, such approaches did not enter the comparison in model validation. However, for future research in the lumbar region of the torso, those kind of stability-related optimization-based models (e.g. Brown and Potvin (2005)) may be involved to compare with EASOM model performance. It is expected that EASOM will be able to achieve comparable model

performance in muscle force and joint loading predictions as those stability-related approaches, with a much less complicated anatomical model.

This dissertation presented a reliable and economical tool in predicting muscle forces (agonist and antagonist) and joint loading. The quantified results from this model can be used as more accurate guidelines in assessing and designing work postures to help reduce the risks of musculoskeletal disorders. In the meantime, it also founded a solid foundation that will help expand applications of EASOM to other body regions (especially the lumbar region of the torso).

References

An, K. N., Hui, F. C., Morrey, B. F., Linscheid, R. L., and Chao, E. Y. (1981). Muscles across the elbow joint - a biomechanical analysis. *Journal of Biomechanics, 14*(10), 659-669.

An, K. N., Kwak, B. M., Chao, E. Y., and Morrey, B. F. (1984). Determination of muscle and joint forces - a new technique to solve the indeterminate problem. *Journal of Biomechanical Engineering-Transactions of the ASME, 106*(4), 364-367.

Andersson, G. B. J. (1998). Epidemiology of low back pain. *Acta Orthopaedica Scandinavica, 69*, 28-31.

Bean, J. C., Chaffin, D. B., and Schultz, A. B. (1988). Biomechanical model calculation of muscle-contraction forces - a double linear-programming method. *Journal of Biomechanics, 21*(1), 59-66.

Beaunis, H. (1889). Recherches physiologiques sur la contraction simultanée des muscles antagonistes. *Arch. Physiol. Norm. Pathol. 5ème Ser., 1*, 55.

Benoit, D. L., and Dowling, J. J. (2006). In vivo assessment of elbow flexor work and activation during stretch-shortening cycle tasks. *Journal of Electromyography and Kinesiology, 16*(4), 352-364.

Bergmark, A. (1989). Stability of the lumbar spine - a study in mechanical engineering. *Acta Orthopaedica Scandinavica, 60*, 3-54.

Bogduk, N., and Twomey, L. T. (Eds.). (1991). *Clinical Anatomy of the Lumbar Spine*. Melbourne: Churchill Livingstone.

Brooks, V. B. (1986). *The Neural Basis of Motor Control*. New York: Oxford University Press.

Brown, S. H. M., and Potvin, J. R. (2005). Constraining spine stability levels in an optimization model leads to the prediction of trunk muscle cocontraction and improved spine compression force estimates. *Journal of Biomechanics, 38*(4), 745-754.

Chaffin, D. B., Andersson, G. B. J., and Martin, B. J. (2006). *Occupational Biomechanics* (4th ed.). Hoboken, NJ: John Wiley and Sons, Inc.

Chang, Y. W., Su, F. C., Wu, H. W., and An, K. N. (1999). Optimum length of muscle contraction. *Clinical Biomechanics, 14*(8), 537-542.

Cheng, C. K., Chen, H. H., Kuo, H. H., Lee, C. L., Chen, W. J., and Liu, C. L. (1998). A three-dimensional mathematical model for predicting spinal joint force distribution during manual liftings. *Clinical Biomechanics, 13*, S59-S64.

Cholewicki, J., McGill, S. M., and Norman, R. W. (1995). Comparison of muscle forces and joint load from an optimization and EMG assisted lumbar spine model - towards development of a hybrid approach. *Journal of Biomechanics, 28*(3), 321-331.

Cholewicki, J., Panjabi, M. M., and Khachatryan, A. (1997). Stabilizing function of trunk flexor-extensor muscles around a neutral spine posture. *Spine, 22*(19), 2207-2212.

Crowninshield, R. D., and Brand, R. A. (1981). A physiologically based criterion of muscle force prediction in locomotion. *Journal of Biomechanics, 14*(11), 793-801.

Deluca, C. J., and Mambrito, B. (1987). Voluntary control of motor units in human antagonist muscles - coactivation and reciprocal activation. *Journal of Neurophysiology, 58*(3), 525-542.

Demeny, G. (1890). Du rôle mécanique des muscles antagonistes. *Arch. Physiol. Sér. 5, 2*, 747.

DOD-HDBK-743A. (1991). Anthropometry of U.S. Military Personnel (metric).

Enoka, R. M. (1994). *Neuromechanical Basis of Kinesiology* (2nd ed.). Champaign, IL: Human Kinetics.

Fang, S. C., Rajasekera, J. R., and Tsao, H. S. J. (1997). *Entropy Optimization and Mathematical Programming*. Boston: Kluwer Academic Publishers Boston.

Feldman, A. G. (1993). The coactivation command for antagonist muscles involving Ib interneurons in mammalian motor control-systems - an electrophysiologically testable model. *Neuroscience Letters, 155*(2), 167-170.

Forster, E., Simon, U., Augat, P., and Claes, L. (2004). Extension of a state-of-the-art optimization criterion to predict co-contraction. *Journal of Biomechanics, 37*(4), 577-581.

Gardner-Morse, M. G., and Stokes, I. A. F. (1998). The effects of abdominal muscle coactivation on lumbar spine stability. *Spine, 23*(1), 86-91.

Gracovetsky, S., Farfan, H. F., and Lamy, C. (1977). Mathematical-model of lumbar spine using an optimized system to control muscles and ligaments. *Orthopedic Clinics of North America, 8*(1), 135-153.

Granata, K. P., and Marras, W. S. (1993). An EMG-assisted model of loads on the lumbar spine during asymmetric trunk extensions. *Journal of Biomechanics, 26*(12), 1429-1438.

Granata, K. P., and Marras, W. S. (1995a). An EMG-assisted model of trunk loading during free-dynamic lifting. *Journal of Biomechanics, 28*(11), 1309-1317.

Granata, K. P., and Marras, W. S. (1995b). The influence of trunk muscle coactivity on dynamic spinal loads. *Spine, 20*(8), 913-919.

Granata, K. P., and Marras, W. S. (2000). Cost-benefit of muscle cocontraction in protecting against spinal instability. *Spine, 25*(11), 1398-1404.

Granata, K. P., and Orishimo, K. F. (2001). Response of trunk muscle coactivation to changes in spinal stability. *Journal of Biomechanics, 34*(9), 1117-1123.

Guisau, S. (1977). *Information Theory with Applications*. New York: McGraw Hill.

Hallett, M., Shahani, B. T., and Young, R. R. (1975). EMG analysis of patients with cerebellar deficits. *Journal of Neurology Neurosurgery and Psychiatry, 38*(12), 1163-1169.

Herzog, W., and Binding, P. (1992). Predictions of antagonistic muscular-activity using nonlinear optimization. *Mathematical Biosciences, 111*(2), 217-229.

Houk, J. C. (1974). Feedback control of muscle: A synthesis of the peripheral mechanisms. In V. B. Mountcastle (Ed.), *Medical Physiology* (13th ed.). St. Louis: C. V. Mosby Co.

Hughes, R. E. (1995). Choice of optimization models for predicting spinal forces in a three-dimensional analysis of heavy work. *Ergonomics, 38*(12), 2476-2484.

Hughes, R. E. (2000). Effect of optimization criterion on spinal force estimates during asymmetric lifting. *Journal of Biomechanics, 33*(2), 225-229.

Hughes, R. E., and Chaffin, D. B. (1995). The effect of strict muscle stress limits on abdominal muscle force predictions for combined torsion and extension loadings. *Journal of Biomechanics, 28*(5), 527-533.

Hughes, R. E., Chaffin, D. B., Lavender, S. A., and Andersson, G. B. J. (1994). Evaluation of muscle force prediction models of the lumbar trunk using surface electromyography. *Journal of Orthopaedic Research, 12*(5), 689-698.

Hultborn, H., Illert, M., and Santini, M. (1976). Convergence on interneurones mediating reciprocal Ia inhibition of motoneurons.1. Disynaptic Ia inhibition of Ia inhibitory interneurones. *Acta Physiologica Scandinavica, 96*(2), 193-201.

Hultborn, H., Jankowsk.E, and Lindstro.S. (1971). Relative contribution from different nerves to recurrent depression of Ia ipsps in motoneurones. *Journal of Physiology-London, 215*(3), 637.

Hultborn, H., Lindstrom, S., and Wigstrom, H. (1979). Function of recurrent inhibition in the spinal-cord. *Experimental Brain Research, 37*(2), 399-403.

Humphrey, D. R., and Reed, D. J. (1983). Separate cortical systems for control of joint movement and joint stiffness: Reciprocal activation and coactivation of antagonist muscles. In J. E. Desmedt (Ed.), *Motor Control Mechanisms in Health and Disease* (pp. 347-372). New York: Raven Press.

Kapur, J. N., and Kesavav, H. K. (1992). *Entropy Optimization Principles with Applications*. MA: Academic Press.

Kee, D., and Chung, M. K. (1996). Comparison of prediction models for the compression force on the lumbosacral disc. *Ergonomics, 39*(12), 1419-1429.

Langenderfer, J., LaScalza, S., Mell, A., Carpenter, J. E., Kuhn, J. E., and Hughes, R. E. (2005). An EMG-driven model of the upper extremity and estimation of long head biceps force. *Computers in Biology and Medicine, 35*(1), 25-39.

Lavender, S. A., Tsuang, Y. H., Hafezi, A., Andersson, G. B. J., Chaffin, D. B., and Hughes, R. E. (1992). Coactivation of the trunk muscles during asymmetric loading of the torso. *Human Factors, 34*(2), 239-247.

Loeb, G. E. (1984). The control and responses of mammalian muscle spindles during normally executed motor tasks. *Exercise Sports Science Review, 12*, 157-204.

Marieb, E. N. (2001). *Human Anatomy and Physiology* (5th ed.). San Francisco: Benjamin Cummings.

Marras, W. S., and Granata, K. P. (1995). A biomechanical assessment and model of axial twisting in the thoracolumbar spine. *Spine, 20*(13), 1440-1451.

Marras, W. S., and Granata, K. P. (1997). Spine loading during trunk lateral bending motions. *Journal of Biomechanics, 30*(7), 697-703.

Marras, W. S., and Mirka, G. A. (1990). Muscle activities during asymmetric trunk angular accelerations. *Journal of Orthopaedic Research, 8*(6), 824-832.

Marras, W. S., and Mirka, G. A. (1992). A comprehensive evaluation of trunk response to asymmetric trunk motion. *Spine, 17*(3), 318-326.

Marras, W. S., and Sommerich, C. M. (1991). A 3-dimensional motion model of loads on the lumbar spine.1. Model structure. *Human Factors, 33*(2), 123-137.

Masters, T. (1993). *Practical Neural Network Recipes in C++*. San Diego, CA: Academic Press.

McConville, J. T., Churchill, T. D., Kaleps, I., Clauser, C. E., and Cuzzi, J. (1980). *Anthropometric Relationships of Body and Body Segment Moments of Inertia* (No. AFAMRL-TR-80-119). Wright-Patterson AFB, OH: Air Force Aerospace Medical Research Laboratory.

McGill, S. M. (1991). Electromyographic activity of the abdominal and low-back musculature during the generation of isometric and dynamic axial trunk torque - implications for lumbar mechanics. *Journal of Orthopaedic Research, 9*(1), 91-103.

McGill, S. M. (1992). A myoelectrically based dynamic 3-dimensional model to predict loads on lumbar spine tissues during lateral bending. *Journal of Biomechanics, 25*(4), 395-414.

McGill, S. M. (1998). Low back exercises: Prescription for the healthy back and when recovering from injury. In *Resources Manual for Guidelines for Exercise Testing and Prescription* (3rd ed.). Baltimore: Williams and Wilkins.

McGill, S. M., and Norman, R. W. (1986). Partitioning of the l4-l5 dynamic moment into disk, ligamentous, and muscular components during lifting. *Spine, 11*(7), 666-678.

Milner, T. E. (2002). Contribution of geometry and joint stiffness to mechanical stability of the human arm. *Experimental Brain Research, 143*(4), 515-519.

Mirka, G. A. (1991). The quantification of EMG normalization error. *Ergonomics, 34*(3), 343-352.

Nielsen, J. B. (1998). Co-contraction of antagonist muscles in man. *Danish Medical Bulletin, 45*(4), 423-435.

Panjabi, M. M. (1992a). The stabilizing system of the spine.1. Function, dysfunction, adaptation, and enhancement. *Journal of Spinal Disorders, 5*(4), 383-389.

Panjabi, M. M. (1992b). The stabilizing system of the spine.2. Neutral zone and instability hypothesis. *Journal of Spinal Disorders, 5*(4), 390-397.

Perrot, P. (1998). *A to Z of Thermodynamics*: Oxford University Press.

Pheasant, S., and Haslegrave, C. M. (2005). *Bodyspace: Anthropometry, Ergonomics and the Design of Work* (3rd ed.). London: Taylor and Francis.

Pigeon, P., Yahia, L., and Feldman, A. G. (1996). Moment arms and lengths of human upper limb muscles as functions of joint angles. *Journal of Biomechanics, 29*(10), 1365-1370.

Praemer, A., Furner, S., and Rice, D. P. (1999). *Musculoskeletal Conditions in the United States*. Chicago, IL: American Academy of Orthopedic Surgeons.

Raikova, R. (1999). About weight factors in the non-linear objective functions used for solving indeterminate problems in biomechanics. *Journal of Biomechanics, 32*(7), 689-694.

Schultz, A. B., Andersson, G., Ortengren, R., Haderspeck, K., and Nachemson, A. (1982a). Loads on the lumbar spine - validation of a biomechanical analysis by measurements of intradiscal pressures and myoelectric signals. *Journal of Bone and Joint Surgery-American Volume, 64*(5), 713-720.

Schultz, A. B., and Andersson, G. B. J. (1981). Analysis of loads on the lumbar spine. *Spine, 6*(1), 76-82.

Schultz, A. B., Andersson, G. B. J., Haderspeck, K., Ortengren, R., Nordin, M., and Bjork, R. (1982b). Analysis and measurement of lumbar trunk loads in tasks involving bends and twists. *Journal of Biomechanics, 15*(9), 669-675.

Schultz, A. B., Cromwell, R., Warwick, D., and Andersson, G. (1987). Lumbar trunk muscle use in standing isometric heavy exertions. *Journal of Orthopaedic Research, 5*(3), 320-329.

Schultz, A. B., Haderspeck, K., Warwick, D., and Portillo, D. (1983). Use of lumbar trunk muscles in isometric performance of mechanically complex standing tasks. *Journal of Orthopaedic Research, 1*(1), 77-91.

Seireg, A., and Arvikar, R. (1989). *Biomechanical Analysis of the Musculoskeletal Structure for Medicine and Sports*. New York: Hemisphere Pub. Corp.

Sherrington, C. S. (1909). Reciprocal innervation of antagonistic muscles. Fourteenth notes. On double reciprocal innervation. *Proceedings of the Royal Society of London. Series B., 91*, 249-268.

Smith, A. M. (1981). The co-activation of antagonist muscles. *Canadian Journal of Physiology and Pharmacology, 59*(7), 733-747.

Smith, M. (1993). *Neural Networks for Statistical Modeling*. New York, NY: Van Nostrand Reinhold.

Stokes, I. A. F., and Gardner-Morse, M. (2001). Lumbar spinal muscle activation synergies predicted by multi-criteria cost function. *Journal of Biomechanics, 34*(6), 733-740.

Suzuki, M., Shiller, D. M., Gribble, P. L., and Ostry, D. J. (2001). Relationship between cocontraction, movement kinematics and phasic muscle activity in single-joint arm movement. *Experimental Brain Research, 140*(2), 171-181.

Terzuolo, C. A., Soechtin.Jf, and Viviani, P. (1973a). Studies on control of some simple motor tasks.1. Relations between parameters of movements and EMG activities. *Brain Research, 58*(1), 212-216.

Terzuolo, C. A., Soechtin.Jf, and Viviani, P. (1973b). Studies on control of some simple motor tasks.2. Cerebellar control of movements in relation to formulation of intentional commands. *Brain Research, 58*(1), 217-222.

Tilney, F., and Pike, F. H. (1925). Muscular coordination experimentally studied in its relation to the cerebellum. *Arch. Neurol. Psychiatry, 13*, 289-334.

Tribus, M., and McIrvine, E. C. (1971). Energy and information. *Scientific American, 225*, 179-188.

Tsirakos, D., Baltzopoulos, V., and Bartlett, R. (1997). Inverse optimization: Functional and physiological considerations related to the force-sharing problem. *Critical Reviews in Biomedical Engineering, 25*(4-5), 371-407.

van Dieen, J. H., and Kingma, I. (2005). Effects of antagonistic co-contraction on differences between electromyography based and optimization based estimates of spinal forces. *Ergonomics, 48*(4), 411-426.

Vonkorff, M., Dworkin, S. F., Leresche, L., and Kruger, A. (1988). An epidemiologic comparison of pain complaints. *Pain, 32*(2), 173-183.

Webster, B. S., and Snook, S. H. (1994). The cost of 1989 workers compensation low-back-pain claims. *Spine, 19*(10), 1111-1116.

Appendix

Table A-1 The EASOM predicted and EMG generated muscle forces, along with the percent errors and average absolute percent errors for muscle force prediction under 30 lbs conditions. In each cell, the first row contains predicted/actual muscle forces, and the second row shows the percent error (in bold font). (BIC(S) – biceps short head; BIC(L) – biceps long head; BRA – brachialis; BRD – brachioradialis; ANC – anconeus; TRI(Lt) – triceps lateral head; TRI(Lg) – triceps long head; TRI(Md) – triceps medial head)

Velocity (°/s)	Angle (°)	Muscle force prediction error							
		BIC(S)	BIC(L)	BRA	BRD	ANC	TRI(Lt)	TRI(Lg)	TRI(Md)
0	45	164.3/302.4 **-45.7%**	205.6/195.8 **5.0%**	652.0/620.7 **5.0%**	111.6/126.9 **-12.0%**	121.0/50.4 **140.3%**	67.9/139.7 **-51.4%**	57.5/85.4 **-32.7%**	66.4/189.3 **-64.9%**
0	90	127.8/191.2 **-33.1%**	162.4/156.3 **3.9%**	575.6/519.7 **10.7%**	91.8/113.2 **-18.8%**	71.4/56.0 **27.6%**	38.7/99.1 **-60.9%**	32.3/61.1 **-47.1%**	37.8/89.9 **-57.9%**
0	135	94.4/106.6 **-11.5%**	119.8/164.1 **-27.0%**	478.7/357.9 **33.7%**	75.0/117.2 **-36.0%**	47.5/48.2 **-1.5%**	23.2/59.9 **-61.3%**	18.8/25.8 **-27.0%**	22.5/58.5 **-61.5%**
20	45	220.7/287.5 **-23.2%**	274.5/196.2 **39.9%**	861.1/813.0 **5.9%**	151.0/140.2 **7.7%**	181.3/70.7 **156.4%**	202.2/221.1 **-8.6%**	198.1/152.7 **29.7%**	201.8/189.6 **6.4%**
20	90	134.4/213.5 **-37.1%**	170.9/152.0 **12.4%**	610.5/532.7 **14.6%**	96.6/105.3 **-8.3%**	80.6/76.6 **5.2%**	73.5/129.9 **-43.4%**	68.9/81.9 **-15.9%**	72.9/66.1 **10.3%**
20	135	98.7/101.5 **-2.8%**	124.9/199.4 **-37.4%**	494.5/448.5 **10.3%**	78.0/95.1 **-18.0%**	56.0/121.7 **-54.0%**	42.4/123.7 **-65.8%**	37.4/40.1 **-6.8%**	41.7/73.4 **-43.2%**
30	45	414.8/250.8 **65.4%**	513.4/178.9 **187.0%**	1608.3/772.8 **108.1%**	285.8/191.8 **49.0%**	382.2/87.2 **338.3%**	662.2/230.1 **187.7%**	707.5/96.4 **634.0%**	669.0/207.4 **222.5%**
30	90	139.1/265.2 **-47.6%**	176.3/160.9 **9.6%**	625.4/489.4 **27.8%**	99.9/77.1 **29.6%**	88.3/81.8 **8.0%**	92.3/130.5 **-29.3%**	88.7/61.6 **44.0%**	91.8/66.0 **39.2%**
30	135	101.3/95.6 **5.9%**	127.9/195.0 **-34.4%**	502.1/467.0 **7.5%**	79.8/112.9 **-29.3%**	60.6/128.1 **-52.7%**	52.5/168.5 **-68.8%**	47.6/52.1 **-8.8%**	51.9/96.7 **-46.4%**
40	45	472.8/372.0 **27.1%**	583.1/185.6 **214.2%**	1809.0/853.4 **112.0%**	326.8/170.7 **91.5%**	445.4/110.1 **304.6%**	793.7/280.0 **183.4%**	851.3/200.9 **323.6%**	802.3/269.4 **197.9%**
40	90	141.4/233.4 **-39.4%**	179.7/172.3 **4.3%**	644.5/596.5 **8.0%**	101.5/64.7 **56.9%**	91.0/70.5 **29.1%**	107.8/152.0 **-29.1%**	106.7/94.2 **13.2%**	107.7/92.0 **17.1%**
40	135	103.0/98.4 **4.7%**	130.1/247.6 **-47.4%**	516.1/470.0 **9.8%**	81.3/99.5 **-18.3%**	63.1/123.0 **-48.7%**	65.0/120.1 **-45.9%**	61.5/67.5 **-8.9%**	64.5/206.6 **-68.8%**
Average absolute percent error		**28.6%**	**51.9%**	**29.5%**	**31.3%**	**97.2%**	**69.6%**	**99.3%**	**69.7%**

i. Data on Muscle Lines of Action

For the single-plane (sagittal) anatomical elbow model (as described in Section 6.5.2), we established an x-y coordinate system in the sagittal plane for identification of the locations for elbow muscle origins and insertions. In this coordinate system, where the origin is the elbow joint, the x-axis is perpendicular to the humerus and pointed towards the front, and the y-axis is along the humerus, connecting the elbow joint and the shoulder joint, and pointed upwards. Table A-2 displays the coordinates (x, y) for origins and insertions (at different elbow flexion angles) for all elbow muscles involved in this study. These coordinate values were calculated from the data in Table I in Chapter IV of Seireg and Arvikar (1989). It should be noted that the scapula (shoulder blade) and humerus (upper arm bone) were assumed to be stationary, with humerus at zero shoulder flexion/extension or adduction/abduction, at all time. Since all elbow muscles originate from either scapula or humerus, origins of these muscles are therefore fixed and independent of the elbow flexion angle.

Table A-2 Coordinates (in cm) for muscle origins and insertions with regard to the elbow joint

	Origin (fixed)	**Insertion** (at different elbow flexion angles)		
		0°	45°	90°
Biceps short head	(1, 32)	(0.8, -5.5)	(4.45, -3.32)	(5.5, 0.8)
Biceps long head	(2.5, 31.5)	(0.8, -5.5)	(4.45, -3.32)	(5.5, 0.8)
Brachialis	(1, 10.5)	(0, -3)	(2.12, -2.12)	(3, 0)
Brachioradialis	(0, 3.5)	(0, -24)	(16.97, -16.97)	(24, 0)
Anconeus	(-1.6, 0.5)	(-1.8, -4)	(1.56, -4.10)	(4, -1.8)
Triceps lateral head	(-0.8, 14.5)	(-1.5, 2.5)	(-2.83, 0.71)	(-2.5, -1.5)
Triceps long head	(-1.5, 28.5)	(-1.5, 2.5)	(-2.83, 0.71)	(-2.5, -1.5)
Triceps medial head	(-1, 10.5)	(-1.5, 2.5)	(-2.83, 0.71)	(-2.5, -1.5)

ii. Force-Length Relationship

An optimization approach was adapted from Chang *et al.* (1999) to calculate the force-length factors. In such an approach, force-length factor (F_l) and passive elastic component (F_{pe}) can be written as functions of muscle strain (ε) and the so-called muscle index of architecture (*ia*) which is the ratio of muscle fiber length to muscle belly length at optimum length) for elbow flexors. Passive components for elbow extensors were omitted. Note that

$$\varepsilon = \frac{ml - oml}{oml} \text{ when } ml > oml ; \tag{A-1}$$

$$\varepsilon = 0 \qquad \text{otherwise} \tag{A-2}$$

where

ε is the muscle strain;

ml is the instantaneous muscle length;

oml is the optimum muscle length.

ml was calculated from instantaneous elbow flexion angle using the regression equations from Pigeon et al. (1996). The optimization formulation was then trying to minimize the sum of squared error between predicted torque (generated by forces calculated from EMG data) and measured torque, i.e.

$$Minimize \quad \sum_{j=1}^{cond} (T_j^p - T_j^m)^2 \tag{A-3}$$

$$Subject\ to \quad T_j^p = \sum_{i=1}^{8} \left(\frac{EMG_i(t)}{EMG_{i,\max}} \times F_l + F_{pe} \right) \times F_v \times PCSA_i \times ma_i \times gain \tag{A-4}$$

where

T_j^p is the predicted torque generated by forces calculated from EMG data at condition *j*;

T_j^m is the measured torque at condition *j*;

cond is the total number of conditions;

$EMG_i(t)$ denotes the raw EMG signal for muscle *i* at time *t* at condition *j*;

$EMG_{i,\max}$ is the maximum EMG for muscle *i* at the current elbow flexion angle;

F_l is the force-length factor for muscle *i* at condition *j*;

F_{pe} is a factor resulting from passive elastic muscle component, for muscle *i* at condition *j*;

F_v is the force-velocity factor for muscle *i* at condition *j*;

$PCSA_i$ denotes the physiological cross sectional area for muscle *i*;

ma_i is the moment arm for muscle *i* at condition *j*;

gain is a constant across all muscles for an individual and shows that person's force generating potential. It represents the maximum force that can be produced per muscle cross sectional area (N/cm^2).

This optimization problem then had five unknowns including the gain and the four elbow flexion angles corresponding to the optimum lengths for all four elbow flexors (or optimum flexion angles). With the resulting optimum flexion angle for each elbow flexor, it was then possible to obtain the optimum muscle length (*oml*) using the regression equations from Pigeon et al. (1996). Subsequently, we were able to calculate muscle strains (ε) (using equation A-1) and ultimately force-length factors (F_l) and passive elastic components (F_{pe}).